CAPITAL UNIVERSITY OF SCIENCE AND TECHNOLOGY, ISLAMABAD

In Silico Exploration and Assessment of Bioactive Compounds from Jerusalem Artichoke for their Efficacy in Breast Cancer via Targeting Receptor Proteins

by

Hira Tahreem

A thesis submitted in partial fulfillment for the degree of Master of Science

in the

Faculty of Health and Life Sciences
Department of Bioinformatics and Biosciences

2026

CERTIFICATE OF APPROVAL

In Silico Exploration and Assessment of Bioactive Compounds from Jerusalem Artichoke for their Efficacy in Breast Cancer via Targeting Receptor Proteins

by

Hira Tahreem

(MBS243018)

THESIS EXAMINING COMMITTEE

S. No.	Examiner	Name	Organization
(a)	External Examiner	Dr. Joham Sarfraz Ali	IST, Islamabad
(b)	Internal Examiner	Dr. Sahar Fazal	CUST, Islamabad

Dr. Sami Ullah Jan
Thesis Supervisor
July, 2026

Dr. Syeda Marriam Bakhtiar
Head
Dept. of Bioinfo. and Biosciences
July, 2026

Dr. Sahar Fazal
Dean
Faculty of Health and Life Sciences
July, 2026

Author's Declaration

I, **Hira Tahreem** hereby state that my MS thesis titled "***In Silico* Exploration and Assessment of Bioactive Compounds from Jerusalem Artichoke for their Efficacy in Breast Cancer via Targeting Receptor Proteins**" is my own work and has not been submitted previously by me for taking any degree from Capital University of Science and Technology, Islamabad or anywhere else in the country/abroad.

At any time if my statement is found to be incorrect even after my graduation, the University has the right to withdraw my MS Degree.

(Hira Tahreem)

Registration No: MBS243018

Plagiarism Undertaking

I solemnly declare that research work presented in this thesis titled "***In Silico* Exploration and Assessment of Bioactive Compounds from Jerusalem Artichoke for their Efficacy in Breast Cancer via Targeting Receptor Proteins**" is solely my research work with no significant contribution from any other person. Small contribution/help wherever taken has been duly acknowledged and that complete thesis has been written by me.

I understand the zero tolerance policy of the HEC and Capital University of Science and Technology towards plagiarism. Therefore, I as an author of the above titled thesis declare that no portion of my thesis has been plagiarized and any material used as reference is properly referred/cited.

I undertake that if I am found guilty of any formal plagiarism in the above titled thesis even after award of MS Degree, the University reserves the right to withdraw/revoke my MS degree and that HEC and the University have the right to publish my name on the HEC/University website on which names of students are placed who submitted plagiarized work.

(Hira Tahreem)

Registration No: MBS243018

Acknowledgement

In the name of Allah, the Most Gracious, the Most Merciful. First and foremost, I express my deepest gratitude to Allah Almighty for His countless blessings, mercy, and guidance, which enabled me to successfully complete this research. I sincerely thank my respected supervisor, Dr. Sami Ullah Jan, for his invaluable guidance, continuous encouragement, and constructive feedback throughout this research. His support and expertise were instrumental in the successful completion of this thesis. I am also grateful to the respected Dean of the Faculty of Health and Life Sciences, the Head of the Department of Bioinformatics and Biosciences, and all the faculty members and staff of Capital University of Science and Technology (CUST), Islamabad, for providing an excellent academic environment and continuous support.

My heartfelt gratitude goes to my parents and family for their unconditional love, prayers, patience, and encouragement, which have always been my greatest source of strength. I would especially like to thank my brother for his constant support and invaluable assistance with the formatting of this thesis. His encouragement is deeply appreciated. I am also sincerely grateful to my dear friends, Faryal Naz Tabassum and Rameen Ahmad, for their continuous encouragement, support, and valuable assistance throughout this journey. Finally, I extend my sincere thanks to all my friends, colleagues, and everyone who contributed, directly or indirectly, to the successful completion of this thesis. On a personal note, I am grateful for the determination and perseverance that enabled me to overcome every challenge and successfully complete this research.

(Hira Tahreem)

Abstract

Breast cancer is among the most commonly diagnosed malignancies and remains a major cause of cancer-related mortality among women worldwide. Despite advances in therapeutic interventions, challenges such as treatment resistance, disease recurrence, and treatment-related adverse effects continue to limit clinical outcomes. Consequently, the exploration of bioactive compounds from natural sources has gained considerable attention in anticancer drug discovery.

The present study investigated the anticancer potential of selected phytochemicals from *Helianthus tuberosus* L. (Jerusalem artichoke) against breast cancer-associated target proteins using *in silico* approaches. The androgen receptor (AR), estrogen receptor alpha (ERα), and human epidermal growth factor receptor 2 (HER2) were selected as molecular targets. The selected phytochemicals were evaluated for their drug-likeness and pharmacokinetic properties using Lipinski's Rule of Five and ADMET analysis. Molecular docking was subsequently performed to investigate the binding affinities of the compounds toward the target proteins, followed by protein–ligand interaction analysis to examine their binding patterns. Lead compound selection was based on the overall evaluation of physicochemical properties, drug-likeness, pharmacokinetic characteristics, molecular docking, and protein–ligand interaction profiles. The selected lead compound was subsequently compared with the reference drug, Tamoxifen.

The findings identified L-tryptophan as the most promising bioactive compound because of its favorable drug-like characteristics, acceptable predicted pharmacokinetic profile, lower predicted toxicity, and favorable protein–ligand interactions with the selected target proteins. Collectively, these findings suggest the therapeutic potential of *Helianthus tuberosus* phytochemicals and provide a computational foundation for the future development of natural product-based lead compounds for breast cancer treatment.

Keywords: Breast cancer, *Helianthus tuberosus*, Jerusalem artichoke, L-tryptophan, Molecular docking, ADMET analysis, Drug-likeness, Protein–ligand interaction, *In silico* drug discovery.

Contents

List of Figures

List of Tables

Abbreviations

ADMET	Absorption, Distribution, Metabolism, Excretion, and Toxicity
AR	Androgen Receptor
BRCA1	Breast Cancer Gene 1
DCIS	Ductal Carcinoma In Situ
EMT	Epithelial–Mesenchymal Transition
ER	Estrogen Receptor
HER2	Human Epidermal Growth Factor Receptor 2
IDC	Invasive Ductal Carcinoma
JA	Jerusalem Artichoke
PDB	Protein Data Bank
PI3K	Phosphoinositide 3-Kinase
PR	Progesterone Receptor
QSAR	Quantitative Structure–Activity Relationship
ROS	Reactive Oxygen Species
STAT	Signal Transducer and Activator of Transcription
UAE	Ultrasound-Assisted Extraction
UHPLC	Ultra-High-Performance Liquid Chromatography

Chapter 1

Introduction

Jerusalem artichoke (JA) or artichoke, scientifically known as *Helianthus tuberosus* L., is a perennial tuberous plant belonging to the Asteraceae family, one of the largest families of flowering plants with more than 25,000 species. The species originated in North America, where it was first cultivated by Native Americans for its edible tubers before being introduced to Europe and Asia. The plant can reach a height of approximately 3 m and develops underground tubers that differ in shape and color.

These tubers are particularly rich in inulin and other nutrients, making them valuable for food, pharmaceutical, and industrial applications. In addition, its shoots and leaves serve as nutritious livestock feed, while its ability to tolerate drought, salinity, and other environmental stresses allows successful cultivation even on marginal lands. Plant growth and tuber formation are strongly influenced by environmental conditions, particularly temperature and photoperiod [1, 2].

Closely related to the common sunflower (*Helianthus annuus*), Jerusalem artichoke is capable of hybridizing with several other *Helianthus* species, enabling the transfer of desirable traits such as disease resistance and stress tolerance. Cytogenetically, it is a perennial hexaploid species ($2n = 6x = 102$) and is classified as an autoallopolyploid. Current evidence suggests that it originated through hybridization between the autotetraploid hairy sunflower and the diploid sawtooth

sunflower. Although these species have evolved over millions of years, many members of the *Helianthus* genus still hybridize naturally, indicating relatively weak reproductive barriers. The genus is estimated to have originated nearly 3 million years ago, while earlier whole-genome duplication and triplication events played an important role in shaping its complex genome [1, 3].

Artichoke is widely recognized as a model crop for fructan metabolism because its tubers accumulate inulin, the principal storage carbohydrate, constituting as much as 80% of the tuber dry matter. The key enzymes involved in inulin synthesis (1-SST and 1-FFT) and degradation (1-FEHI and 1-FEHII) have been identified, and their corresponding genes have been cloned and functionally characterized [1, 3].

Owing to its hexaploid genome, artichoke is likely to contain additional unexplored gene copies. Recent genomic studies have generated a 21-Gb chromosome-level genome assembly, providing insights into its polyploid origin, chromosome synteny with common sunflower, and the evolution of genes associated with inulin metabolism, thereby supporting future genetic improvement and industrial applications of this crop [1, 4].

Artichoke, also known as sunroot, earth apple, topinambur, or sunchoke, has been cultivated for over 2000 years. It was domesticated in India during the first millennium B.C. and later introduced to Europe in the 16th century, where it spread rapidly before its cultivation declined with the widespread adoption of potato. Owing to its nutritional and medicinal value, interest in the crop was revived during the 19th century. Today, artichoke is cultivated worldwide, particularly in France, the United States, Canada, Germany, Poland, Hungary, China, Japan, and Russia [3, 4].

The species comprises more than 300 cultivars and hybrids that differ in tuber yield, biomass production, and ornamental characteristics. The plant grows up to 3 m tall and produces underground tubers of varying shapes, sizes, and colors that serve as storage organs for inulin, a fructan with important nutritional and industrial value. Tuber development occurs over approximately 24 weeks and

involves four stages: creeping stem formation, tuber initiation, tuber swelling, and tuber maturation [4].

Above-ground structures consist of erect, branched stems and alternately arranged leaves that can be harvested several times annually for high-protein forage or silage. The leaves are rich in essential amino acids, particularly methionine and lysine, and contain higher calcium levels than the tubers, whereas magnesium is moderate and potassium and phosphorus are comparatively lower [4]. The plant bears composite inflorescences typical of the Asteraceae family, contributing to both reproduction and ornamental value. Specialized anatomical features, including stomata and trichomes, enhance tolerance to various abiotic and biotic stresses, enabling the plant to thrive in saline, waterlogged, marginal, and coastal environments [5].

Artichoke is a high-biomass forage crop widely used as fresh fodder, hay, and silage for livestock. Both its herbage and tubers are rich in carbohydrates and contain up to 17% protein with a balanced amino acid composition, making it a nutritious feed resource. Its high nutritional and bioactive value contributes to improved livestock health and productivity [6, 7]. Artichoke is recognized as a valuable forage crop due to its high nutritional value and biomass productivity, contributing to improved livestock performance, including enhanced milk production, weight gain, and egg yield [6]. The crop is widely cultivated in temperate regions and exhibits remarkable adaptability to diverse soils and environmental stresses, such as drought and frost.

In addition, endophytic bacterial inoculation has been reported to improve drought tolerance and tuber yield under water-limited conditions [8]. Owing to its high carbohydrate and inulin content, artichoke is also considered a promising bioenergy crop for bioethanol production and other sustainable industrial applications [9].

Medicinal plants have played an essential role in healthcare for centuries and continue to provide a rich source of biologically active molecules for pharmaceutical research. A considerable number of modern therapeutic agents have been developed from naturally occurring plant metabolites, and herbal medicines remain an important component of primary healthcare in many regions of the world. Owing

to their diverse phytochemical composition, medicinal plants exhibit numerous pharmacological effects, including antioxidant, anti-inflammatory, antimicrobial, antidiabetic, and anticancer activities. These biological properties have encouraged extensive research into their potential for the management and prevention of chronic diseases [10].

Among these, *Helianthus tuberosus* L. has attracted considerable attention owing to its adaptability to diverse environmental conditions and its potential applications in food, feed, bioenergy, and pharmaceuticals. Its tubers are rich in inulin, fructose, vitamins, and minerals, contributing to their nutritional and functional value [11]. *Helianthus tuberosus* is characterized by a diverse phytochemical composition comprising both primary and secondary metabolites.

The primary metabolites predominantly include carbohydrates, amino acids, organic acids, and quaternary ammonium compounds such as betaine, whereas secondary metabolites comprise phenolic acids, flavonoids, sesquiterpene lactones, chlorophylls, and carotenoids. These phytochemicals are associated with diverse pharmacological activities and contribute significantly to the plant's therapeutic potential [10, 11]. Hydroxycinnamic acids, including chlorogenic, caffeic, and ferulic acids, are abundant in the tubers, leaves, stems, and flowers of artichoke and contribute significantly to its antioxidant activity by scavenging reactive oxygen species. Multiple caffeoylquinic acid isomers have also been identified, particularly in the leaves, indicating considerable phytochemical diversity [12].

The diverse phytochemicals present in *Helianthus tuberosus* confer multiple biological activities, such as antioxidant, anti-inflammatory, antifungal, and cytotoxic effects. These beneficial properties suggest that the plant may serve as a promising natural source of therapeutic agents for combating oxidative stress-related diseases, including diabetes, cardiovascular disorders, and various forms of cancer. Consequently, its rich phytochemical profile has attracted considerable interest for applications in nutraceuticals, functional foods, and pharmaceutical development [13]. Despite the extensive nutritional and industrial importance of *Helianthus tuberosus*, its therapeutic potential against breast cancer remains insufficiently explored. The present study selected this plant because of its diverse

phytochemical composition, particularly its abundance of biologically important primary metabolites that participate in essential metabolic processes and have been reported to possess antioxidant and cytoprotective properties.

Since oxidative stress and abnormal cellular signaling contribute significantly to breast cancer progression, these metabolites may offer promising therapeutic value. Moreover, compared with many extensively investigated medicinal plants, *H. tuberosus* has received relatively limited attention in computational anticancer drug discovery. This knowledge gap provided a strong scientific basis for investigating its metabolites as potential inhibitors of key proteins involved in metastatic breast cancer through molecular docking and ADMET analysis.

Breast cancer develops when genetic and cellular alterations in breast tissue lead to the uncontrolled proliferation of abnormal cells, resulting in tumor formation, local invasion, and metastasis to distant organs [14]. Globally, more than two million new cases are diagnosed each year, with approximately 670,000 deaths annually. Although it predominantly affects women, nearly 1% of cases occur in men. Considerable disparities in incidence, mortality, and survival exist between developed and developing countries. Early screening, greater public awareness, and improved access to treatment have enhanced survival in developed regions, whereas delayed diagnosis and limited healthcare resources continue to adversely affect outcomes in developing countries [15, 16].

Breast cancer typically develops from epithelial cells located within the mammary ducts or the milk-producing lobules, giving rise to ductal and lobular carcinomas, respectively. Tumors may remain confined to their site of origin (*in situ*) or progress to invasive disease capable of spreading through the lymphatic and circulatory systems. Its development is multifactorial, involving genetic, hormonal, environmental, and lifestyle-related factors [14, 17].

Inherited genetic mutations make up to 5–10% of cases, whereas 20–30% are linked to modifiable risk factors such as obesity, tobacco use, alcohol consumption, unhealthy lifestyle habits, and exposure to environmental pollutants or ionizing radiation. Prolonged exposure to estrogen and progesterone further promotes cellular

proliferation and increases the risk of malignant transformation [14]. Breast cancer is categorized into four principal molecular subtypes which are luminal A, luminal B, HER2-enriched, and basal-like, according to the expression of estrogen receptor (ER), progesterone receptor (PR), human epidermal growth factor receptor 2 (HER2), and the proliferation marker Ki-67. Among these, triple-positive breast cancer (TPBC), which expresses ER, PR, and HER2 simultaneously, represents approximately 10–15% of all breast cancer cases. This subtype is driven by estrogen receptor signaling together with HER2-mediated pathways, which promote tumor growth, progression, and therapeutic resistance [15]. Owing to its molecular heterogeneity, TPBC presents significant clinical challenges, with differences in tumor genetics, the tumor microenvironment, and patient-specific factors contributing to variable treatment responses.

Moreover, variation in tumor-infiltrating lymphocyte levels further influences prognosis and therapeutic outcomes [15, 18]. Consequently, effective treatment requires personalized strategies that integrate endocrine therapy with targeted molecular approaches. A comprehensive understanding of the molecular mechanisms and signaling pathways involved in breast cancer progression is therefore essential for developing precision therapies and improving clinical outcomes.

Triple-positive breast cancer (TPBC) is defined by the simultaneous expression of ER, PR, and HER2, all of which contribute to tumor growth and survival. ER and PR regulate hormone-dependent growth, whereas HER2 enhances proliferative and survival signaling. Crosstalk among these receptors further influences tumor progression and therapeutic response [15]. Therefore, understanding the biological roles of these receptors is fundamental for the developing the targeted therapies for breast cancer. Estrogen regulates cellular proliferation, differentiation, and survival through genomic and non-genomic signaling pathways. In the genomic signaling pathway, estrogen activates ERα and ERβ by binding to these receptors, leading to receptor dimerization and regulation of genes associated with cell-cycle progression, cellular proliferation, and apoptosis.

Activated estrogen receptors further modulate gene expression through interactions with transcription factors, including AP-1 and SP-1, while also stimulating

the PI3K/AKT and MAPK signaling cascades. Conversely, the non-genomic pathway is mediated by membrane-associated estrogen receptors, which rapidly initiate intracellular signaling events that regulate cellular proliferation, survival, and metabolic processes [15, 19]. The androgen receptor (AR) is a steroid hormone-activated nuclear receptor that is expressed in a significant proportion of breast cancer cases.

Following androgen binding, the receptor undergoes conformational activation, forms dimers, and translocates to the nucleus, where it binds to androgen response elements (AREs) to regulate the expression of genes associated with cellular proliferation, differentiation, apoptosis, and survival. In addition to this classical genomic mechanism, AR modulates several intracellular signaling pathways, including PI3K/AKT, mTOR, ERK, and Wnt/β-catenin. The functional role of AR depends on the molecular subtype of breast cancer, where it may either suppress tumor growth or promote disease progression. Consequently, AR has emerged as an important molecular target for breast cancer therapy [20].

Aromatase, encoded by the *CYP19A1* gene on chromosome 15, is the principal enzyme responsible for estrogen biosynthesis through the conversion of androgens into estrogens. Elevated aromatase activity enhances local estrogen production, thereby promoting ER-dependent tumor growth. Although aromatase inhibitors are widely used to suppress estrogen synthesis, prolonged therapy may cause adverse effects, including bone loss, cognitive impairment, skeletal fragility, and therapeutic resistance.

Therefore, the development of improved aromatase inhibitors and alternative therapeutic strategies remains an important area of breast cancer research [21].

1.1 Problem Statement

Breast cancer, particularly hormone-dependent types like triple-positive breast cancer, is a major global health issue with increasing incidence and therapy resistance. Current treatments targeting pathways are effective but limited by side

effects and resistance. Hence, there is a need to identify novel natural compounds targeting key molecular pathways.

1.2 Hypothesis

Jerusalem artichoke (*Helianthus tuberosus* L.) contains numerous bioactive compounds which may have anticancer potential. However, its role in breast cancer mechanisms remains underexplored and requires further investigation.

1.3 Aims

To explore bioactive phytochemicals in Jerusalem artichoke (*Helianthus tuberosus* L.) and evaluate its potential therapeutic association with breast cancer through molecular docking.

1.4 Objectives

i. To identify the bioactive compounds of *Helianthus tuberosus* L. through phytochemical database screening.

ii. To select the identified compounds based on their reported medicinal properties.

iii. To characterize the interactions and binding affinities of the selected phytochemicals against breast cancer target proteins through molecular docking.

Chapter 2

Literature Review

2.1 Jerusalem Artichoke

Helianthus tuberosus L., commonly known as Jerusalem artichoke, is well known for its adaptability to diverse environmental conditions. Owing to its rich chemical composition and diverse biological properties, Jerusalem artichoke has attracted increasing scientific interest in recent years [22]. The whole plant of Jerusalem artichoke, including its tubers, leaves, and flowers, is shown in Figure 2.1.

2.2 Taxonomy

This species is characterized by its tuber-forming ability and remarkable tolerance to both biotic and abiotic stresses, enabling its widespread cultivation across diverse geographical regions. As a member of the *Helianthus* genus, it is closely related to several economically important species, highlighting its taxonomic and agricultural significance [22].

In addition, *Helianthus tuberosus* crop also has applications in the food, pharmaceutical, and industrial sectors.

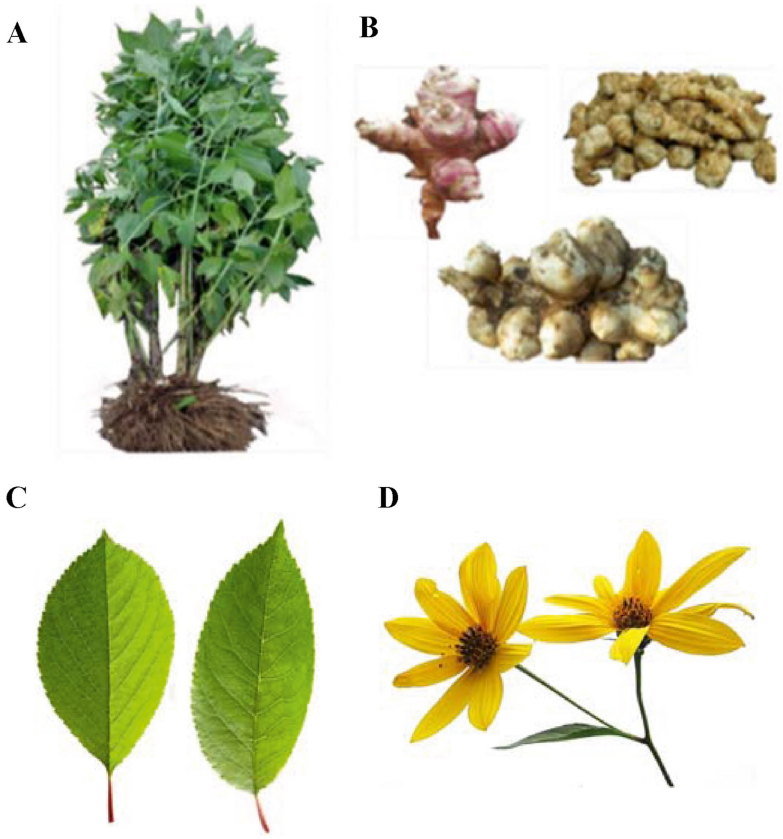

FIGURE 2.1: Morphology of *Helianthus tuberosus* L., illustrating (A) the whole plant, (B) underground tubers, (C) leaves, and (D) flowers [7].

Its taxonomic classification is based on morphological and physiological characteristics, while its ability to synthesize bioactive compounds, particularly inulin, enhances its nutritional, functional, and economic value [22]. The taxonomic classification of *Helianthus tuberosus* L., obtained from the PubChem database, is presented in Table 2.1 [23].

TABLE 2.1: Taxonomic classification of *Helianthus tuberosus* L.

Taxonomic Rank	**Classification**
Kingdom	Plantae
Order	Asterales
Family	Asteraceae (Compositae)
Subfamily	Asteroideae
Tribe	Heliantheae
Genus	*Helianthus* L. (sunflower)
Species	*Helianthus tuberosus* L.

2.3 Genomic and Phylogenetic Evidence

Recent genomic studies have provided valuable insights into the taxonomy and evolution of *Helianthus tuberosus*. Genome-level analyses revealed that the species possesses a large, highly heterozygous genome with considerable variation among different accessions, reflecting substantial intraspecific genetic diversity and supporting its taxonomic classification [24]. Furthermore, chloroplast genome analyses have clarified the phylogenetic position of *Helianthus tuberosus*. Its complete chloroplast genome exhibits a typical quadripartite structure and indicates a close evolutionary relationship with *Helianthus petiolaris*, providing additional molecular evidence for its evolutionary lineage and taxonomic placement [25].

2.4 Medicinal Properties

Helianthus tuberosus is a perennial medicinal plant recognized for its broad range of biological activities, including antioxidant, anti-inflammatory, antidiabetic, and anticancer effects. Different plant parts, such as the tubers, leaves, and aerial tissues, have shown promising pharmacological potential. Among these, the antidiabetic activity is primarily associated with the presence of inulin and its related compounds. In addition, *Helianthus tuberosus* exhibits antimicrobial and wound-healing properties and has been reported to improve blood pressure regulation, lipid metabolism, body weight management, and immune function. These biological activities highlight its potential as a functional food and a valuable source of bioactive compounds for pharmaceutical applications [10, 22, 26]. The major medicinal properties of *H. tuberosus* are discussed in the following sections.

2.4.1 Antioxidant

The antioxidant activity of *Helianthus tuberosus* is principally related to its high content of phenolic compounds, flavonoids, and inulin [27]. Both fresh extracts and processed products derived from JA tubers exhibit considerable antioxidant

potential, while freeze-dried tubers retain substantial amounts of phenolic compounds, indicating that appropriate processing preserves their antioxidant constituents and functional value [28]. Leaf-derived flavonoids also exhibit strong radical-scavenging activity in *in vitro* assays, whereas inulin contributes to antioxidant defence by maintaining catalase and peroxidase activities during post-harvest storage [29, 30].

Furthermore, incorporation of JA tuber powder into functional foods, such as healthy crackers, enhances *in vitro* antioxidant activity owing to its high phenolic and flavonoid contents [31]. Overall, these findings emphasize the importance of *Helianthus tuberosus* as a rich source of natural antioxidants and a promising functional food ingredient.

2.4.2 Anti-Inflammatory

Helianthus tuberosus possesses notable anti-inflammatory properties that are largely linked to its polysaccharides, phenolic compounds, and flavonoids, which suppress pro-inflammatory mediators and regulate inflammatory signaling pathways [32]. Among these, polysaccharides play a major role by reducing the expression of inflammatory cytokines, particularly tumor necrosis factor-alpha (TNF-α) and interleukin-6 (IL-6) [33]. They also exhibit antiviral activity against respiratory syncytial virus while reducing virus-induced inflammation and have demonstrated *in vivo* therapeutic effects by accelerating wound healing and promoting tissue regeneration. Furthermore, incorporation of JA tuber powder into functional foods enhances *in vitro* anti-inflammatory activity because of its high polysaccharide and phenolic content [34, 35]. These findings indicate that *Helianthus tuberosus* exhibits natural anti-inflammatory activity.

2.4.3 Antidiabetic

Artichoke has been widely investigated for its antidiabetic properties, which are mainly attributed to inulin and related polysaccharides. Experimental studies

in streptozotocin-induced diabetic mice demonstrated that artichoke extracts reduced blood glucose levels, enhanced insulin secretion, improved pancreatic β-cell function, and promoted glycemic control [36].

In type 2 diabetes mellitus (T2DM) models, inulin supplementation beneficially modulated gut microbiota and metabolic profiles, leading to improved glucose tolerance, reduced hepatic lipid accumulation, and lower insulin resistance [37]. Clinical studies further reported reductions in postprandial blood glucose and glucose-dependent insulinotropic polypeptide (GIP) concentrations following artichoke consumption, supporting its potential as a functional food for glycemic control [38].

2.4.4 Anticancer

Helianthus tuberosus L. has emerged aas a rich source of bioactive phytochemicals with potential anticancer activity, owing to its cytotoxic, antimetastatic, and pro-apoptotic properties. *In vitro* studies using MCF-7 breast cancer cells demonstrated that tuber and shell extracts induce dose- and time-dependent cell death while exhibiting minimal toxicity toward normal mammary epithelial cells (MCF-12A). These extracts inhibited tumor cell adhesion and invasion and induced apoptosis, as confirmed by TMRE and AnnexinV/7AAD staining, providing mechanistic evidence for their selective anticancer activity [39].

The anticancer potential of artichoke has also been demonstrated in other epithelial cancer models. Combined extracts of artichoke and fennel seeds significantly reduced the viability of oral squamous carcinoma cells by activating apoptotic pathways and suppressing cell proliferation [40]. Similarly, studies in melanoma cell lines reported reduced cell proliferation, induction of apoptosis, and cell-cycle arrest following treatment with artichoke extracts, further supporting the ability of artichoke-derived phytochemicals to disrupt tumor progression [41]. Furthermore, these findings highlight the broad-spectrum anticancer potential of *Helianthus tuberosus* and support its further investigation as a natural source of therapeutic agents.

2.5 Phytochemical and Nutritional Composition

Helianthus tuberosus L. contains high level bioactive phytochemicals, including phenolic acids, flavonoids, and sesquiterpene lactones, which are responsible for its diverse pharmacological activities. Phenolic acids, such as chlorogenic, caffeic, and ferulic acids, exhibit strong antioxidant activity by scavenging reactive oxygen species and reducing oxidative stress. Flavonoids possess antioxidant, anti-inflammatory, and antimicrobial properties while regulating cellular signaling pathways.

Sesquiterpene lactones have also demonstrated cytotoxic and anticancer activities by inducing apoptosis and suppressing tumor growth. Together, these phytochemicals led to the antioxidant, anti-inflammatory, antidiabetic, and anticancer potential of *H. tuberosus* through the modulation of molecular pathways involved in cell proliferation, apoptosis, and immune regulation [10, 11].

2.5.1 Primary Metabolites and Tuber Constituents

In addition to secondary metabolites, *Helianthus tuberosus* tubers contain a diverse range of primary metabolites that contribute to their nutritional and functional value. Carbohydrates are the major constituents, with inulin serving as the principal storage polysaccharide, accompanied by fructose, glucose, sucrose, and fructooligosaccharides. These carbohydrates are largely responsible for the prebiotic and health-promoting properties of Jerusalem artichoke. The tubers also provide proteins, essential amino acids, vitamins, and minerals, further enhancing their nutritional importance [7, 22]. Among the naturally occurring amino acids are lysine, isoleucine, glutamic acid, aspartic acid, and tryptophan, together with biologically important compounds such as betaine. These metabolites participate in various physiological processes and have attracted increasing interest because of their nutritional value, favorable safety profile, and therapeutic potential in computational and experimental drug discovery studies [42]. The major primary metabolites reported in artichoke tubers are listed in Table 2.2.

TABLE 2.2: Major primary metabolites reported in *Helianthus tuberosus* tubers.

Class	**Representative Compounds**	**Biological Significance**	**Ref**
Carbohydrates	Hexose, β-D-Glucose, Fructose, Sucrose	Primary energy source and essential components of carbohydrate metabolism.	[42]
Fructans	Inulin, Fructooligosaccharides	Storage carbohydrates with prebiotic properties that support gut health and glucose metabolism.	[22]
Amino acids	L-Tryptophan, L-Isoleucine, L-Glutamic acid, L-Lysine, L-Aspartic acid	Essential for protein synthesis, cellular metabolism, and various physiological processes.	[42]
Other metabolites	Betaine	Functions as an osmoprotectant and methyl donor, contributing to cellular homeostasis and metabolic regulation.	[42]

2.5.2 Phenolic Compounds

Phenolic compounds in *Helianthus tuberosus* L. exhibit considerable variation in response to environmental conditions, particularly drought stress. Water deficiency has been reported to increase total phenolic content (TPC) in leaves and stems, while tubers show comparatively smaller changes. In addition, the accumulation of individual phenolics, such as *p*-coumaric acid, varies among genotypes,

indicating that both genetic and environmental factors influence phenolic biosynthesis and antioxidant capacity [43].

Comparative analyses of different plant organs revealed that leaves possess the highest total phenolic content and antioxidant activity, with chlorogenic acid and dicaffeoylquinic acids identified as the major phenolic constituents contributing to these properties [12]. Furthermore, optimization of microwave-assisted extraction (MAE) significantly improved the recovery of phenolic compounds from artichoke tubers, supporting their potential application in nutraceutical and functional food development [44].

2.5.3 Flavonoids

Flavonoids in *Helianthus tuberosus* contribute significantly to its antioxidant properties. Optimized ultrasound-assisted extraction (UAE) has been shown to improve flavonoid recovery from tubers, resulting in enhanced antioxidant activity, highlighting the importance of extraction conditions in maximizing flavonoid yield and bioactivity [45]. Flavonoid content is also influenced by environmental and post-harvest conditions. Moderate doses of gamma irradiation have been reported to increase flavonoid accumulation, indicating that controlled stress can stimulate secondary metabolite biosynthesis and enhance the nutritional and therapeutic value of artichoke tubers [46]. The aerial parts of *H. tuberosus*, particularly the leaves, contain a diverse range of flavonoids, including quercetin, kaempferol, and isorhamnetin derivatives. These compounds contribute to the antioxidant potential of the plant and support its applications in nutraceuticals and functional foods [47].

2.5.4 Sesquiterpene Lactones

Sesquiterpene lactones are important bioactive constituents of *Helianthus tuberosus* that have attracted considerable attention because of their pharmacological

potential. These compounds exhibit diverse biological activities, including antitrypanosomal effects, which are largely attributed to their reactive chemical structures and interactions with biological targets [48]. In addition, sesquiterpene lactones have been identified in processed artichoke-derived products, indicating their stability during food processing and potential contribution to the functional properties of these products [49]. Quantitative analysis using UHPLC identified multiple sesquiterpene lactones in *H. tuberosus* leaves, with their abundance varying according to geographical location and harvesting time, suggesting that environmental conditions influence their biosynthesis and accumulation [50].

2.5.5 Carotenoids and Chlorophylls

Carotenoids and chlorophylls are key bioactive pigments in *Helianthus tuberosus*, playing essential roles in the plant's functional properties and antioxidant potential. Studies indicate that both aerial tissues and tubers contain a range of carotenoids, including α-carotene, β-carotene, γ-carotene, lutein, lycopene, and zeaxanthin, which contribute to photoprotection and free radical scavenging activity. These pigments are present alongside chlorophyll species in green tissues, emphasizing their significance in photosynthesis and mitigation of oxidative stress. The distribution and relative abundance of these pigments have been shown to vary according to plant organ and developmental stage, reflecting dynamic regulation of pigment biosynthesis in *H. tuberosus*. Furthermore, biochemical profiling of leaf protein concentrates confirms that aerial tissues are particularly rich in phytochemicals, highlighting the nutritional and functional value of these pigments for potential applications in functional foods and nutraceuticals [2, 47].

2.5.6 Minerals and Vitamins

The nutritional composition of *Helianthus tuberosus* has been widely investigated, establishing its importance as a functional food with significant health benefits.

Previous studies have demonstrated that artichoke is a rich source of essential minerals, particularly potassium, along with appreciable amounts of calcium, magnesium, and iron, all of which contribute to its physiological and dietary value. In addition to its mineral richness, the plant is notably abundant in inulin, a storage polysaccharide recognized for its well-documented prebiotic effects. The presence of these nutrients, together with trace levels of vitamins, highlights the therapeutic and nutritional potential of *H. tuberosus* and supports its utilization in the formulation of health-promoting food products [51]. Further research has explored the biochemical variability of artichoke in response to agronomic practices. Studies assessing the impact of fertilization and irrigation regimes have revealed significant variations in nutrient accumulation, particularly in mineral content such as potassium, indicating that environmental and cultivation factors substantially influence the plant's nutritional profile.

Moreover, the detection of amino acids within plant tissues suggests that artichoke also contributes protein-related nutritional components. Collectively, these findings demonstrate that both inherent plant characteristics and external agronomic conditions play a critical role in shaping the compositional and nutritional attributes of artichoke [52]. Numerous bioactive compounds derived from *H. tuberosus* have been investigated in various experimental models and reported to possess diverse pharmacological properties [10]. A summary of representative compounds, their plant source, experimental models, and associated pharmacological activities is presented in Table 2.3.

2.6 Inulin and Fructan

The inulin content in artichoke typically ranges from 15–20%, depending on cultivar and processing conditions. Partial hydrolysis of inulin produces fructooligosaccharides (FOS), which improve the textural properties, water-binding capacity, and stability of food products, making artichoke inulin valuable for bakery, dairy, and gluten-free formulations [53]. The biosynthesis of inulin in *H. tuberosus* is regulated by enzymes involved in fructan formation and chain elongation.

TABLE 2.3: Representative bioactive compounds identified in *H. tuberosus* and their reported pharmacological activities [10].

Bioactive Compound	**Plant Part**	**Experimental Model**	**Reported Pharmacological Activity**
Chlorogenic acid	Tuber	*In vitro* (Inflammatory cell models)	Antioxidant and anti-inflammatory
Ferulic acid	Tuber	*In vitro* (Cancer and metabolic cell models)	Antioxidant and antidiabetic
Kaempferol-3-*O*-glucoside	Leaves	*In vitro* (Microbial and oxidative stress assays)	Antioxidant and antimicrobial
Butein	Leaves	*In vitro* (Cancer cell lines)	Anticancer through apoptosis induction
Heliangin	Aerial parts	*In vitro* (RAW 264.7 macrophages)	Anti-inflammatory activity
Kaurenoic acid	Flowers	*In vitro* (Bacterial and immune cell models)	Antibacterial and anti-inflammatory
Vanillin	Whole plant	*In vitro* (Cell-based assays)	Antidiabetic and anti-inflammatory
Ethyl acetate fraction	Tuber	*In vitro* (HepG2 and NIH 3T3 cells)	Enhanced glucose metabolism and wound healing
Phenolic-rich	Tuber and leaves	*In vitro* (HaCaT and BJ fibroblasts)	Antioxidant activity with minimal cytotoxicity
Inulin-rich	Tuber	Human (Older adults)	Improved postprandial glucose regulation and gut microbiota
4,15-Isoatriplicolide	Whole plant	*In vitro* (Cancer cell lines)	Anticancer activity

Its β-(2→1) glycosidic linkages and degree of polymerization determine its physicochemical and biological properties, supporting its applications as a soluble dietary fiber in nutraceutical and functional food products [54].

As a non-digestible carbohydrate, inulin resists digestion in the upper gastrointestinal tract and is fermented by beneficial gut microbiota selectively, including *Bifidobacterium* and *Lactobacillus* species.

This fermentation promotes gut health, improves mineral bioavailability, regulates glycemic and lipid metabolism, and reduces inflammatory responses, highlighting its potential in managing metabolic and gastrointestinal disorders [55]. Endophytic microorganisms also influence inulin metabolism by participating in fructan

synthesis and hydrolysis, thereby affecting inulin accumulation and fructooligosaccharide production.

These interactions offer opportunities to improve inulin yield and functionality through targeted agronomic and microbial management strategies [56].

2.7 Breast Cancer

Breast cancer develops due to the uncontrolled growth of epithelial cells in breast tissue, most commonly originating from the ducts or lobules.

It spread to nearby tissues and distant organs such as the bone, liver, and lungs. Globally, breast cancer is the most commonly diagnosed cancer in women and remains a major health concern.

Around 2.3 million new cases occur each year worldwide. Although advances in diagnosis and treatment have improved patient outcomes, the disease burden is still higher in low- and middle-income countries, mainly due to late diagnosis and limited access to healthcare facilities [57].

Breast cancer is now understood as a complex disease caused by the interaction of genetic, hormonal, and environmental factors. Its development involves different molecular changes, including mutations in oncogenes, loss of tumor suppressor gene function, and abnormal activation of signaling pathways that control cell growth and survival.

The increasing number of cases worldwide is also linked to lifestyle changes, reproductive factors, and an aging population. Despite improvements in early detection and targeted therapies, differences in survival rates still exist between developed and developing countries, showing the need for better screening methods and more effective treatment strategies [58].

2.8 Types of Breast Cancer

2.8.1 Ductal Carcinoma

Ductal carcinoma is the most common histological type of breast cancer, originating from the epithelial lining of the breast ducts. It includes both ductal carcinoma *in situ* (DCIS), which remains confined within the ductal system, and invasive ductal carcinoma (IDC), which has the ability to breach the basement membrane and invade surrounding breast tissue.

DCIS is considered a non-invasive precursor lesion with the potential to progress into invasive disease if left untreated. Histologically, ductal carcinoma is characterized by abnormal cellular proliferation, varying nuclear grades, and the presence of microcalcifications in many cases. Its progression from *in situ* to invasive form involves disruption of normal epithelial architecture and accumulation of genetic and molecular alterations that enhance tumor aggressiveness [59].

2.8.2 Lobular Carcinoma

Lobular carcinoma is the second most common type of breast cancer and arises from the milk-producing lobules of the breast. The invasive form, invasive lobular carcinoma (ILC), is characterized by a distinct single-file pattern of tumor cell infiltration due to loss of cell adhesion, most commonly associated with inactivation of the CDH1 gene encoding E-cadherin.

This loss of cellular cohesion contributes to its diffuse growth pattern, making it more difficult to detect clinically and radiologically compared to ductal carcinoma. ILC is frequently hormone receptor-positive and often lacks HER2 overexpression, typically aligning with luminal molecular subtypes. Although it tends to grow more slowly than ductal carcinoma, it is often diagnosed at a more advanced stage due to its subtle clinical presentation and infiltrative nature [60].

2.8.3 Molecular Subtypes of Breast Cancer

Breast cancer is also classified into molecular subtypes based on the expression of estrogen receptor (ER), progesterone receptor (PR), and human epidermal growth factor receptor 2 (HER2). This classification includes Luminal A, Luminal B, HER2-enriched, and triple-negative breast cancer (TNBC), each exhibiting distinct biological behavior and clinical outcomes.

Luminal A tumors are typically ER-positive, PR-positive, and HER2-negative, with low proliferation rates and favorable prognosis. Luminal B tumors show higher proliferation rates, expressing HER2 which has outcome in a more aggressive course.

HER2-enriched tumors are characterized by overexpression of HER2 and are associated with rapid tumor growth but respond well to targeted therapies. TNBC lacks expression of ER, PR, and HER2 and is considered the most aggressive subtype with limited targeted treatment options [61].

A comparison of the molecular characteristics and corresponding therapeutic approaches of the major breast cancer subtypes is presented in Table 2.4.

TABLE 2.4: Molecular characteristics and therapeutic approaches of the subtypes of breast cancer [19].

Characteristic	**Luminal A**	**Luminal B**	**HER2-enriched**	**Triple-negative**
ERα Status	+ve	+ve	-ve	-ve
PR Status	+ve	+ve/Low	-ve	-ve
HER2 Status	-ve	+ve/-ve	+ve	-ve
Ki-67 Expression	Low	High	High	High
Prognosis	Good	Intermediate	Intermediate	Poor
Primary Treatment	Endocrine therapy	Endocrine therapy ± chemotherapy	Anti-HER2 targeted therapy	Chemo–therapy

2.9 Mechanism

Breast cancer develops through complex molecular and cellular alterations that disrupt the normal regulation of cell growth and differentiation, leading to malignant transformation. One of the major mechanisms involves hormone receptor signaling. In hormone receptor-positive breast cancer, estrogen binds to the estrogen receptor (ER) and regulates genes associated with cell proliferation and survival, while progesterone receptor (PR) expression serves as a marker of active estrogen signaling. Dysregulation of this pathway promotes sustained proliferative signaling and tumor progression [62].

Another key mechanism involves the overexpression of human epidermal growth factor receptor 2 (HER2), which activates downstream signaling pathways that enhance cell proliferation, survival, and therapeutic resistance, resulting in a more aggressive tumor phenotype [63, 64]. Cell cycle dysregulation also plays a critical role in breast cancer progression. Aberrant activation of the Cyclin D1–CDK4/6 complex promotes uncontrolled cell proliferation, while resistance to CDK4/6 inhibitors may arise through retinoblastoma (RB) loss or activation of compensatory signaling pathways [65].

Epithelial–mesenchymal transition (EMT) is another important process that enhances tumor cell migration, invasion, and metastasis through the loss of epithelial characteristics and acquisition of mesenchymal traits. The molecular mechanism of EMT regulation by non-coding RNAs and nanocarriers is illustrated in Figure 2.2. Metastatic spread to distant organs, including the bone, lung, liver, and brain, is the primary cause of poor clinical outcomes in breast cancer [63, 64]. Drug resistance remains a major challenge in breast cancer treatment. It develops through activation of alternative signaling pathways, genetic and epigenetic alterations, and suppression of apoptosis, reducing the effectiveness of endocrine therapy, chemotherapy, and targeted treatments and contributing to disease recurrence [62].

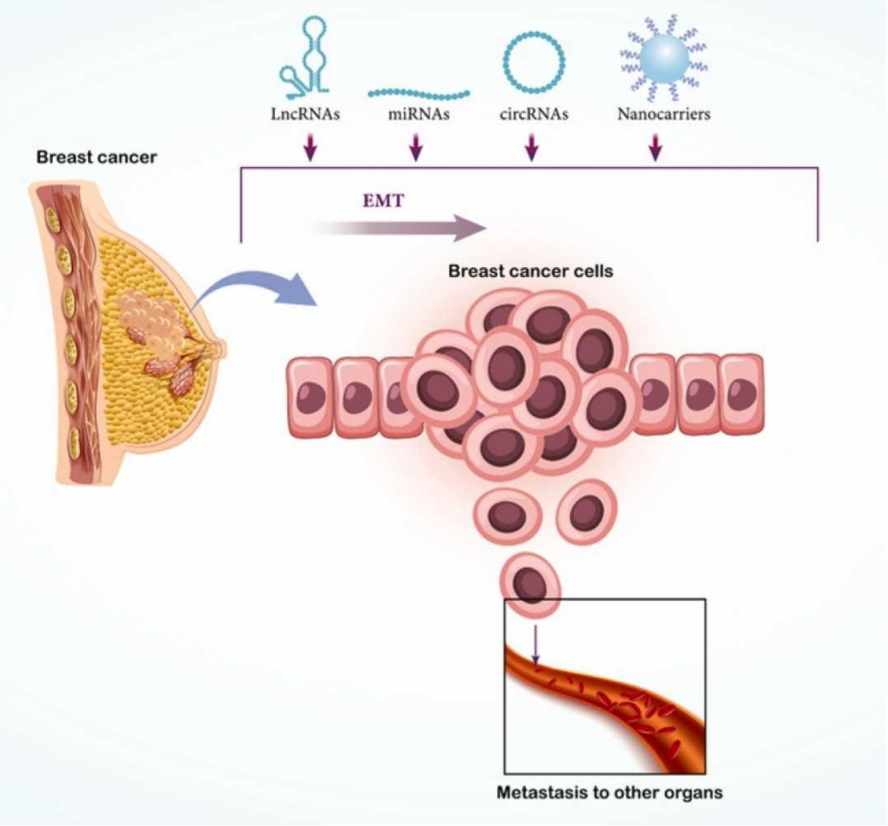

FIGURE 2.2: Regulation of Epithelial-Mesenchymal Transition (EMT) by non-coding RNAs and nanocarriers, leading to the metastasis of breast cancer cells into the circulatory system [63].

2.10 Pathways

The PI3K/AKT/mTOR signaling pathway is a central regulatory cascade involved in breast cancer progression and is frequently altered in malignant cells. Activation of this pathway occurs through receptor tyrosine kinases, leading to PI3K activation, AKT phosphorylation, and subsequent mTOR signaling, which regulates protein synthesis, metabolism, proliferation, and survival.

Dysregulation of this pathway promotes tumor growth and contributes to resistance against targeted therapies [66]. In addition to its role in development of breast cancer, the PI3K/AKT/mTOR pathway is an important therapeutic target. Plant-derived bioactive compounds have been shown to suppress this signaling cascade and reactivate apoptotic pathways, highlighting their potential as adjunct

therapeutic agents for breast cancer treatment [67]. Several receptor proteins, including Androgen Receptor (AR), Estrogen Receptor Alpha (ERα), and Human Epidermal Growth Factor Receptor 2 (HER2), play pivotal roles in regulating hormone signaling, cellular proliferation, and tumor survival, making them important molecular targets for breast cancer therapy [19, 20]. The major signaling events associated with estrogen receptor-mediated activation of the PI3K/AKT and MAPK pathways are illustrated in Figure 2.3.

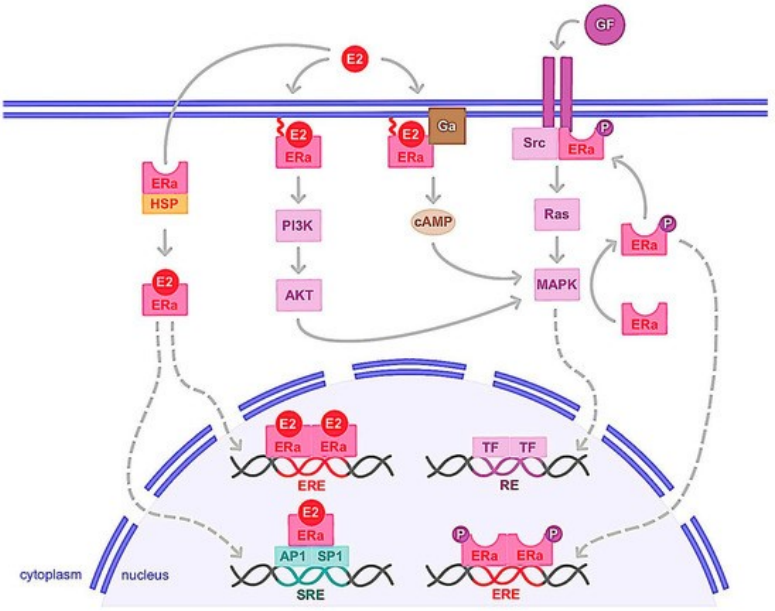

FIGURE 2.3: Overview of estrogen receptor signaling mechanisms involved in breast cancer [19].

Human Epidermal Growth Factor Receptor 2 (HER2), encoded by the *ERBB2* gene on chromosome 17q21, is a transmembrane receptor tyrosine kinase that regulates cell proliferation and survival. HER2 activation stimulates the PI3K/AKT and MAPK signaling mechanisms, promoting tumor growth and progression. Consequently, HER2 overexpression or amplification is associated with aggressive breast cancer, making HER2 an important therapeutic target [68].

DNA repair pathways are essential for maintaining genomic stability in breast cancer cells. The tumor suppressor genes *BRCA1* and *BRCA2* are key components of the homologous recombination pathway responsible for repairing DNA double-strand breaks. Germline mutations in these genes impair DNA repair, resulting in genomic instability and an increased risk of hereditary breast and ovarian cancers.

These defects also increase the sensitivity of BRCA-mutated tumors to poly (ADP-ribose) polymerase (PARP) inhibitors through synthetic lethality, making PARP inhibition an important strategy in personalized breast cancer treatment [69, 70].

2.11 Treatment

The treatment of breast cancer has advanced considerably with the emergence of precision medicine, which tailors therapeutic strategies according to the molecular and genetic profile of individual tumors. This approach utilizes biomarkers, including hormone receptor status and HER2 expression, to guide treatment selection, improve therapeutic efficacy, and reduce unnecessary toxicity, thereby enabling personalized disease management [71]. Conventional treatment modalities, including chemotherapy, hormonal therapy, and targeted therapy, remain central to breast cancer management and are increasingly combined to improve clinical outcomes.

Chemotherapeutic agents disrupt DNA synthesis and cell division, whereas hormonal therapies inhibit estrogen-mediated signaling in hormone receptor-positive tumors. Targeted therapies, particularly those directed against HER2, selectively inhibit oncogenic signaling pathways. Combination therapies further improve treatment response and help overcome therapeutic resistance by targeting multiple molecular pathways simultaneously [72]. The major conventional and combination treatment strategies for breast cancer based on tumor type and disease stage are illustrated in Figure 2.4.

Recent advances have also focused on phytochemical-based nanocarrier systems for breast cancer therapy. These systems encapsulate plant-derived bioactive compounds to improve targeted drug delivery, bioavailability, and stability while reducing systemic toxicity. By overcoming limitations such as poor solubility and rapid degradation of phytochemicals, nanocarrier-based delivery represents a promising strategy for improving anticancer efficacy [73].

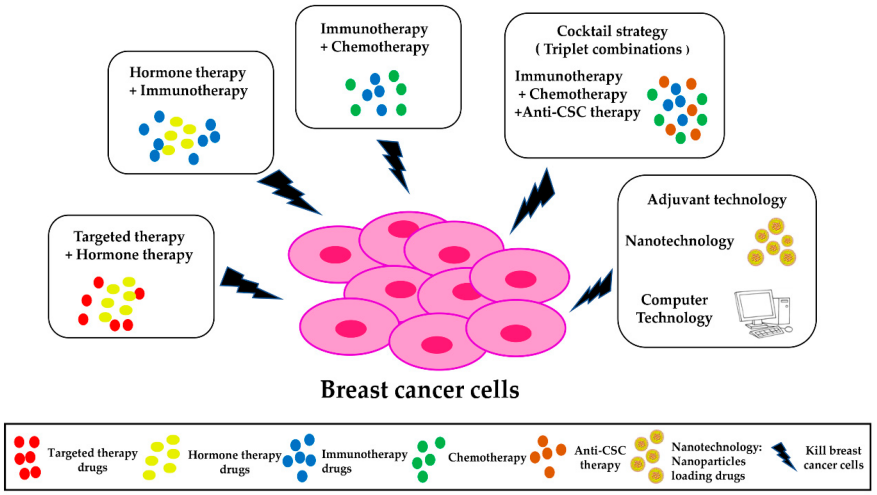

FIGURE 2.4: Illustrates the major conventional and combination treatment strategies for breast cancer based on tumor type and stage [72].

2.12 Phytochemicals and Breast Cancer

Phytochemicals are plant-derived bioactive compounds that play important roles in the prevention and treatment of breast cancer. They exert chemopreventive effects by suppressing cell proliferation, inducing apoptosis, regulating oxidative stress, and exhibiting antioxidant and anti-inflammatory activities [74]. In addition, phytochemicals regulate cell cycle progression, inhibit metastasis, modulate intracellular signaling pathways, and may enhance the efficacy of conventional therapies while helping to overcome drug resistance [75].

Among these compounds, inulin-type fructans exert indirect anticancer effects by modulating the gut microbiota and influencing host metabolic and immune responses. Moreover, the combined administration of inulin and sulforaphane has been shown to suppress estrogen receptor-negative breast cancer through inhibition of the PI3K/AKT/mTOR signaling pathway [76, 77].

Flavonoids also exhibit potent anticancer activity by modulating the mTOR signaling pathway, promoting apoptosis, and suppressing abnormal cell proliferation [78]. Similarly, *Helianthus tuberosus* extracts have demonstrated selective cytotoxicity against MCF-7 breast cancer cells by reducing cell viability, inducing

apoptosis, and inhibiting metastatic behavior, highlighting their potential as a natural source of anticancer agents [79].

2.13 Other Plants in Breast Cancer Progression

Medicinal plant-derived nutraceuticals are increasingly recognized as complementary agents in breast cancer management because of their diverse biological activities.

These bioactive compounds exhibit anticancer effects by regulating signaling pathways, suppressing abnormal cell proliferation, and inducing programmed cell death. Their ability to target multiple molecular mechanisms simultaneously proves as supportive therapeutic agents for treating breast cancer [80].

2.13.1 *Curcuma longa* in Breast Cancer

Curcuma longa has been widely investigated for its anticancer potential against breast cancer, particularly triple-negative breast cancer. Experimental studies have shown that its extract modulates key regulators of apoptosis, including p53 and survivin, leading to activation of caspase-3-dependent pathways, enhanced programmed cell death, and reduced cancer cell viability [81].

In combination with *Phyllanthus niruri*, *Curcuma longa* exhibits enhanced antiproliferative activity against MDA-MB-231 breast cancer cells, suggesting that plant-based combination therapies may improve treatment efficacy [82].

In addition, *Curcuma longa* possesses anti-metastatic properties by downregulating metastasis-related proteins, including MMP-9 and Rac-1, thereby reducing the migration and invasive potential of highly metastatic breast cancer cells [83].

2.13.2 *Camellia sinensis* in Breast Cancer

Camellia sinensis (green tea) has been extensively investigated for its anticancer activity against breast cancer. Its extracts exhibit cytotoxic and antiproliferative effects by reducing the viability of breast cancer cells [84].

Recent studies have further enhanced its therapeutic potential through the biosynthesis of silver nanoparticles using *Camellia sinensis* (CsAgNPs). These nanoparticles induce oxidative stress, disrupt cellular homeostasis, activate apoptotic pathways, and inhibit breast cancer cell proliferation, highlighting their potential as plant-based nanotherapeutic agents [85].

In addition, *Camellia sinensis* has been reported to inhibit the STAT signaling pathway, thereby suppressing oncogenic signaling, cell proliferation, and tumor progression, supporting its potential in breast cancer prevention and targeted therapy [86].

2.13.3 *Vitis vinifera* in Breast Cancer

The antioxidant and anticancer potential of *Vitis* species has been widely investigated in breast cancer. An optimized extract of *Vitis labrusca* (Isabella grape) demonstrated significant antioxidant activity and cytotoxic effects against breast cancer cells, suggesting that grape-derived phytoconstituents reduce tumor cell viability through oxidative stress modulation [87].

Network pharmacology studies have shown that *Vitis vinifera* phytochemicals interact with multiple molecular targets involved in cell proliferation, survival, and apoptosis, highlighting their potential as multi-target therapeutic agents [88].

Molecular docking and network-based analyses further demonstrated their ability to modulate key proteins associated with breast cancer signaling pathways, supporting their role in inhibiting oncogenic signaling [89].

In addition, exosome-like nanoparticles derived from *Vitis vinifera* (Kyoho grapes) have shown promise as drug delivery systems by improving targeted delivery, bioavailability, and therapeutic efficacy in breast cancer treatment [90].

2.13.4 *Nigella sativa* in Breast Cancer

Nigella sativa has been investigated for its anticancer potential in breast cancer through computational and experimental studies. Bioactive compounds derived from *Nigella sativa* target neuropilins, key regulators of tumor growth and angiogenesis, suggesting their potential to inhibit breast cancer progression [91]. Network pharmacology and experimental studies further demonstrated that *Nigella sativa* bioactive compounds interact with multiple signaling pathways involved in tumor cell proliferation, survival, and apoptosis, highlighting their multi-target mechanism of action [92]. In addition, *Nigella sativa* seed oil has shown synergistic anticancer effects when combined with conventional cytotoxic agents, enhancing therapeutic efficacy and supporting its potential as an adjuvant in breast cancer chemotherapy [93].

2.13.5 *Zingiber officinale* in Breast Cancer

Zingiber officinale (ginger) has been extensively investigated for its anticancer activity against breast cancer. Its bioactive constituents inhibit breast cancer development by suppressing malignant cell proliferation and survival, supporting its potential as a natural therapeutic agent [94]. In combination with *Terminalia chebula*, *Zingiber officinale* has demonstrated enhanced anticancer activity in DMBA-induced breast cancer models through inhibition of the mTOR signaling pathway, highlighting its role in regulating tumor growth and survival [95]. Recent studies have also explored ginger-mediated green-synthesized zinc oxide (ZnO) nanoparticles, which exhibit enhanced cytotoxicity and tumor-targeting potential in three-dimensional breast cancer models, demonstrating their promise as nanotherapeutic agents [96].

2.14 Molecular Docking

Molecular docking is a computational, structure-based approach used to investigate the interactions between small molecules and biological macromolecules, particularly proteins. In drug discovery, it is widely applied to predict the most favorable binding pose of a ligand within the active site of a target protein and to estimate the strength of the interaction. This technique relies on molecular recognition, where the structural and physicochemical compatibility between a ligand and its receptor determines the stability of the protein–ligand complex, making molecular docking a fundamental tool for virtual screening and structure-based drug design [97].

Depending on the degree of ligand and receptor flexibility, docking approaches are classified as rigid, semi-flexible, or flexible. Among these, flexible docking is considered more biologically relevant because it accounts for conformational changes during ligand binding, thereby improving the physiological accuracy of predicted interactions. Docking algorithms use scoring functions to assess protein–ligand interactions, including hydrogen bonding, hydrophobic contacts, van der Waals forces, and electrostatic interactions, in order to predict binding affinity and the stability of the resulting complex [97].

To supplement the static predictions obtained from molecular docking, molecular dynamics (MD) simulations are widely used to examine the dynamic behavior and stability of protein–ligand complexes under physiological conditions. Whereas molecular docking identifies the most favorable binding orientation, MD simulations provide additional insights into conformational flexibility, interaction persistence, and structural stability over time, thereby improving the biological relevance and predictive reliability of computational drug discovery studies [98].

In addition, molecular docking serves as an essential tool for virtual screening and lead identification by rapidly assessing large chemical libraries against disease-related molecular targets. This strategy accelerates the discovery of promising lead compounds while reducing the time, cost, and experimental resources required for conventional drug development, and also supports the identification of

molecules with potential multi-target activity. Recent advances in computational pharmacology and structure-based drug design have further enhanced docking accuracy and expanded its applications in the discovery of novel therapeutic agents, particularly for complex diseases such as cancer [99].

Beyond its computational applications, molecular docking is regarded as both an analytical and interpretative approach, integrating concepts from structural biology, physical chemistry, and computational modeling. Therefore, reliable docking outcomes depend not only on computational algorithms but also on the critical interpretation of binding poses, scoring functions, and docking parameters [100].

2.15 Molecular Docking Studies in Breast Cancer

Molecular docking has become an important computational approach in breast cancer drug discovery for identifying and evaluating bioactive compounds targeting cancer-associated proteins. In early-stage drug design, docking is often combined with quantitative structure activity relationship (QSAR) analysis to assess the binding potential of synthetic compounds. For example, pyrimidine–coumarin–triazole conjugates have demonstrated favorable interactions with breast cancer-related targets, highlighting the value of *in silico* screening in the rational design of anticancer agents [101]. Natural product-derived hybrid molecules have also been extensively investigated using molecular docking. Curcumin-derived hybrid conjugates exhibited strong binding affinity toward breast cancer-associated proteins, suggesting that structural modification of natural compounds can enhance their therapeutic potential [102].

Molecular dynamics (MD) simulation is frequently combined with molecular docking to validate docking results and evaluate the stability of ligand–protein complexes under physiological conditions. Studies involving natural compounds targeting overexpressed breast cancer receptors have demonstrated stable docked complexes, improving the reliability of computational predictions [103].

The integration of molecular docking with experimental validation has further strengthened confidence in *in silico* findings. Flavonoids such as naringin have shown strong binding affinity toward breast cancer-related targets, supported by experimental evidence of anticancer activity [104]. In addition, network toxicology combined with molecular docking has been used to investigate the interactions of environmental chemicals with breast cancer-related targets, expanding the application of docking to disease mechanism studies and environmental risk assessment [105].

Chapter 3

Methodology

Figure 3.1 illustrates the overall workflow followed in this study to evaluate the anticancer potential of bioactive compounds isolated from *Helianthus tuberosus* using *in silico* approaches.

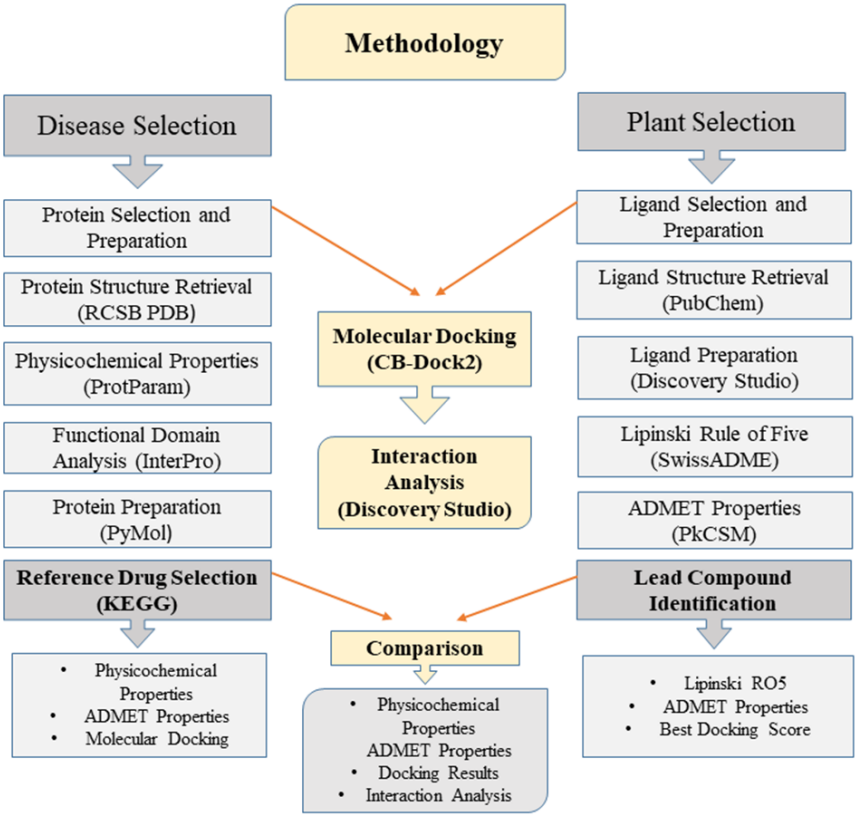

FIGURE 3.1: Methodological workflow for the *in silico* evaluation of bioactive compounds from *Helianthus tuberosus* against breast cancer-associated target proteins.

3.1 Disease Selection

Breast cancer was selected as the target disease in the present study because it remains one of the most significant health challenges affecting women worldwide. It is the most frequently diagnosed malignancy among women and continues to be a major contributor to cancer-related mortality. The disease is characterized by uncontrolled proliferation of abnormal cells within breast tissue, with the potential to invade surrounding tissues and metastasize to distant organs. Its development is multifactorial, involving genetic susceptibility, hormonal imbalance, environmental factors, and lifestyle-related influences [106].

Among the different types, hormone-dependent breast cancer is mainly regulated by estrogen-driven signaling pathways that significantly contribute to tumor development. The binding of estrogen to its receptors initiates signaling events that regulate genes controlling cellular proliferation, division, and survival. Although various treatments such as hormone therapy, chemotherapy, and targeted therapies are available, their success is often limited due to resistance, side effects, and recurrence [107]. Therefore, breast cancer was selected in this study to investigate alternative therapeutic options, particularly natural plant-based compounds, which may provide safer and more effective approaches for inhibiting cancer progression.

3.2 Protein Selection and Preparation

The preparation and characterization of the selected target proteins for molecular docking are presented in this section.

3.2.1 Selection of Target Proteins

Target proteins associated with breast cancer progression were selected for molecular docking based on their documented biological significance. AR, ERα, and

HER2 were selected for this study because of their critical involvement in the molecular mechanisms underlying breast cancer.

Their regulatory roles in hormone signaling, cellular proliferation, and tumor survival have established them as important therapeutic targets for breast cancer drug discovery [108, 109].

3.2.2 Retrieval of Protein Structures

The required 3D structures of the selected breast cancer target proteins were retrieved from the RCSB Protein Data Bank (RCSB PDB) (https://www.rcsb.org/) and saved in PDB format for subsequent analyses.

3.2.3 Physicochemical Characterization of Target Proteins

The ProtParam tool available on the ExPASy server was used to characterize the physicochemical properties (https://web.expasy.org/protparam/) of the selected proteins. Their FASTA sequences were retrieved from the Protein Data Bank and analyzed using ProtParam. The calculated parameters included mw, pI, instability index, aliphatic index, and grand average of hydropathicity (GRAVY), which provided information on the physicochemical characteristics and predicted stability of the target proteins [110].

3.2.4 Functional Domain Characterization

The InterPro database (https://www.ebi.ac.uk/interpro/) was used to identify the conserved functional domains present in the selected proteins. Protein sequences were analyzed to identify conserved domains, families, and functional regions. Pfam annotations integrated within InterPro were used to determine biologically important domains associated with ligand binding and protein activity.

3.2.5 Protein Preparation

The retrieved protein structures were prepared using PyMOL (https://pymol.org/). Before molecular docking, the retrieved protein structures were cleaned by eliminating water molecules, heteroatoms, and co-crystallized ligands that could interfere with ligand binding. Hydrogen atoms were then added to obtain stable protein structures, and the prepared files were stored in PDB format for subsequent computational analyses.

3.3 Selection of Target Plant

Jerusalem artichoke (*Helianthus tuberosus*) was selected because of its reported medicinal value and diverse phytochemical composition. Evidence from previous studies indicates that *Helianthus tuberosus* contains a variety of bioactive compounds with antioxidant, anti-inflammatory, and anticancer activities. Owing to these pharmacological properties, it was considered a suitable source for identifying potential therapeutic compounds against breast cancer [2, 4].

3.4 Ligand Identification and Preparation

The selection and preparation of phytochemical ligands obtained from *Helianthus tuberosus* are described in this section, including the steps followed before computational evaluation.

3.4.1 Selection of Ligands

The phytochemical ligands were selected from *Helianthus tuberosus* using the PubChem Taxonomy database. Within the Chemicals and Bioactivities section, the Food Compounds category was examined, and only compounds reported to be

present in the tubers with available chemical structures suitable for computational analysis were included. Accordingly, ten phytochemicals were selected for further investigation: Hexose, Betaine, β-D-Glucose, Inulin, L-Tryptophan, PNPP disodium hexahydrate, L-Isoleucine, L-Glutamic acid, L-Lysine, and L-Aspartic acid [22].

3.4.2 Retrieval of Ligand Structures

The three-dimensional chemical structures of the selected phytochemical compounds were obtained from the PubChem database in Structure Data File (SDF) format (https://pubchem.ncbi.nlm.nih.gov/). PubChem is a publicly accessible chemical repository that offers comprehensive information on molecular structures, chemical properties, and related physicochemical characteristics, making it a reliable source for computational studies.

3.4.3 Ligand Refinement

The retrieved ligand structures were energy-minimized using BIOVIA Discovery Studio Visualizer:
(https://discover.3ds.com/discovery-studio-visualizer-download) to improve their structural stability before molecular docking. Energy minimization was performed to eliminate unfavorable molecular conformations and reduce steric strain, resulting in geometrically optimized structures. The optimized ligands were then exported in the required file formats for subsequent docking and computational analyses.

3.5 Virtual Screening

A virtual screening approach was performed before molecular docking to examine the drug-like properties and pharmacokinetic behavior of the selected phytochemicals.

3.5.1 Lipinski's Rule of Five

The drug-likeness of the selected phytochemicals was evaluated using the SwissADME web server (https://www.swissadme.ch/) according to Lipinski's RO5. Parameters including mol-weight, LogP, HBD, HBA, and rotatable-bonds were analyzed to assess the compounds' suitability as potential oral drug candidates [111].

i. Mol. Weight $\leq$ 500 Da

ii. HB donors (HBD) $\leq$ 5

iii. HB Acceptors (HBA) $\leq$ 10

iv. (LogP) $\leq$ 5

v. No. of RB $<$ 10

Compounds satisfying these criteria are regarded as promising candidates for further drug development studies.

3.5.2 ADMET Property Prediction

The pharmacokinetic and toxicity profiles of the selected phytochemicals were predicted using the pkCSM web server (https://biosig.lab.uq.edu.au/pkcsm/). Parameters related to absorption, distribution, metabolism, excretion, and toxicity (ADMET) were evaluated to assess the compounds' drug-like behavior and safety for subsequent analyses [112].

3.6 Molecular Docking

Molecular docking was conducted using the CB-Dock2 server (https://cadd.labshare.cn/cb-dock2/) to evaluate the binding interactions between the selected phytochemicals and the target proteins. The prepared protein and ligand structures

were submitted to the server, which automatically detected binding cavities and predicted ligand binding poses.

The resulting complexes were ranked according to their binding affinity, and the top-scoring docked conformations were selected for subsequent analysis [113].

3.7 Protein–Ligand Interaction Analysis

The protein–ligand interactions of the docked complexes were examined using BIOVIA Discovery Studio Visualizer. Binding interactions, including H-bonds, hydrophobic- contacts, electrostatic-interactions, salt-bridges, and pi-mediated interactions, were analyzed to evaluate the binding mode and stability of the complexes.

3.8 Lead Compound Identification

Lead compound identification was carried out by considering the collective results of drug-likeness screening, ADMET analysis, molecular docking, and interaction studies. Compounds exhibiting favorable physicochemical and pharmacokinetic properties, minimal predicted toxicity, high binding affinity, and stable protein–ligand interactions were regarded as potential lead compounds for further investigation.

3.9 Drug Selection and Screening

This section presents the process of identifying, selecting, and evaluating a reference drug for comparison with the selected lead compound.

3.9.1 Identification of Reference Drug

The Kyoto Encyclopedia of Genes and Genomes (KEGG) database was utilized to select an appropriate reference drug for this study. Approved breast cancer therapeutics and their associated hormone signaling pathways were identified from the database to support comparative evaluation.

3.9.2 Drug Selection

The identified drugs were screened based on their mechanism of action, physicochemical properties, pharmacokinetic profiles, and therapeutic significance. Information related to physicochemical characteristics and mechanisms of action was retrieved from the PubChem and KEGG databases, respectively, whereas ADMET properties were evaluated using the pkCSM web server.

3.9.3 Reference Drug Docking

The reference drug was docked with the target proteins using the CB-Dock2 server under the same conditions applied to the phytochemicals. The resulting binding affinities and protein–ligand interaction patterns were evaluated and compared to determine the relative binding performance of the selected compounds.

3.10 Comparative Analysis of the Lead Compound and the Reference Drug

The lead phytochemical and the reference drug were comparatively evaluated based on their physicochemical properties, drug-likeness, ADMET profiles, molecular docking performance, and protein–ligand interaction patterns. This analysis was carried out to determine the therapeutic potential of the lead phytochemical relative to the reference drug.

Chapter 4

Results

4.1 Selection, Retrieval, and Preparation of Target Proteins

The results associated with the selection, extraction, and preparation of selected breast cancer target proteins are described in this section. Selected proteins were processed and prepared for further computational studies such as molecular docking and interactions analysis.

4.1.1 Three-Dimensional Structure of Proteins

Three-dimensional (3D) protein structures provide essential insights into the biological functions and molecular mechanisms of proteins. The spatial conformation of a protein is determined by its amino acid sequence and stabilized through hydrogen bonding, electrostatic interactions, hydrophobic effects, and van der Waals forces.

Protein organization comprises four structural levels: primary, secondary, tertiary, and quaternary, with the tertiary structure representing the overall three-dimensional folding of a polypeptide chain. Knowledge of protein structures is fundamental to bioinformatics, structural biology, and drug discovery because it

enables the identification of functional domains, active sites, and protein–ligand binding regions.

Protein structures are determined experimentally using X-ray crystallography, nuclear magnetic resonance (NMR) spectroscopy, and cryo-electron microscopy (cryo-EM), whereas computational prediction methods provide reliable alternatives when experimental structures are unavailable [114].

The three-dimensional structures of the selected breast cancer-associated target proteins, namely the androgen receptor (AR), estrogen receptor alpha (ERα), and human epidermal growth factor receptor 2(HER2), corresponding to PDB IDs 3RLL, 3ERT, and 8U8X, respectively, were retrieved from the RCSB Protein Data Bank (PDB) in PDB format for subsequent protein preparation, molecular docking, and protein–ligand interaction analyses. The three-dimensional structures of AR, ERα, and HER2 are shown in Figures 4.1, 4.2, and 4.3, respectively.

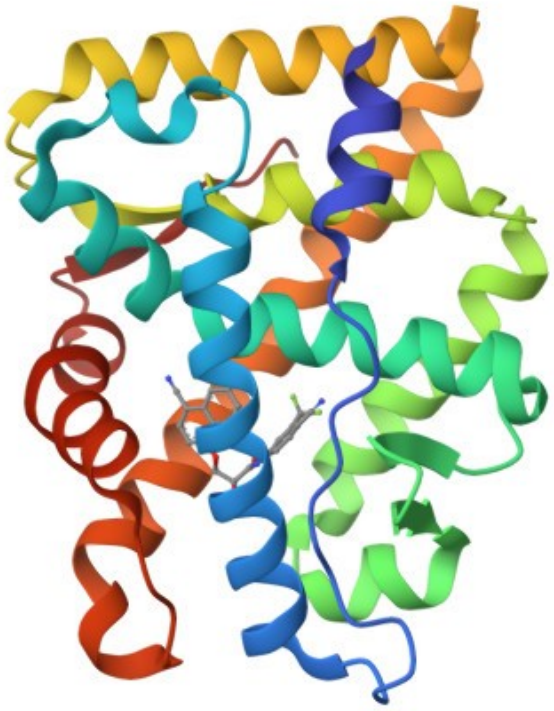

FIGURE 4.1: 3D Structure of the Androgen Receptor Protein.

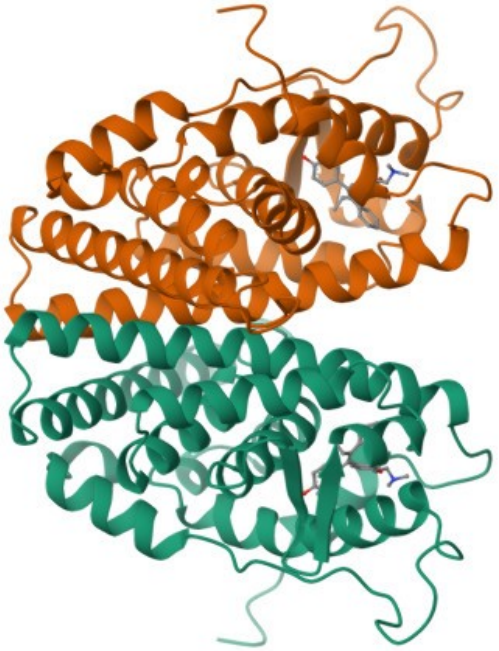

FIGURE 4.2: 3D Structure of the Estrogen receptor Alpha Protein.

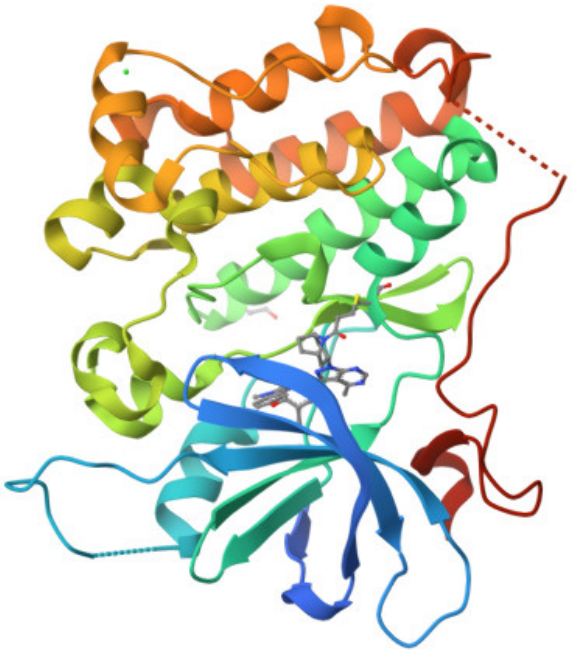

FIGURE 4.3: Three-dimensional structure of the HER2 protein receptor.

4.1.2 Physicochemical Characteristics

The physicochemical characteristics of proteins are fundamental determinants of their structural organization, functional behavior, and potential applications in therapeutic and computational research. These properties influence how proteins fold into their native three-dimensional conformations, maintain structural stability under physiological conditions, and interact with surrounding biomolecules. Key characteristics, including hydrophobicity, charge distribution, hydrogen-bonding capacity, molecular size, and surface properties, collectively govern protein folding, conformational stability, and biological function [115]. Disruptions in these physicochemical interactions may result in protein misfolding, loss of biological activity, or aggregation.

Furthermore, protein solubility is strongly influenced by the balance between hydrophilic and hydrophobic regions as well as the overall electrostatic profile. Reduced solubility can promote protein aggregation, thereby affecting structural stability and biological function. In addition, physicochemical properties influence protein distribution, membrane interactions, formulation stability, purification efficiency, and storage conditions. They may also affect immunogenicity, as unstable conformations or exposed hydrophobic regions can increase immune recognition [115].

Therefore, comprehensive physicochemical characterization is essential for understanding protein behavior and is widely employed in bioinformatics, structural biology, and structure-based drug discovery. Although molecular docking can be performed without prior physicochemical characterization of the receptor proteins, this analysis was included in the present study to obtain a better understanding of their fundamental biochemical properties before docking. Parameters such as mol. weight, theoretical isoelectric point (pI), stability, and hydropathicity provide useful information about the overall characteristics of the selected proteins and help describe their structural and biochemical nature.

While these properties do not directly influence docking scores or binding affinity calculations, they provide supporting information that aids in the characterization

of the receptor proteins and facilitates the interpretation of protein–ligand interaction results. Therefore, physicochemical analysis served as a complementary step to molecular docking rather than a mandatory requirement.

TABLE 4.1: Predicted physicochemical characteristics of the androgen receptor (AR) obtained using the ExPASy ProtParam server.

Sr. No.	**Properties**	**Results**
1	Amino acid residues	247
2	Predicted isoelectric point (pI)	8.97
3	Molecular weight	28750.79 Da
4	Negatively charged residues (Asp + Glu)	23
5	Positively charged residues (Arg + Lys)	28
6	Total atoms	4059
7	Extinction coefficient (cystine bonds assumed)	32680 $M^{-1}cm^{-1}$
8	Extinction coefficient (reduced cysteines)	32430 $M^{-1}cm^{-1}$
9	Predicted half-life	>20h (mammalian), >20h (yeast)
10	Protein instability index	41.83 (Unstable protein)
11	Aliphatic index	95.87
12	GRAVY score	0.017
13	Formula	$C_{1309}H_{2039}N_{347}O_{346}S_{18}$

The physicochemical properties of the selected target proteins were predicted using the ExPASy ProtParam server. The theoretical isoelectric point (pI) values indicated that the androgen receptor (AR) is basic, whereas ERα and HER2 are acidic proteins [116]. Protein stability was evaluated using the instability index,

where values greater than 40 indicate unstable proteins and values below 40 indicate stable proteins

TABLE 4.2: Predicted physicochemical characteristics of the estrogen receptor alpha (ERα) obtained using the ExPASy ProtParam server.

Sr. No.	**Properties**	**Results**
1	Amino acid residues	261
2	Predicted isoelectric point (pI)	6.49
3	Molecular weight	29811.16 Da
4	Negatively charged residues (Asp + Glu)	29
5	Positively charged residues (Arg + Lys)	26
6	Total atoms	4235
7	Extinction coefficient (cystine bonds assumed)	24200 $M^{-1}cm^{-1}$
8	Extinction coefficient (reduced cysteines)	23950 $M^{-1}cm^{-1}$
9	Predicted half-life	30 h (mammalian), >20 h (yeast), >10 h (*E. coli*)
10	Protein instability index	40.41 (Unstable protein)
11	Aliphatic index	111.34
12	GRAVY score	0.067
13	Formula	$C_{1331}H_{2152}N_{358}O_{373}S_{21}$

According to this criterion, all three target proteins were predicted to be unstable. The aliphatic index values suggested relatively high thermostability for all selected proteins. Analysis of the grand average of hydropathicity (GRAVY) indicated that AR and ERα are slightly hydrophobic, whereas HER2 is slightly hydrophilic,

suggesting differences in their surface characteristics and interactions with aqueous environments [117].

Collectively, these physicochemical parameters describe the structural characteristics of the selected proteins and provide a basis for their application in molecular docking and subsequent computational analyses. The physicochemical properties of AR, ERα, and HER2 are listed in Tables 4.1, 4.2, and 4.3, respectively.

TABLE 4.3: Predicted physicochemical characteristics of the HER2 receptor obtained using the ExPASy ProtParam server.

Sr. No.	**Properties**	**Results**
1	Amino acid residues	348
2	Predicted isoelectric point (pI)	5.80
3	Molecular weight	39473.59 Da
4	Negatively charged residues (Asp + Glu)	47
5	Positively charged residues (Arg + Lys)	39
6	Total atoms	5549
7	Extinction coefficient (cystine bonds assumed)	51255 $M^{-1}cm^{-1}$
8	Extinction coefficient (reduced cysteines)	50880 $M^{-1}cm^{-1}$
9	Predicted half-life	30 h (mammalian), >20 h (yeast), >10 h (*E. coli*)
10	Protein instability index	47.70 (Unstable protein)
11	Aliphatic index	93.22
12	GRAVY score	−0.218
13	Formula	$C_{1757}H_{2780}N_{482}O_{509}S_{21}$

4.1.3 Functional Domain Analysis

Proteins consist of one or more functional domains that are responsible for their biological activities and molecular interactions [118]. Although the identification of functional domains is not essential for performing molecular docking, it was included in this study to better understand the biological characteristics of the selected target proteins.

The identification of conserved domains confirms the functional identity of the proteins and supports their selection as biologically relevant receptors for docking analysis. This information also provides a clearer biological context for interpreting the predicted protein–ligand interactions.

Functional domains were identified using the InterPro database based on Pfam annotations. The FASTA sequences of the selected proteins were retrieved from the RCSB Protein Data Bank (PDB) and submitted to InterPro for domain prediction and functional characterization that can be shown in Figures 4.4, 4.6, and 4.7.

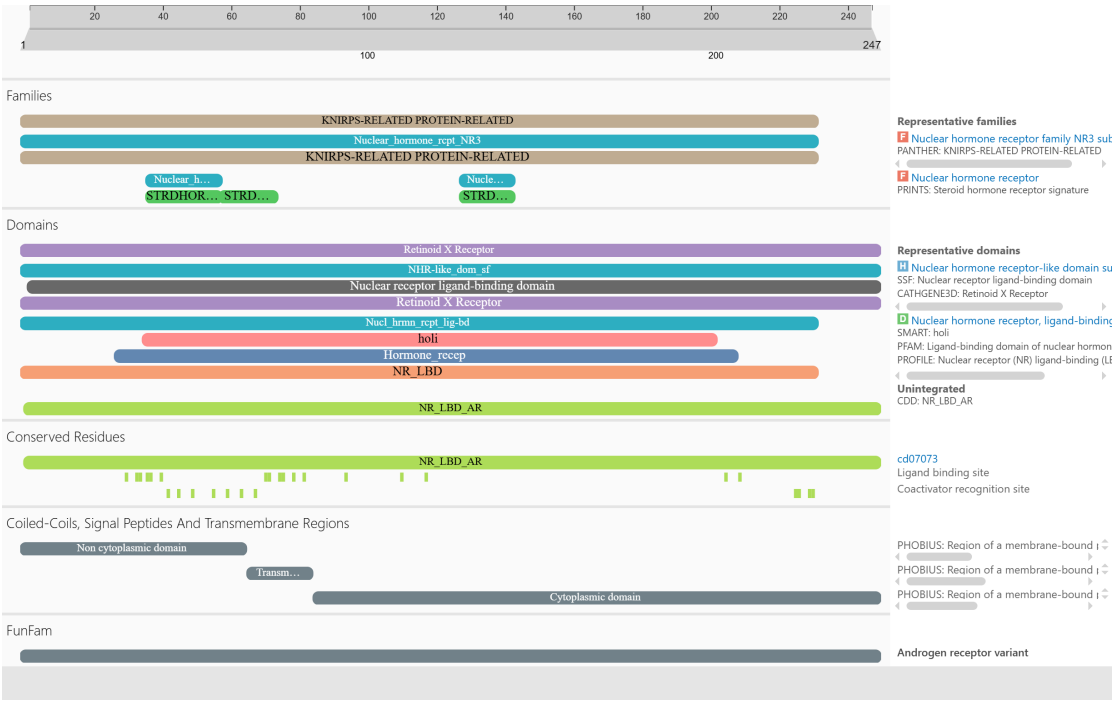

FIGURE 4.4: Functional domains, conserved residues, and ligand-binding regions of the androgen receptor (3RLL) identified using the InterPro database based on Pfam domain annotations.

4.1.4 Protein Refinement

Protein refinement was carried out before docking using PyMOL software. In this process, ligands, heteroatoms, and water molecules were eliminated to obtain a clean and prepared protein structure for molecular docking studies. Refined structures of AR, ERα, and HER2 is shown in Figure 4.5, 4.8,and 4.9.

FIGURE 4.5: Refined 3D Structure of the AR Protein.

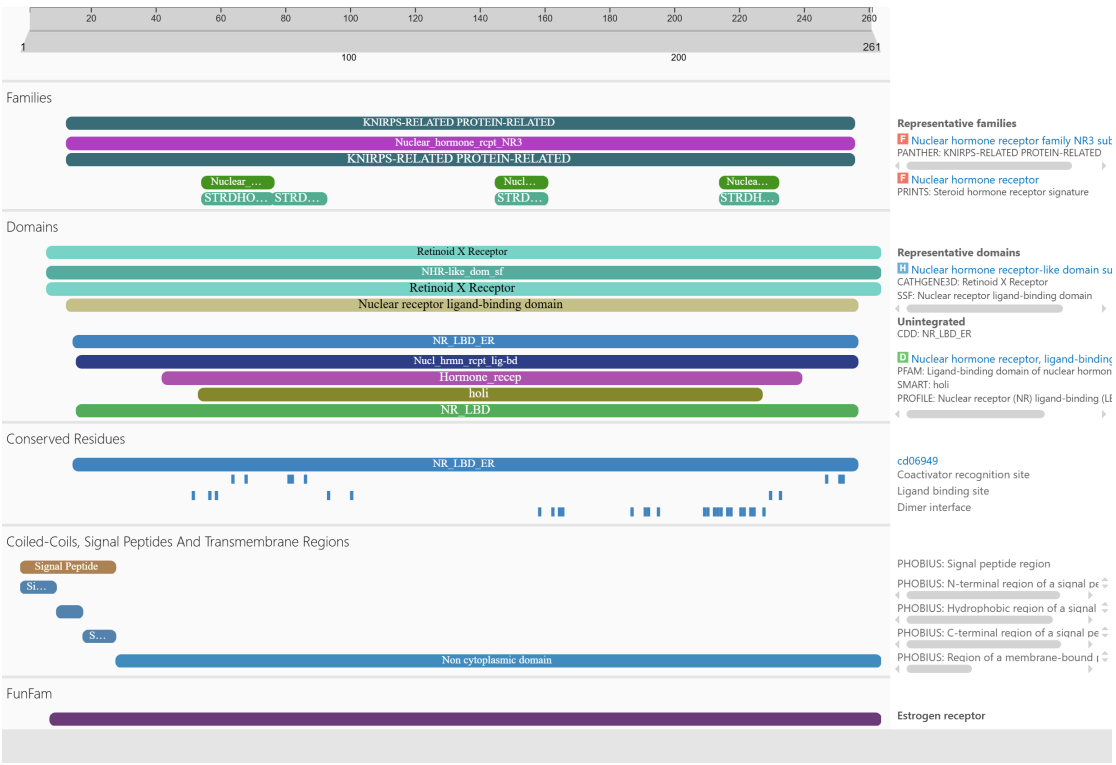

FIGURE 4.6: Functional domains, conserved residues, and ligand-binding regions of estrogen receptor alpha (3ERT) identified using the InterPro database based on Pfam domain annotations.

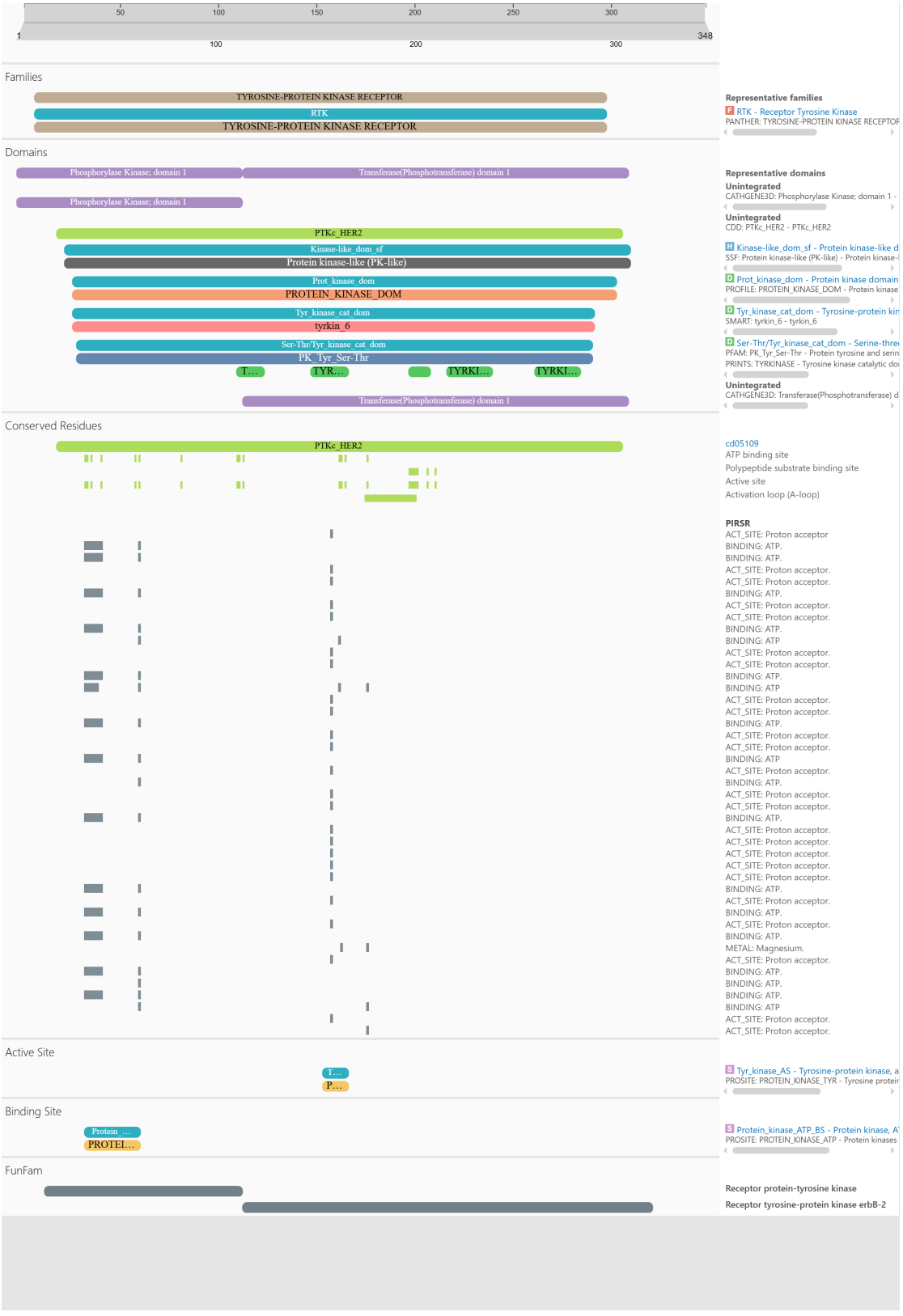

FIGURE 4.7: Functional domains, conserved residues, and ligand-binding regions of HER2 (8U8X) identified using the InterPro database based on Pfam domain annotations.

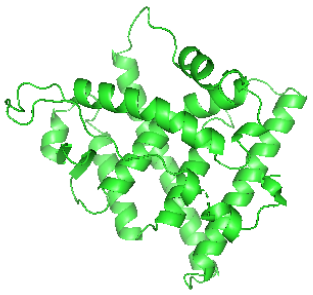

FIGURE 4.8: Refined 3D Structure of the ERα Protein.

FIGURE 4.9: Refined 3D Structure of the HER2 Protein.

4.2 Selection, Retrieval, and Preparation of Ligands

The selection of phytochemicals was performed using the PubChem Taxonomy database for *Helianthus tuberosus* (Jerusalem artichoke). Initially, a targeted search was conducted using the plant name 'Jerusalem artichoke." The corresponding database entry contained several sections, including Names and Identifiers, Related Records, Chemicals and Bioactivities, BioAssays, Proteins, Literature, Patents, Classification, and Information Sources.

Within the Chemicals and Bioactivities section, four categories were available: Tested Compounds, Metabolites, Natural Products, and Food Compounds. For this study, the Food Compounds category was selected because it provided compounds specifically reported for *Helianthus tuberosus* tubers. The remaining categories were not considered, as the objective of this study was to investigate tuber-derived compounds suitable for molecular docking analysis. A total of ten ligands were retrieved from the Food Compounds section.

Their chemical structures were downloaded from PubChem in a suitable structural format for subsequent physicochemical characterization, ADMET evaluation, and molecular docking analyses.

TABLE 4.4: Physicochemical properties and chemical structures of the selected tuber-derived ligands (PubChem) (Part I).

Ligand	**PubChem CID**	**MF**	**Mol. Weight**	**Structure**
Hexose	206	$C_6H_{12}O_6$	180.16 g/mol	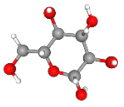
Betaine	247	$C_5H_{11}NO_2$	117.15 g/mol	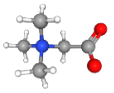
β-D-Glucose	64689	$C_6H_{12}O_6$	180.16 g/mol	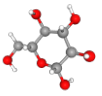
Inulin	5045177	$C_{18}H_{32}O_{16}$	504.40 g/mol	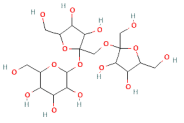
L-Tryptophan	6923516	$C_{11}H_{12}N_2O_2$	204.22 g/mol	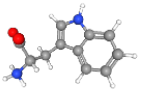

This selection strategy ensured the use of tuber-derived compounds with available structural information for computational investigation against breast cancer target proteins.

The corresponding PubChem compound names of the selected ligands were Hexose, Betaine, Beta-D-Glucopyranose, GlyTouCan:G19464BO, (2S)-2-ammonio-3-(1H-indol-3-yl)propanoate, PNPP disodium hexahydrate, 2-Azaniumyl-3-methylpentanoate, CID 88747398, (2S)-2-amino-6-azaniumylhexanoate, and (2S)-2-aminobutanedioate. Their chemical structures were retrieved from the PubChem database for subsequent computational analyses.

4.2.1 Physicochemical Properties and Structural Analysis of Ligands

The molecular properties, chemical structures, and PubChem information of the chosen tuber-derived phytochemicals are presented in Tables 4.4 and 4.5.

TABLE 4.5: Physicochemical properties and chemical structures of the selected tuber-derived ligands (PubChem) (Part II).

Ligand	PubChem CID	MF	Mol. Weight	Structure
PNPP	24802402	$C_6H_{16}NNa_2O_{12}P$	371.14 g/mol	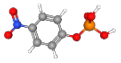
L-Isoleucine	57397079	$C_6H_{13}NO_2$	131.17 g/mol	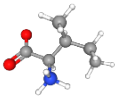
L-Glutamic acid	88747398	$C_5H_9NO_4$	147.13 g/mol	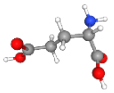
L-Lysine	168007633	$C_6H_{14}N_2O_2$	146.19 g/mol	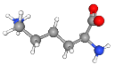
L-Aspartic acid	173074227	$C_4H_7NO_4$	133.10 g/mol	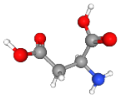

4.2.2 Ligand Refinement

Prior to docking, ligand structures were energy minimized using Discovery Studio to achieve stable conformations. This optimization improved their suitability for subsequent molecular docking studies.

4.3 Screening of Bioactive Compounds for Lead Compound Selection

4.3.1 Virtual Screening Based on Lipinski's Rule of Five

The drug-likeness of the selected phytochemicals was evaluated using physicochemical parameters obtained from the SWISS ADME web server and assessed according to Lipinski's RO5. According to this guideline, compounds are considered more likely to possess favorable oral bioavailability when they have a molecular weight $\leq$ 500 Da, LogP $\leq$ 5, no more than 10 H-bond acceptors, and no more than 5 H-bond donors [119].

As shown in Table 4.6, eight of the ten evaluated compounds fulfilled all Lipinski criteria, suggesting good oral drug potential. In contrast, Inulin and the PNPP compound showed multiple rule violations and were therefore considered less favorable for oral administration. Based on these findings, only compounds meeting the Lipinski requirements were advanced for molecular docking studies.

TABLE 4.6: Evaluation of the selected compounds according to Lipinski's RO5 SwissADME.

Compound	**MW**	**LogP**	**HBA**	**HBD**	**RB**	**Lipinski**
Hexose	180.16	-3.24	6	5	1	Yes
Betaine	117.15	0.76	2	0	2	Yes
β-D-Glucose	180.16	-3.24	6	5	1	Yes
Inulin	504.44	-5.54	16	11	9	No
L-Tryptophan	204.23	0.92	2	2	3	Yes
PNPP	371.14	-1.88	12	6	3	No
L-Isoleucine	131.17	-0.02	2	1	3	Yes
L-Glutamic acid	147.13	-1.19	5	2	4	Yes
L-Lysine	146.19	-0.59	3	2	5	Yes
L-Aspartic acid	133.10	-1.49	5	1	3	Yes

4.4 ADMET Properties

Evaluation of absorption, distribution, metabolism, excretion, and toxicity (ADMET) properties is an important component of the drug development process.

As it helps predict the pharmacokinetic characteristics and safety of potential therapeutic compounds [120].

4.4.1 Absorption

The absorption properties of the selected phytochemicals were predicted using the pkCSM web server, and the corresponding results are summarized in Tables 4.7 and 4.8. The compounds exhibited a broad range of water solubility values, from 0.723 to −3.455 log mol/L.

Among them, Betaine showed the greatest aqueous solubility, whereas the PNPP compound displayed the lowest solubility. Predicted Caco-2 permeability values varied considerably across the compounds. Betaine demonstrated the highest permeability, followed by the L-tryptophan and L-isoleucine compound, indicating a greater ability to cross intestinal epithelial membranes. In contrast, Inulin and PNPP compound exhibited comparatively lower permeability values.

Human intestinal absorption predictions revealed notable differences among the selected phytochemicals. Betaine showed the highest absorption rate (100%), while L-isoleucine and L-tryptophan compounds also exhibited favorable absorption profiles. Conversely, Inulin and PNPP compound displayed poor intestinal absorption, suggesting limited oral uptake.

All compounds showed low skin permeability values, indicating weak transdermal absorption potential. In addition, none of the selected phytochemicals were predicted to inhibit P-glycoprotein I or II. However, Betaine, Inulin, and the L-tryptophan were identified as P-glycoprotein substrates. Overall, the absorption

analysis indicated that Betaine, L-isoleucine, and L-tryptophan compounds possess the most promising absorption properties among the evaluated phytochemicals.

TABLE 4.7: Absorption properties of ligands (Hexose to L-tryptophan).

Sr. No.	Characteristic	Hexose	Betaine	β-D-Glucose	Inulin	L-tryptophan
1	Water solubility (log mol/L)	-1.377	0.723	-1.377	-1.111	-2.891
2	Caco-2 permeability	-0.249	1.440	-0.249	-0.490	0.800
3	Intestinal absorption (%)	21.51	100.00	21.51	0.00	75.06
4	Skin permeability	-3.041	-2.780	-3.041	-2.735	-2.735
5	P-gp substrate	No	Yes	No	Yes	Yes
6	P-gp I inhibitor	No	No	No	No	No
7	P-gp II inhibitor	No	No	No	No	No

TABLE 4.8: Absorption properties of ligands (PNPP disodium hexahydrate to L-aspartic acid).

Sr. No.	Characteristic	PNPP	L-Isoleucine	L-Glutamic acid	L-Lysine	L-Aspartic acid
1	Water solubility (log mol/L)	-3.455	-2.887	-2.892	-2.887	-2.890
2	Caco-2 permeability	-0.367	0.742	-0.219	-0.208	-0.197
3	Intestinal absorption (%)	13.82	84.69	23.47	41.95	21.07
4	Skin permeability	-2.735	-2.752	-2.735	-2.735	-2.735
5	P-gp substrate	No	No	No	No	No
6	P-gp I inhibitor	No	No	No	No	No
7	P-gp II inhibitor	No	No	No	No	No

4.4.2 Distribution

The pkCSM web server was used to predict the distribution properties of the selected phytochemicals, and the corresponding parameters are presented in Table 4.9. The VDss values varied from -1.015 to 0.148 log L/kg.

Among the analyzed compounds, Hexose and β-D-Glucose showed the highest distribution volumes, indicating a greater tendency to partition into tissues, whereas

PNPP exhibited the lowest VDss value, suggesting more limited tissue distribution.

The fraction unbound (Fu) values varied between 0.404 and 0.875, reflecting differences in plasma protein binding. Betaine displayed the highest unbound fraction, indicating increased availability in systemic circulation, while Glutamic acid showed the lowest value.

Blood-brain barrier permeability (log BB) values ranged from -2.086 to 0.099. L-Isoleucine and L-tryptophan compounds exhibited comparatively higher log BB values, whereas PNPP and Inulin demonstrated the lowest values, indicating minimal ability to cross the blood-brain barrier.

A similar trend was observed for CNS permeability (log PS), with values ranging from -5.536 to -2.804. Betaine showed the highest CNS permeability, while PNPP and Inulin displayed the lowest permeability values.

Collectively, these findings indicate moderate distribution profiles for most compounds with generally limited penetration into the central nervous system.

Table 4.9: Distribution properties of ligands.

Compound	**VDss (log L/kg)**	**Fu**	**BBB (log BB)**	**CNS (log PS)**
Hexose	0.148	0.820	-0.943	-3.636
Betaine	-0.304	0.875	-0.214	-2.804
β-D-Glucose	0.148	0.820	-0.943	-3.636
Inulin	-0.248	0.538	-1.469	-5.113
L-tryptophan	-0.140	0.555	0.016	-2.909
PNPP disodium hexahydrate	-1.015	0.511	-2.086	-5.536
L-Isoleucine	-0.559	0.448	0.099	-3.009
L-Glutamic acid	-0.317	0.404	-0.282	-3.176
L-Lysine	-0.519	0.461	-0.121	-3.141
L-Aspartic acid	-0.508	0.445	-0.309	-3.172

4.4.3 Metabolism

Metabolism-related parameters of the selected phytochemicals were predicted using the pkCSM web server, and the corresponding results are presented in Tables 4.10 and 4.11. None of the compounds were predicted to act as substrates of CYP2D6 or inhibitors of CYP1A2, CYP2C19, CYP2C9, CYP2D6, and CYP3A4. The PNPP compound was the only phytochemical identified as a CYP3A4 substrate, whereas all other compounds were predicted to be non-substrates. Overall, the results suggest a low likelihood of cytochrome P450-associated drug-drug interactions.

TABLE 4.10: Metabolism properties of ligands (Hexose to L-tryptophan).

Sr. No.	Characteristic	Hexose	Betaine	β-D-Glucose	Inulin	L-tryptophan
1	CYP2D6 Substrate	No	No	No	No	No
2	CYP3A4 Substrate	No	No	No	No	No
3	CYP1A2 Inhibitor	No	No	No	No	No
4	CYP2C19 Inhibitor	No	No	No	No	No
5	CYP2C9 Inhibitor	No	No	No	No	No
6	CYP2D6 Inhibitor	No	No	No	No	No
7	CYP3A4 Inhibitor	No	No	No	No	No

TABLE 4.11: Metabolism properties of ligands (PNPP disodium hexahydrate to L-aspartic acid).

Sr. No.	Characteristic	PNPP	L-Isoleucine	L-Glutamic acid	L-Lysine	L-Aspartic acid
1	CYP2D6 Substrate	No	No	No	No	No
2	CYP3A4 Substrate	Yes	No	No	No	No
3	CYP1A2 Inhibitor	No	No	No	No	No
4	CYP2C19 Inhibitor	No	No	No	No	No
5	CYP2C9 Inhibitor	No	No	No	No	No
6	CYP2D6 Inhibitor	No	No	No	No	No
7	CYP3A4 Inhibitor	No	No	No	No	No

4.4.4 Excretion

Excretion-related parameters of the selected phytochemicals were predicted using the pkCSM web server, and the corresponding results are presented in Table 4.12.

Total clearance values varied between -2.262 and 1.562 log mL/min/kg. Among the evaluated compounds, Inulin demonstrated the highest clearance rate, with the L-tryptophan also showing comparatively high clearance, indicating efficient elimination.

Conversely, the PNPP compound exhibited the lowest clearance value, suggesting prolonged retention in the body. The remaining phytochemicals showed intermediate clearance values.

Furthermore, none of the compounds were predicted to be substrates of the organic cation transporter 2 (OCT2), indicating that OCT2-mediated renal excretion is unlikely to play a significant role in their elimination.

TABLE 4.12: Predicted excretion properties of the selected ligands obtained using the pkCSM web server.

No.	Compound	Total Clearance (log mL/min/kg)	OCT2 Substrate
1	Hexose	0.626	No
2	Betaine	0.326	No
3	β-D-Glucose	0.626	No
4	Inulin	1.562	No
5	L-tryptophan	0.840	No
6	PNPP disodium hexahydrate	-2.262	No
7	L-Isoleucine	0.544	No
8	L-Glutamic acid	0.801	No
9	L-Lysine	0.785	No
10	L-Aspartic acid	0.593	No

4.4.5 Toxicity

Toxicity-related parameters of the selected phytochemicals were predicted using the pkCSM web server, and the corresponding results are presented in Tables 4.13 and 4.14. AMES toxicity predictions indicated that all compounds were non-mutagenic except the PNPP compound, which showed potential mutagenic activity. None of the phytochemicals were predicted to inhibit hERG I channels, while only Inulin was identified as a hERG II inhibitor, suggesting an overall low risk of cardiotoxic effects.

The maximum tolerated dose (MTD) values ranged from 0.280 to 1.896 log mg/kg/-day. The predicted acute oral toxicity (LD_{50}) values varied between 1.214 and 2.800 mol/kg, with Inulin exhibiting the highest LD_{50} value, indicating comparatively lower acute toxicity. Skin sensitization potential was observed for Betaine and the PNPP compound, whereas the remaining phytochemicals were predicted to be non-sensitizers.

Overall, the toxicity analysis demonstrated favorable safety profiles for the majority of the selected phytochemicals.

TABLE 4.13: Toxicity properties of ligands (Hexose to L-tryptophan).

No.	**Characteristic**	**Hexose**	**Betaine**	**β-D-Glucose**	**Inulin**	**L-tryptophan**
1	AMES	No	No	No	No	No
2	Max tolerated dose	1.896	0.838	1.896	0.733	0.764
3	hERG I	No	No	No	No	No
4	hERG II	No	No	No	Yes	No
5	LD50 (mol/kg)	1.214	1.654	1.214	2.800	2.338
6	LOAEL (log mg/kg/day)	3.897	0.254	3.897	4.162	0.791
7	Hepatotoxicity	No	No	No	No	No
8	Skin sensitisation	No	Yes	No	No	No
9	*T. pyriformis* toxicity	0.285	-0.057	0.285	0.285	0.283
10	Minnow toxicity	5.083	2.970	5.083	15.565	2.297

TABLE 4.14: Toxicity properties of ligands (PNPP disodium hexahydrate to L-aspartic acid).

No.	Characteristic	PNPP	L-Isoleucine	L-Glutamic acid	L-Lysine	L-Aspartic acid
1	AMES	Yes	No	No	No	No
2	Max tolerated dose	0.280	1.069	0.893	1.163	1.164
3	hERG I	No	No	No	No	No
4	hERG II	No	No	No	No	No
5	LD50 (mol/kg)	1.331	2.029	2.442	2.059	2.354
6	LOAEL (log mg/kg/day)	2.104	0.220	1.962	-0.263	0.750
7	Hepatotoxicity	No	No	No	No	No
8	Skin sensitisation	Yes	No	No	No	No
9	*T. pyriformis* toxicity	0.309	-0.202	0.281	0.246	0.273
10	Minnow toxicity	3.204	2.883	3.191	3.004	3.626

Following the evaluation of drug-likeness and ADMET properties, Inulin and PNPP disodium hexahydrate were not considered for molecular docking studies. Inulin was excluded because of multiple violations of Lipinski's RO5 and its lack of predicted intestinal absorption, whereas PNPP disodium hexahydrate was excluded because of its poor absorption characteristics and positive AMES toxicity. Consequently, only phytochemicals demonstrating favorable pharmacokinetic and safety profiles were advanced for molecular docking analysis.

4.5 Molecular Docking

Molecular docking is a widely applied computational method in drug discovery that facilitates the prediction of binding modes and interaction strengths between ligands and target proteins [121]. In this study, the docking potential of selected phytochemicals from *Helianthus tuberosus* (Jerusalem artichoke) against breast cancer-associated target proteins was investigated using the CB-Dock2 server. The molecular docking results of the selected phytochemicals against the androgen receptor (AR) are presented in Tables 4.15 and 4.16.

The binding affinities ranged from −3.9 to −7.6 kcal/mol.

Among the evaluated compounds, L-tryptophan exhibited the most favorable docking score (−7.6 kcal/mol), whereas Betaine showed the lowest binding affinity (−3.9 kcal/mol).

TABLE 4.15: Molecular docking results of selected phytochemicals against the androgen receptor (AR) (Hexose to L-Tryptophan).

Ligand	**Docking Score (kcal/mol)**	**Cavity Volume (Å^3)**	**Structure**
Hexose	-5.6	2398	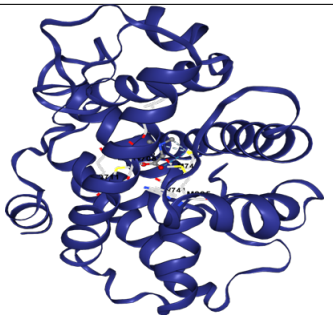
Betaine	-3.9	2398	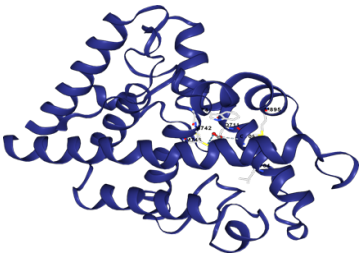
β-D-Glucose	-5.6	2398	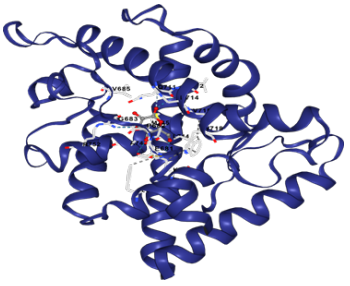
L-Tryptophan	-7.6	2398	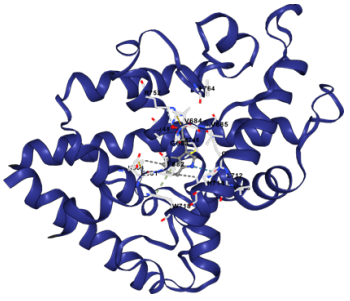

These findings indicate that L-tryptophan possesses a stronger binding affinity toward the AR than the other selected phytochemicals.

TABLE 4.16: Molecular docking results of selected phytochemicals against the Androgen Receptor (AR) (L-Isoleucine to L-Aspartic acid).

Ligand	**Docking Score (kcal/mol)**	**Cavity Volume ($Å^3$)**	**Structure**
L-Isoleucine	-4.7	2398	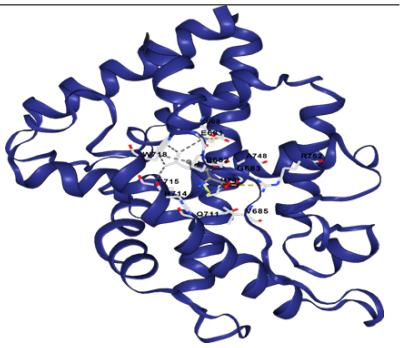
L-Glutamic acid	-5.0	2398	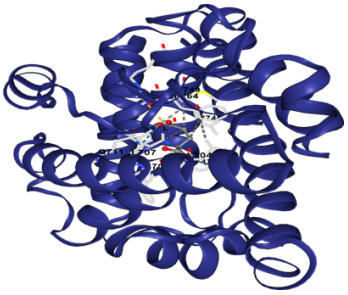
L-Lysine	-4.5	2398	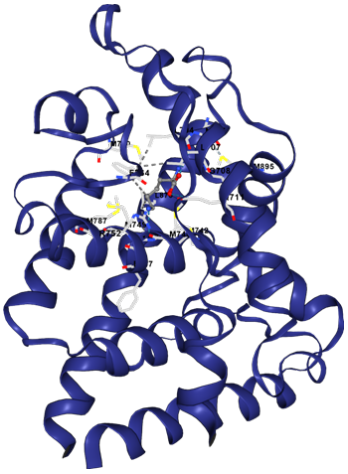
L-Aspartic acid	-4.2	2398	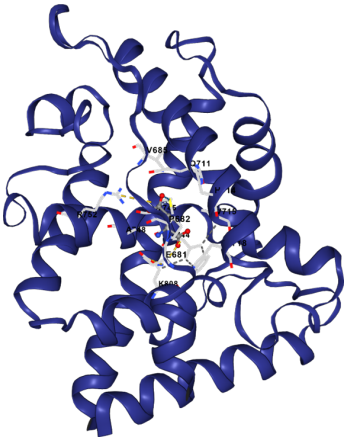

The molecular docking results of the selected phytochemicals against the estrogen receptor alpha (ERα) are presented in Tables 4.17 and 4.18.

TABLE 4.17: Molecular docking results of selected phytochemicals against the estrogen receptor alpha (ERα) (Hexose to L-Tryptophan).

Ligand	**Docking Score (kcal/mol)**	**Cavity Volume (Å^3)**	**Structure**
Hexose	-5.6	1983	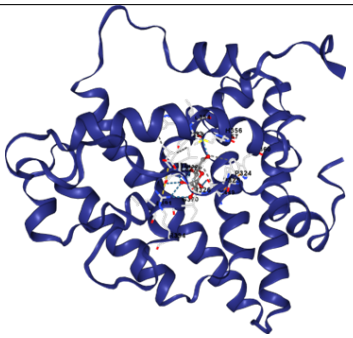
Betaine	-3.9	1983	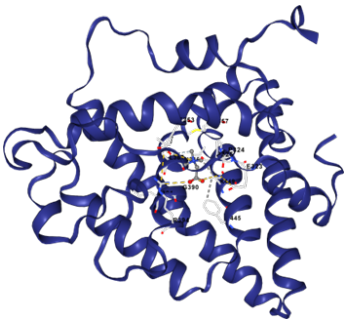
β-D-Glucose	-5.7	1983	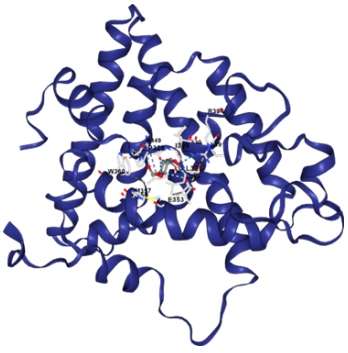
L-Tryptophan	-7.0	1983	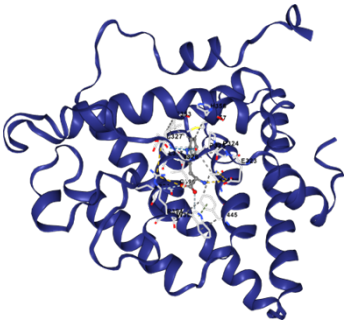

The docking scores spanned from -3.9 to -7.0 kcal/mol. Among the evaluated compounds, L-tryptophan exhibited the strongest binding affinity with a docking

score of −7.0 kcal/mol, indicating the most favorable interaction with the ERα.

TABLE 4.18: Molecular docking results of selected phytochemicals against the estrogen receptor alpha (ERα) (L-Isoleucine to L-Aspartic acid).

Ligand	**Docking Score (kcal/mol)**	**Cavity Volume ($Å^3$)**	**Structure**
L-Isoleucine	-5.1	1983	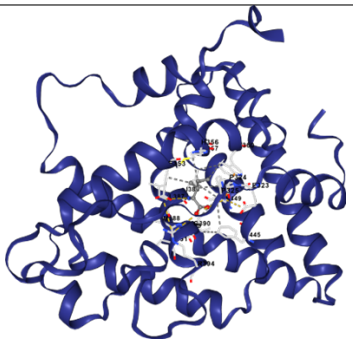
L-Glutamic acid	-4.6	1983	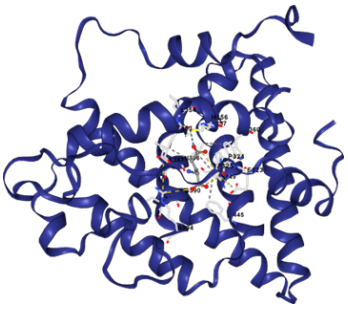
L-Lysine	-4.8	1983	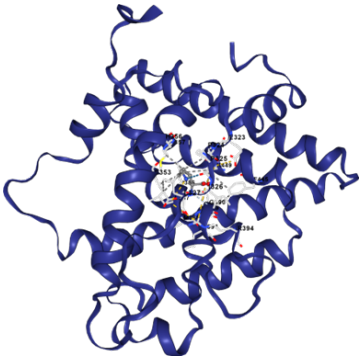
L-Aspartic acid	-4.5	1983	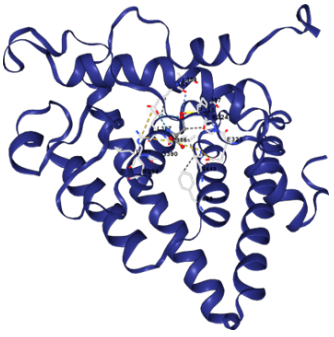

The molecular docking results of the selected phytochemicals against the HER2 are presented in Tables 4.19 and 4.20.

The docking scores ranged from −3.9 to −7.4 kcal/mol.

TABLE 4.19: Molecular docking results of selected phytochemicals against the HER2 (Hexose to L-Tryptophan).

Ligand	**Docking Score (kcal/mol)**	**Cavity Volume ($Å^3$)**	**Structure**
Hexose	-5.4	1099	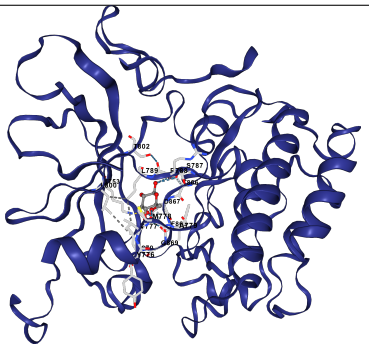
Betaine	-3.9	1099	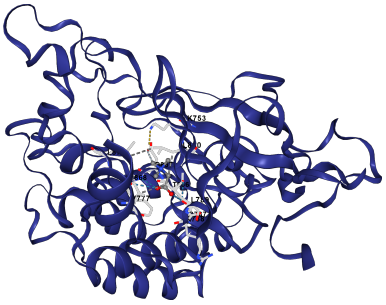
β-D-Glucose	-5.5	1099	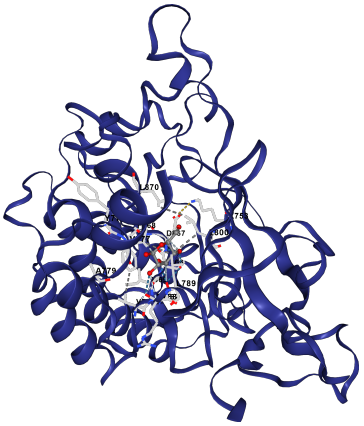
L-Tryptophan	-7.4	1099	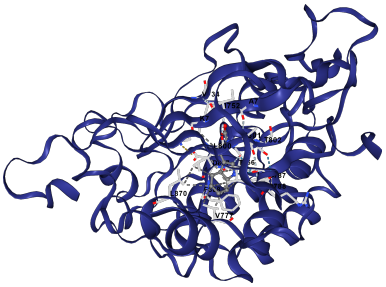

Among the evaluated compounds, L-tryptophan exhibited the most favorable docking score (−7.4 kcal/mol), indicating the strongest interaction with the HER2 receptor.

TABLE 4.20: Molecular docking results of selected phytochemicals against the HER2 (L-Isoleucine to L-Aspartic Acid)

Ligand	**Docking Score (kcal/mol)**	**Cavity Volume (Å^3)**	**Structure**
L-Isoleucine	-5.1	1099	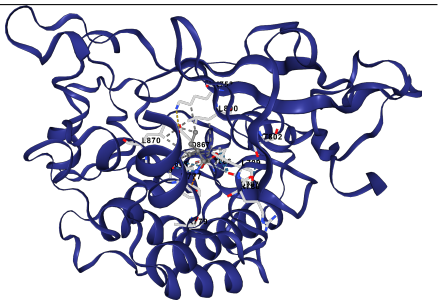
L-Glutamic acid	-5.0	1099	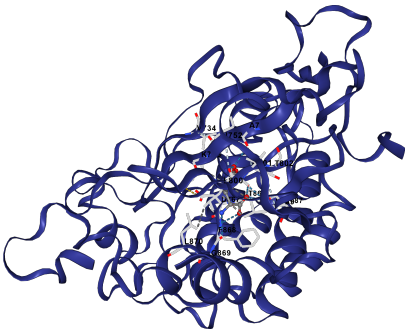
L-Lysine	-5.0	1099	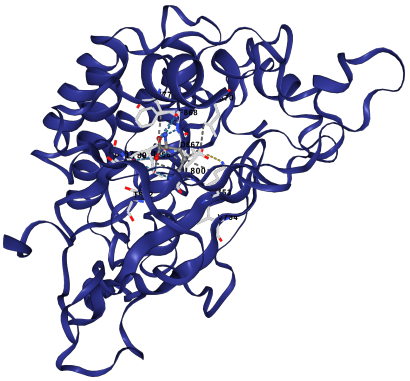
L-Aspartic acid	-4.5	1099	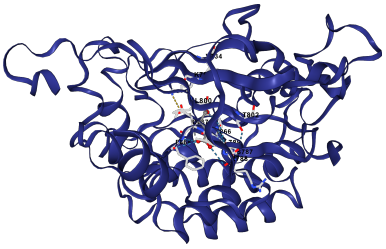

4.5.1 Ligand and Protein Interaction Analysis

The interactions between the selected target proteins and their corresponding ligands were further examined using Discovery Studio Visualizer. The docked protein–ligand complexes generated by the CB-Dock2 server were analyzed to identify the key binding residues and characterize the intermolecular interactions involved, including hydrogen bonding, hydrophobic contacts, electrostatic interactions, and van der Waals forces.

4.5.1.1 Interaction Analysis Hexose with the Androgen Receptor

The molecular interaction analysis of Hexose with the androgen receptor (AR) is shown in Figure 4.10. Hexose formed four conventional hydrogen bonds with Lys808 (2.89 Å), Glu681 (2.66 Å), Gln711 (2.30 Å), and Arg752 (3.10 Å), stabilizing the protein–ligand complex through its multiple hydroxyl groups on the non-aromatic pyranose ring.

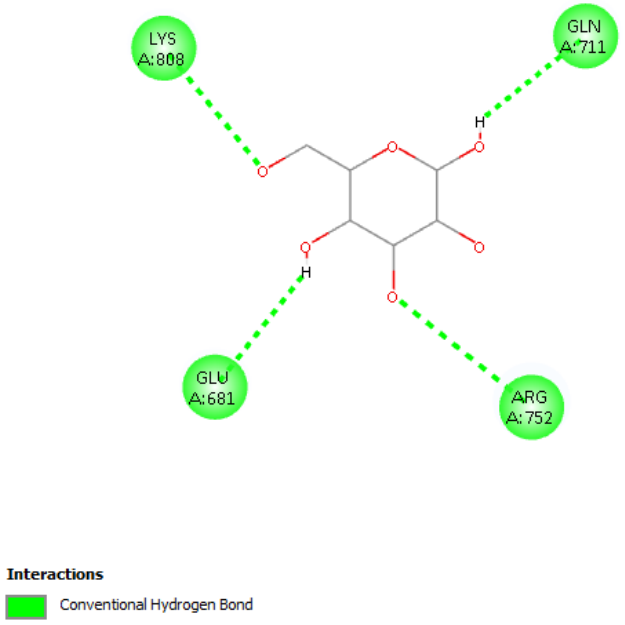

FIGURE 4.10: Molecular interaction analysis of Hexose with the androgen receptor (AR).

4.5.1.2 Betaine–AR Interaction Analysis

The molecular interaction analysis of Betaine with the androgen receptor (AR) is shown in Figure 4.11. The ligand established two conventional hydrogen bonds with Gln711 (3.09 Å) and Trp741 (3.13 Å). In addition, two carbon hydrogen bonds were formed with Gly708 (3.30 Å) and Leu704 (3.66 Å). These interactions were primarily mediated by the ligand's carbonyl and tertiary amine functional groups, thereby contributing to the stability of the protein–ligand complex within the receptor binding site.

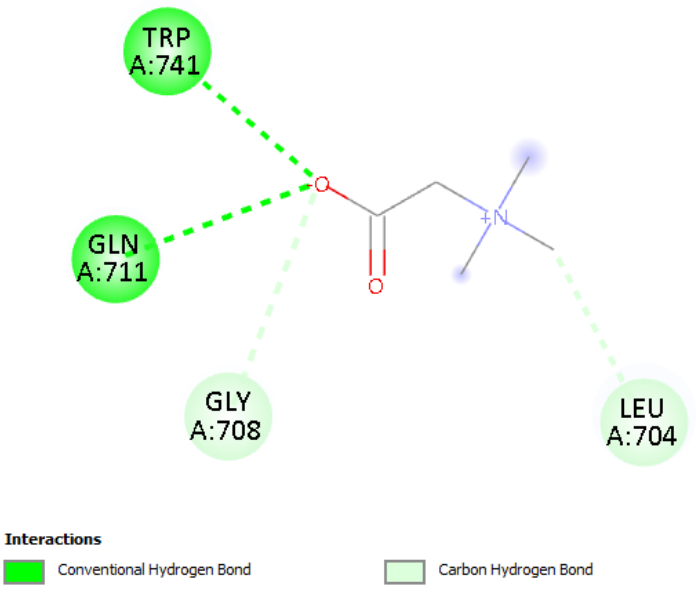

FIGURE 4.11: Molecular interaction analysis of Betaine with the androgen receptor (AR).

4.5.1.3 β-D-Glucose–AR Interaction Analysis

The molecular interaction analysis of β-D-Glucose with the androgen receptor (AR) is shown in Figure 4.12. The ligand formed three conventional hydrogen bonds with Glu681 (2.57 Å), Lys808 (2.95 Å), and Arg752 (3.11 Å), establishing

favorable interactions within the receptor binding pocket. The presence of multiple hydroxyl groups in the non-aromatic pyranose ring facilitated hydrogen-bond formation, thereby contributing to the stability of the protein–ligand complex.

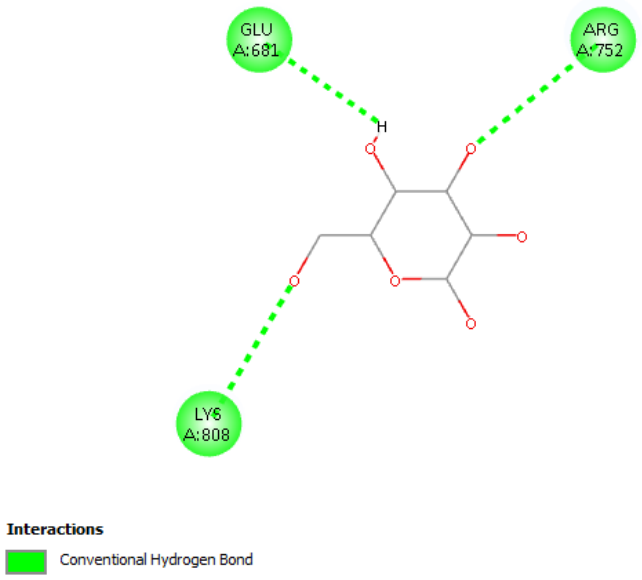

FIGURE 4.12: Molecular interaction analysis of β-D-Glucose with the androgen receptor (AR).

4.5.1.4 L-Tryptophan–AR Interaction Analysis

The molecular interaction analysis of L-tryptophan with the androgen receptor (AR) is shown in Figure 4.13. The ligand formed four conventional hydrogen bonds with Gly683 (1.93 Å), Pro682 (2.30 Å), Val685 (2.98 Å), and Gln711 (2.72 Å), establishing favorable interactions within the receptor binding pocket. In addition, an attractive charge interaction with Glu681 (2.68 Å) and a salt bridge interaction with Arg752 (3.76 Å) were observed. The indole ring of L-tryptophan participated in multiple π-mediated interactions, including one π–σ interaction with Met745, one π–π T-shaped interaction with Trp718, and three π–alkyl interactions involving Ala748, Pro682, and Met745. An unfavorable donor–donor interaction was also detected with Val715. Overall, the predominance of favorable interactions contributed to the stabilization of the protein–ligand complex.

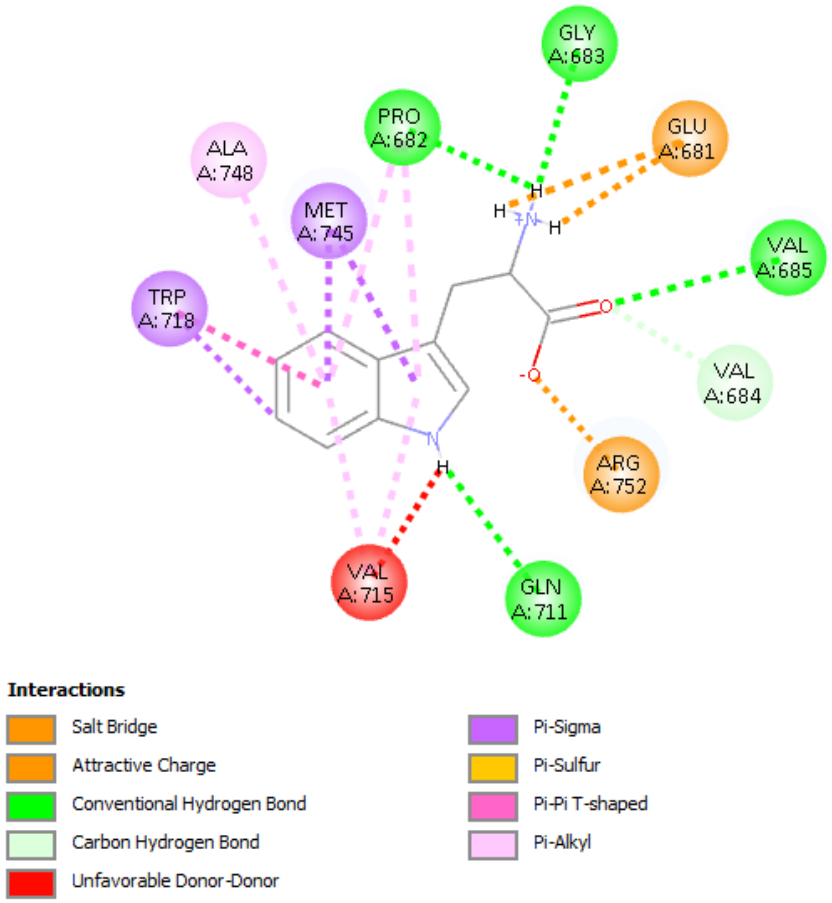

FIGURE 4.13: Molecular interaction analysis of L-tryptophan with the androgen receptor (AR).

4.5.1.5 L-Isoleucine–AR Interaction Analysis

The molecular interaction analysis of L-isoleucine with the androgen receptor (AR) is shown in Figure 4.14. The ligand formed three conventional hydrogen bonds with Pro682 (2.90 Å), Gly683 (2.06 Å), and Val685 (2.96 Å), establishing favorable interactions within the receptor binding pocket.

In addition, two attractive charge interactions were observed with Glu681 and Arg752, whereas one unfavorable positive–positive interaction was detected with Arg752. The branched aliphatic side chain of L-isoleucine further established two alkyl interactions with Val715 and Met745, thereby enhancing the stability of the protein–ligand complex.

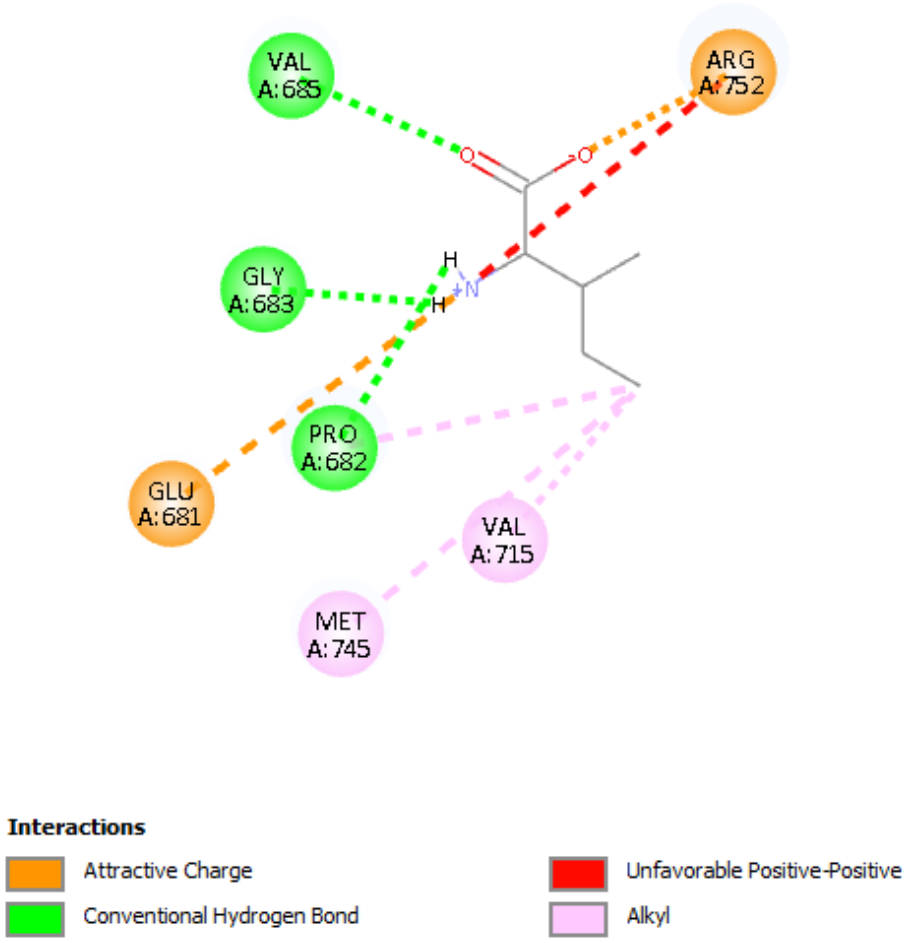

FIGURE 4.14: Molecular interaction analysis of L-isoleucine with the androgen receptor (AR).

4.5.1.6 L-Glutamic Acid–AR Interaction Analysis

The molecular interaction analysis of L-glutamic acid with the androgen receptor (AR) is shown in Figure 4.15. The ligand established three conventional hydrogen bonds with Gln711 (1.95 Å), Phe764 (2.39 Å), and Arg752 (3.00 Å), establishing favorable interactions within the receptor binding pocket.

The amino and carboxyl groups of L-glutamic acid played a key role in hydrogen-bond formation, thereby enhancing the stability of the protein–ligand complex.

Furthermore, a single unfavorable donor–donor interaction was detected with Arg752; however, the overall binding pattern remained favorable because of the presence of multiple stabilizing interactions.

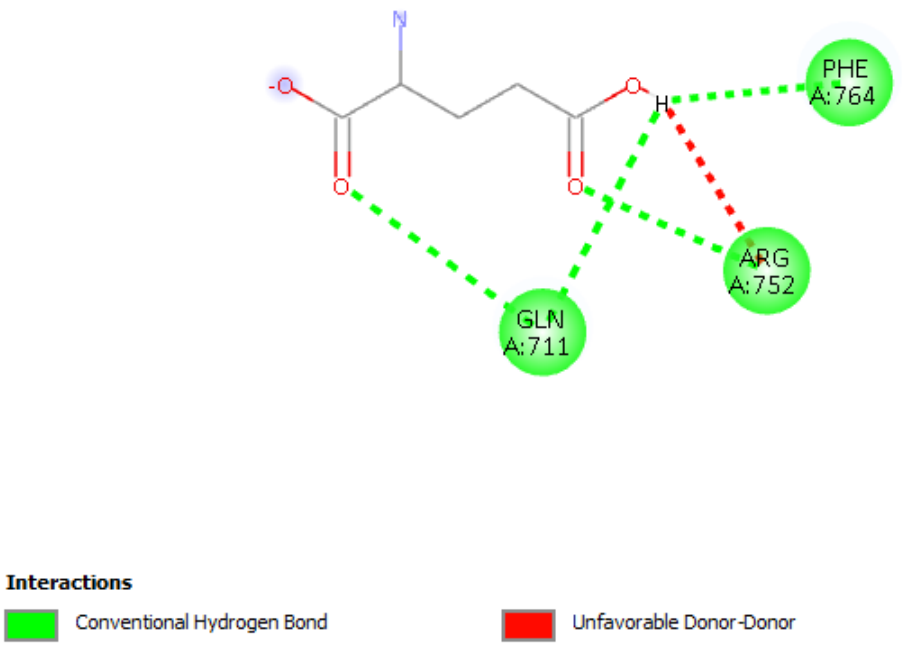

FIGURE 4.15: Molecular interaction analysis of L-glutamic acid with the androgen receptor (AR).

4.5.1.7 L-Lysine–AR Interaction Analysis

The molecular interaction analysis of L-lysine with the androgen receptor (AR) is shown in Figure 4.16. The ligand established one conventional hydrogen bond with Gln711 (2.94 Å) and one salt bridge interaction with Arg752 (3.23 Å), establishing favorable interactions within the receptor binding pocket.

In addition, a π–cation interaction was observed with Trp718, whereas an unfavorable positive–positive interaction was detected with Lys808.

The amino and carboxyl functional groups of L-lysine contributed to electrostatic and hydrogen-bond interactions, thereby enhancing the stability of the protein–ligand complex.

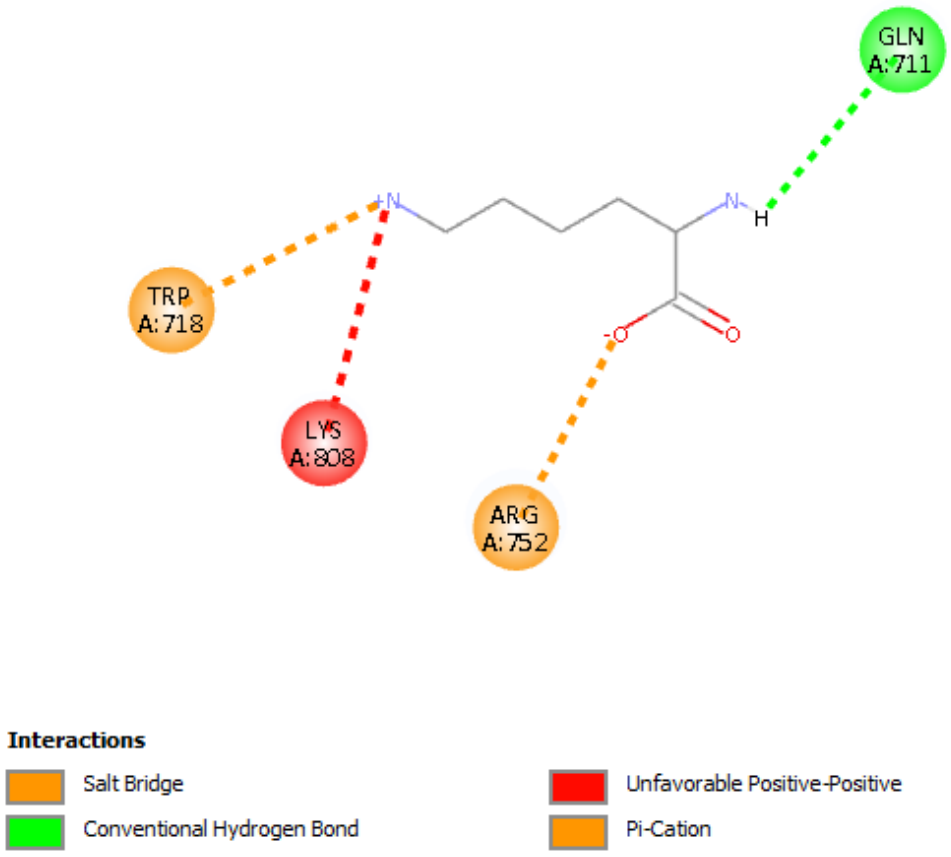

FIGURE 4.16: Molecular interaction analysis of L-lysine with the androgen receptor (AR).

4.5.1.8 L-Aspartic Acid–AR Interaction Analysis

The molecular interaction analysis of L-aspartic acid with the androgen receptor (AR) is shown in Figure 4.17. The ligand established two conventional hydrogen bonds with Gln711 (3.05 Å) and Trp741, together with one carbon hydrogen bond with Gly708 (3.01 Å), establishing favorable interactions within the receptor binding pocket.

Furthermore, a π–anion interaction involving Trp741 was observed, contributing to the stabilization of the protein–ligand complex. The amino and carboxyl functional groups of L-aspartic acid facilitated hydrogen-bonding and electrostatic interactions, thereby supporting stable binding within the receptor binding pocket.

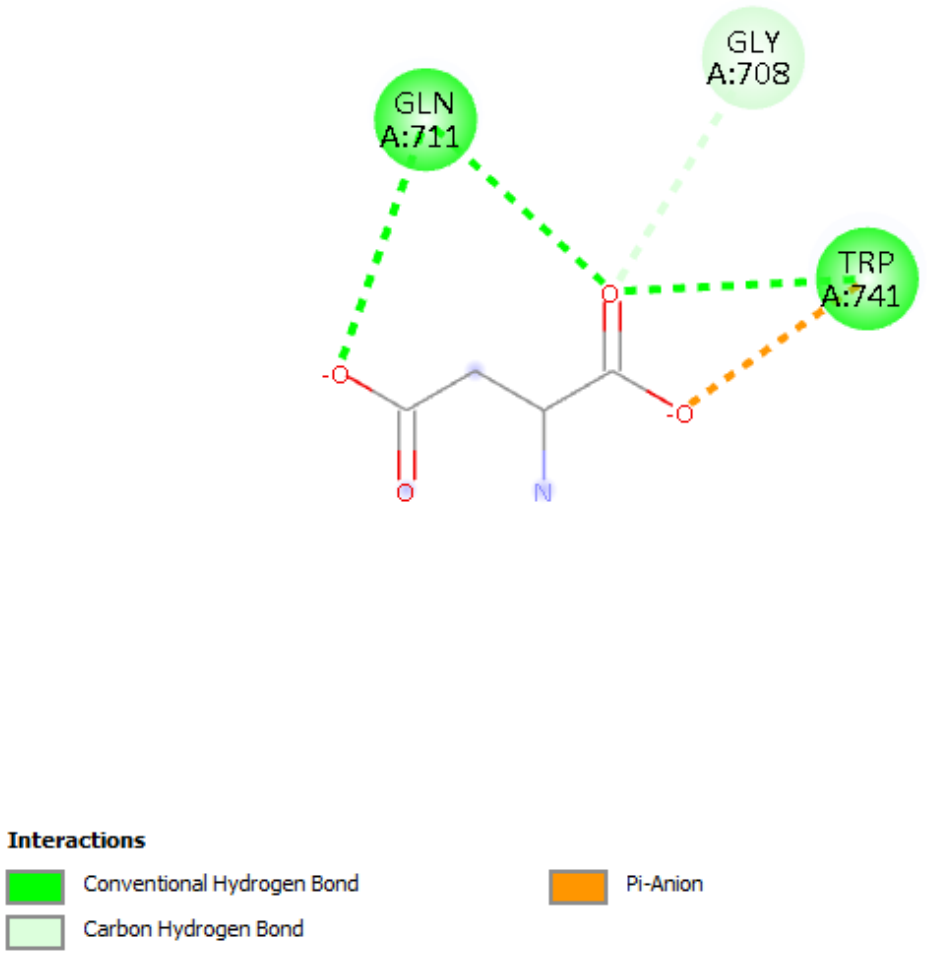

FIGURE 4.17: Molecular interaction analysis of L-aspartic acid with the androgen receptor (AR).

4.5.1.9 Hexose–ERα Interaction Analysis

The molecular interaction analysis of Hexose with the estrogen receptor alpha (ERα) is shown in Figure 4.18. The ligand established two conventional hydrogen bonds with Lys449 (3.03 Å) and Glu353 (2.60 Å), establishing favorable interactions within the receptor binding pocket.

The presence of multiple hydroxyl groups on the non-aromatic pyranose ring promoted hydrogen-bond formation, thereby contributing to the stability of the protein–ligand complex and facilitating effective binding within the active site.

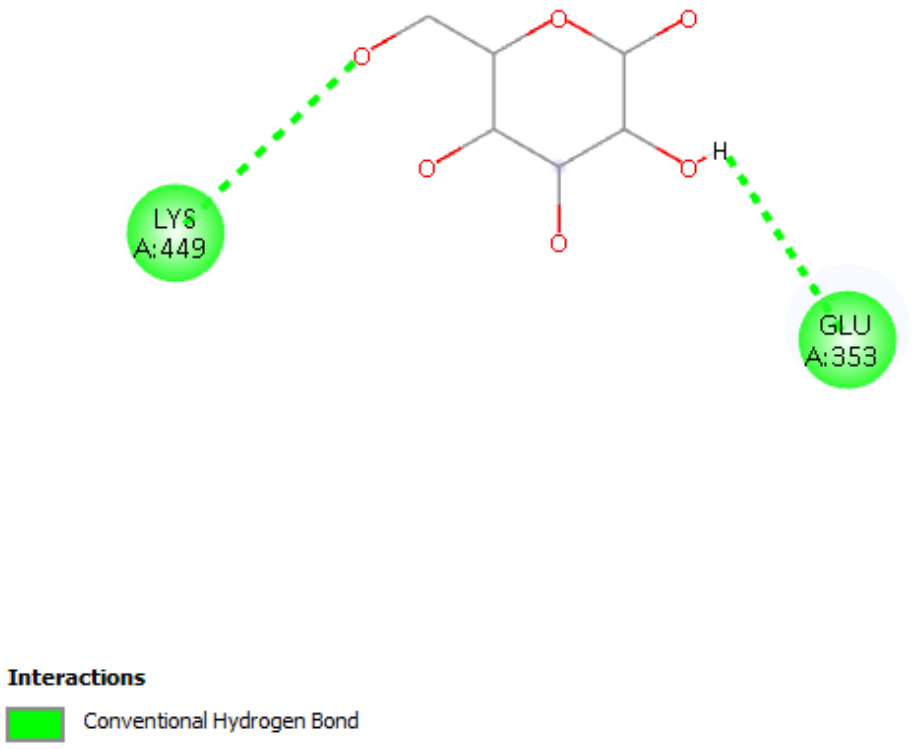

FIGURE 4.18: Molecular interaction analysis of Hexose with the Estrogen receptor Alpha (ERα).

4.5.1.10 Betaine–ERα Interaction Analysis

The molecular interaction analysis of Betaine with the estrogen receptor alpha (ERα) is shown in Figure 4.19. The ligand formed one conventional hydrogen bond with Arg394 and three attractive charge interactions involving Arg394, Lys449, and Glu353.

In addition, salt bridge interactions were established with Lys449 and Glu353. Two carbon hydrogen bonds involving Ile386 (2.96 Å) and Glu353 were also observed.

The quaternary ammonium and carboxyl functional groups of Betaine facilitated these electrostatic and hydrogen-bond interactions, thereby contributing to the stabilization of the protein–ligand complex within the receptor binding pocket.

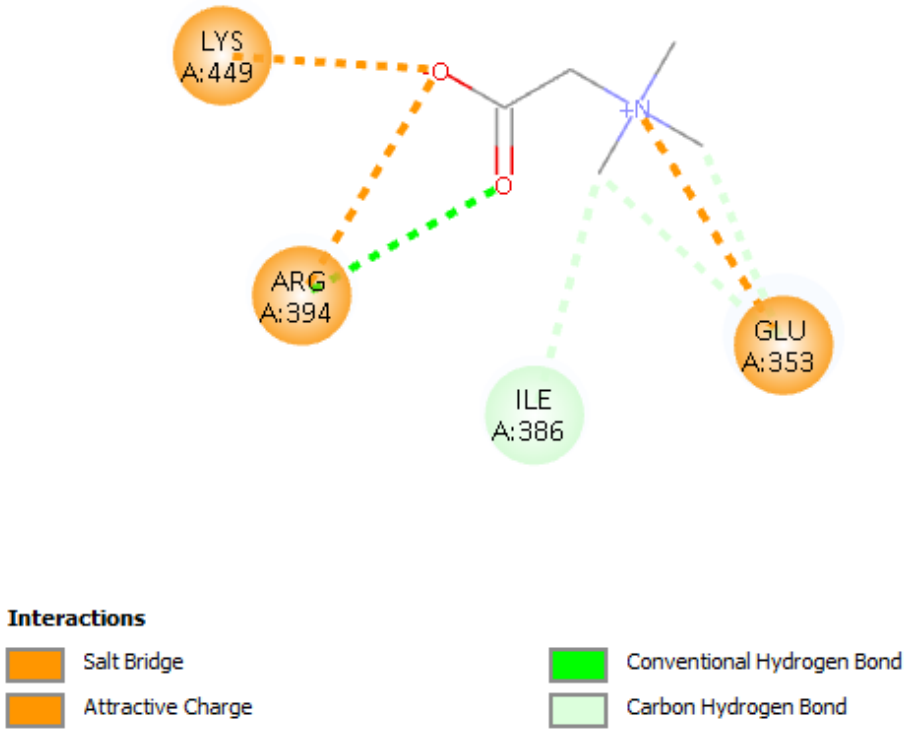

FIGURE 4.19: Molecular interaction analysis of Betaine with the estrogen receptor alpha (ERα).

4.5.1.11 β-D-Glucose–ERα Interaction Analysis

The molecular interaction analysis of β-D-Glucose with the estrogen receptor alpha (ERα) is shown in Figure 4.20. The ligand formed one conventional hydrogen bond with Glu353 (2.44 Å), establishing favorable interactions within the receptor binding pocket. The non-aromatic pyranose ring and its multiple hydroxyl groups facilitated hydrogen-bond formation, thereby contributing to the stabilization of the protein–ligand complex.

In addition, one unfavorable donor–donor interaction was observed with Arg394 (2.23 Å); however, the overall interaction profile remained favorable because of the predominance of stabilizing interactions.

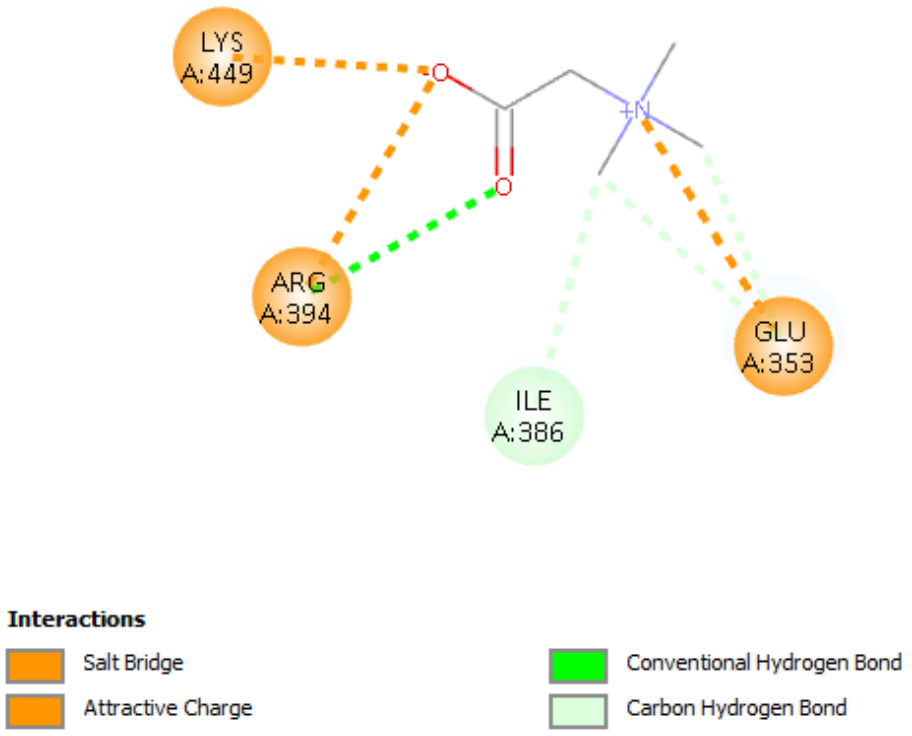

FIGURE 4.20: Molecular interaction analysis of β-D-Glucose with the estrogen receptor alpha (ERα).

4.5.1.12 L-Tryptophan–ERα Interaction Analysis

The molecular interaction analysis of L-tryptophan with the estrogen receptor alpha (ERα) is shown in Figure 4.21. The ligand established three conventional hydrogen bonds with Glu323, Arg394 (3.25 Å), and Pro325 (2.68 Å), together with one attractive charge interaction with Glu323 (2.23 Å).

In addition, one carbon hydrogen bond was observed with Trp393. The indole ring of L-tryptophan further participated in one π–sulfur interaction with Met357 and two π–alkyl interactions with Pro324, thereby contributing to the stabilization of the protein–ligand complex within the receptor binding pocket.

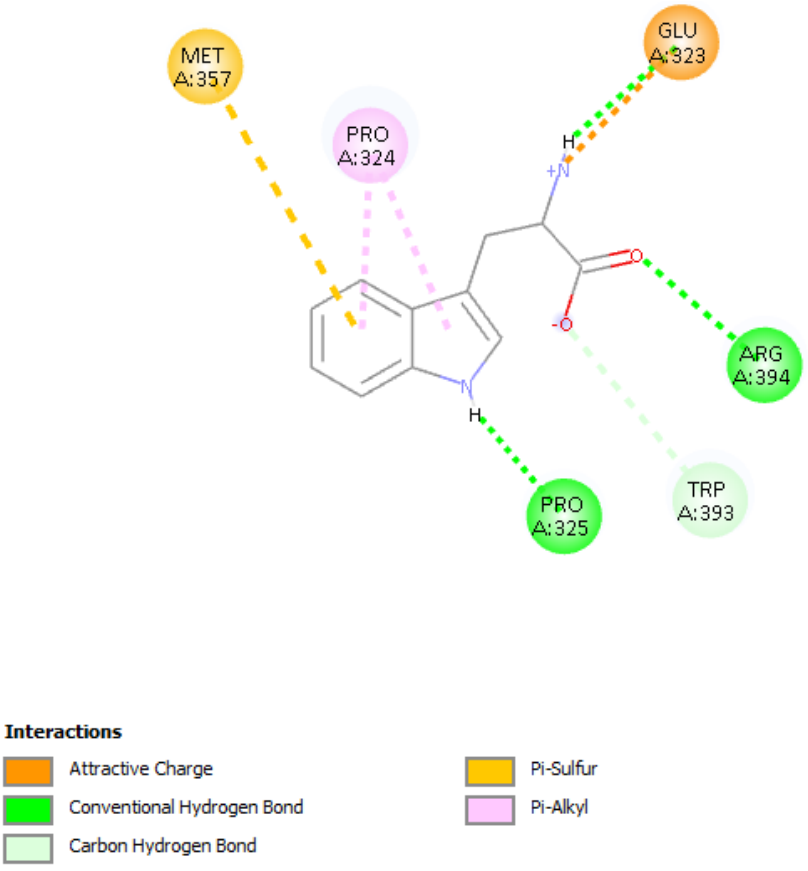

FIGURE 4.21: Molecular interaction analysis of L-tryptophan with the estrogen receptor alpha (ERα).

4.5.1.13 L-Isoleucine–ERα Interaction Analysis

The molecular interaction analysis of L-isoleucine with the estrogen receptor alpha (ERα) is shown in Figure 4.22. The ligand formed three conventional hydrogen bonds, including two interactions with Ile386 (2.75 Å) and one interaction with Arg394 (3.00 Å), establishing favorable interactions within the receptor binding pocket. In addition, two attractive charge interactions were observed with Arg394 and Glu353, while salt bridge interactions were established with Lys449 and Glu353. A carbon hydrogen bond was also formed with Gly390 (2.72 Å). Although the ligand lacks an aromatic ring, its branched aliphatic side chain participated in one alkyl interaction with Met357 and three π–alkyl interactions involving Pro324 and Trp360. Overall, these interactions contributed to the stabilization of the protein–ligand complex within the receptor binding pocket.

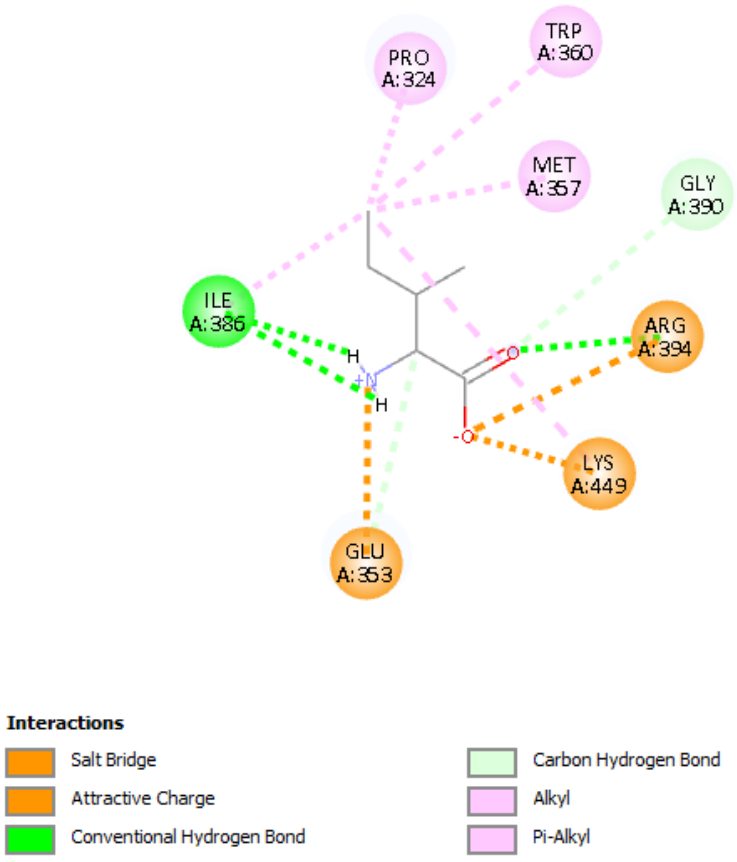

FIGURE 4.22: Molecular interaction analysis of L-isoleucine with the estrogen receptor alpha (ERα).

4.5.1.14 L-Glutamic Acid–ERα Interaction Analysis

The molecular interaction analysis of L-glutamic acid with the estrogen receptor alpha (ERα) is shown in Figure 4.23. The ligand formed one conventional hydrogen bond with Lys449 (2.99 Å) and one attractive charge interaction with Arg394 (3.04 Å), establishing favorable interactions within the receptor binding pocket.

Furthermore, a salt bridge interaction with Lys449 was identified, further strengthening ligand binding. The amino and carboxyl functional groups of L-glutamic acid facilitated hydrogen-bonding and electrostatic interactions, thereby contributing to the stability of the protein–ligand complex.

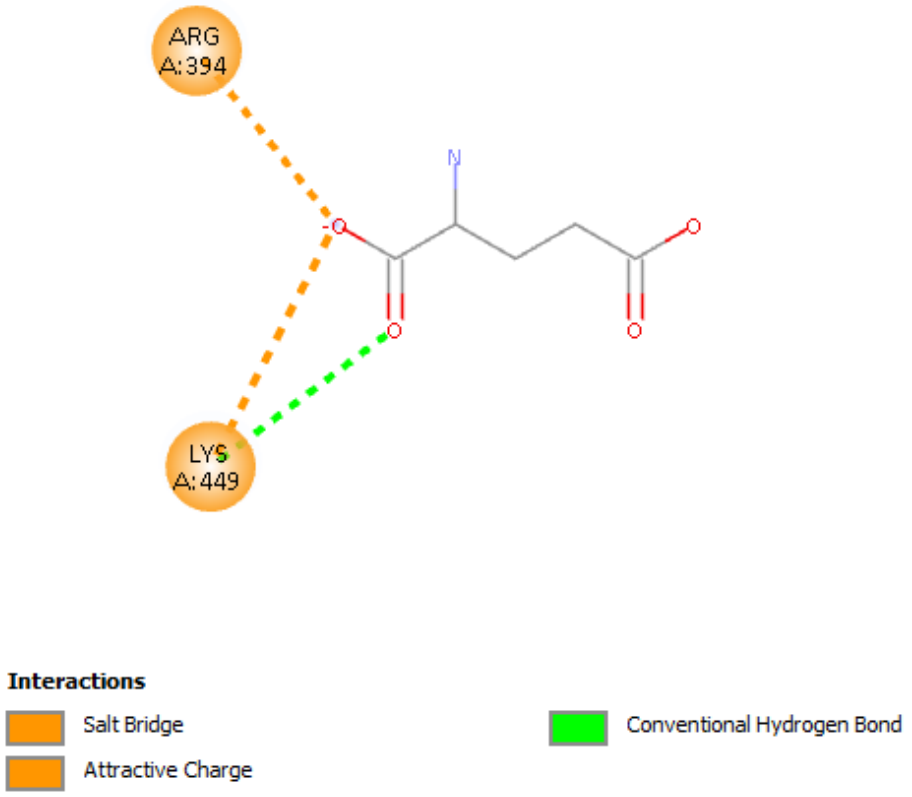

FIGURE 4.23: Molecular interaction analysis of L-glutamic acid with (ERα).

4.5.1.15 L-Lysine–ERα Interaction Analysis

The molecular interaction analysis of L-lysine with the estrogen receptor alpha (ERα) is shown in Figure 4.24. The ligand formed four conventional hydrogen bonds, including two interactions with Ile386, one interaction with Arg394 (3.22 Å), and one interaction with Pro325 (2.46 Å), establishing favorable interactions within the receptor binding pocket.

In addition, two attractive charge interactions were observed with Lys449 and Glu353, while a salt bridge interaction was established with Lys449.

The amino and carboxyl functional groups of L-lysine facilitated these hydrogen-bonding and electrostatic interactions, thereby contributing to the stabilization of the protein–ligand complex within the receptor binding pocket.

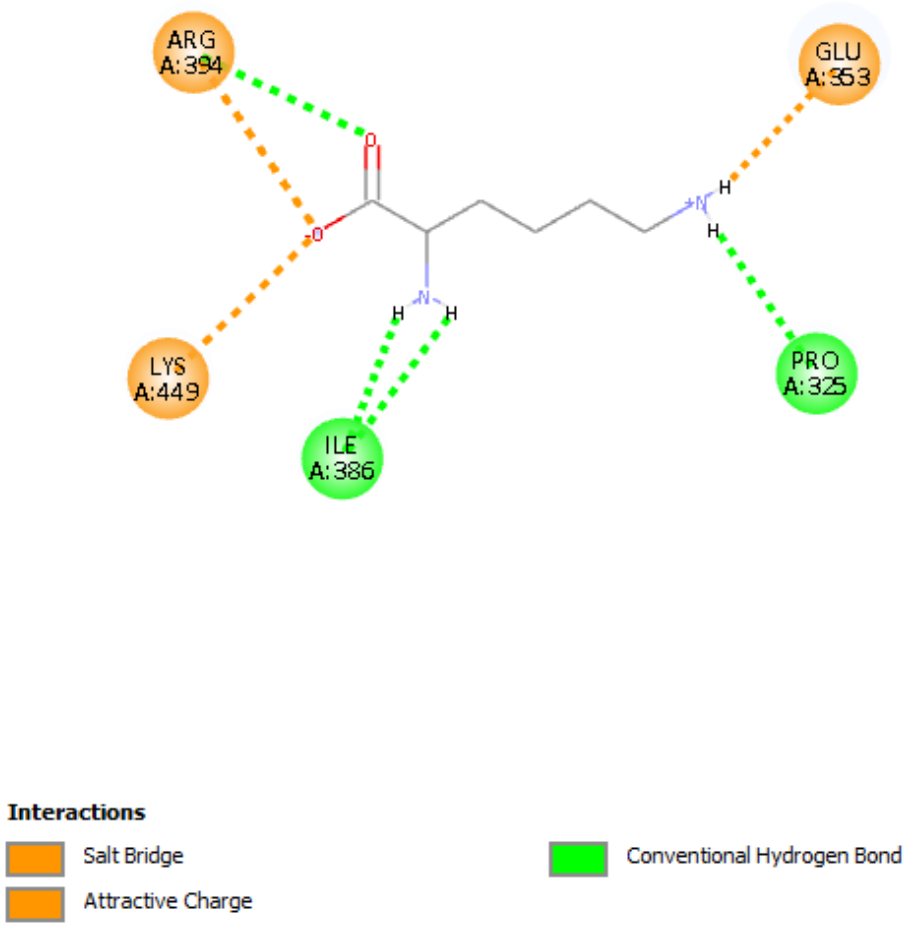

FIGURE 4.24: Molecular interaction analysis of L-lysine with (ERα).

4.5.1.16 L-Aspartic Acid–ERα Interaction Analysis

The molecular interaction analysis of L-aspartic acid with the estrogen receptor alpha (ERα) is shown in Figure 4.25. The ligand formed one conventional hydrogen bond and one attractive charge interaction with Arg394 (3.02 Å), establishing favorable interactions within the receptor binding pocket. In addition, one carbon hydrogen bond was observed with Gly390 (5.35 Å), while a salt bridge interaction was established with Lys449.

A π–anion interaction involving Trp360 further contributed to the stabilization of the protein–ligand complex. The amino and carboxyl functional groups of L-aspartic acid facilitated hydrogen-bonding and electrostatic interactions, thereby

contributing to stable binding within the receptor binding pocket.

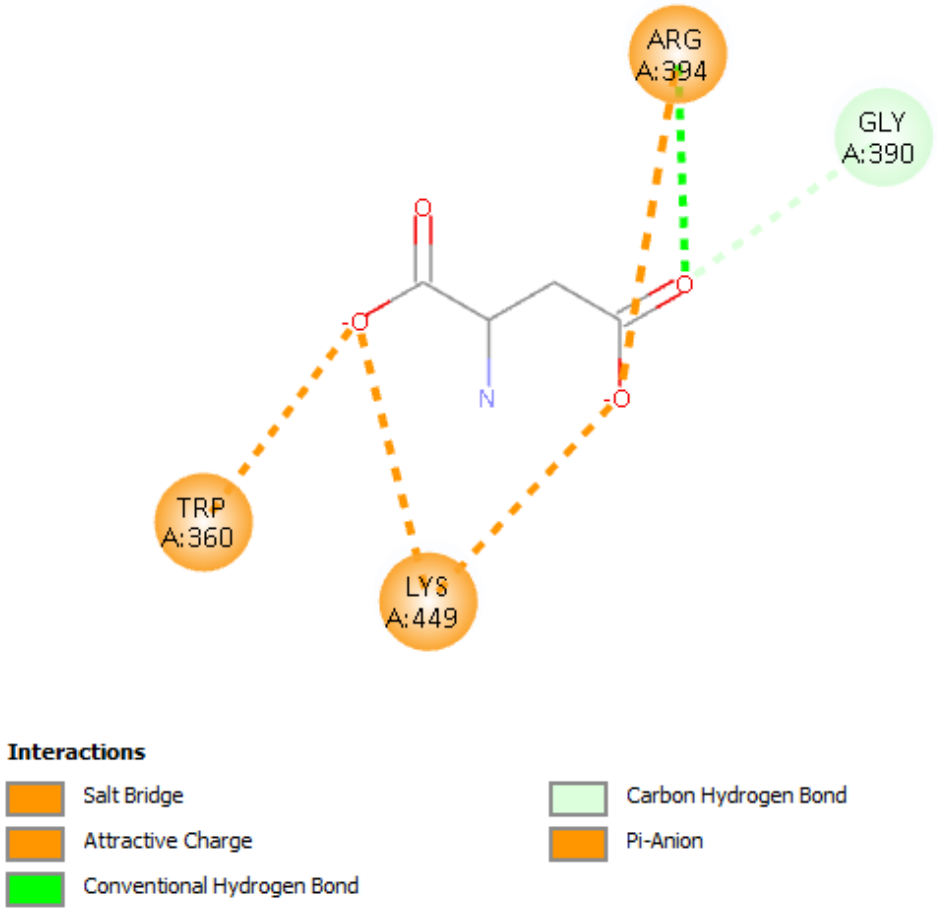

FIGURE 4.25: Molecular interaction analysis of L-aspartic acid with the estrogen receptor alpha (ERα).

4.5.1.17 Hexose–HER2 Interaction Analysis

The molecular interaction analysis of Hexose with the HER2 is shown in Figure 4.26. The ligand established three conventional hydrogen bonds with Val777 (2.07 Å), Ser787 (3.01 Å), and Thr866 (2.77 Å), establishing favorable interactions within the receptor binding pocket. In addition, two unfavorable donor–donor interactions were observed with Phe868 at distances of 2.49 Å and 2.71 Å.

The multiple hydroxyl groups present on the pyranose ring of Hexose promoted hydrogen-bond formation with key active-site residues, thereby contributing to

the stabilization of the protein–ligand complex despite the presence of unfavorable donor–donor interactions.

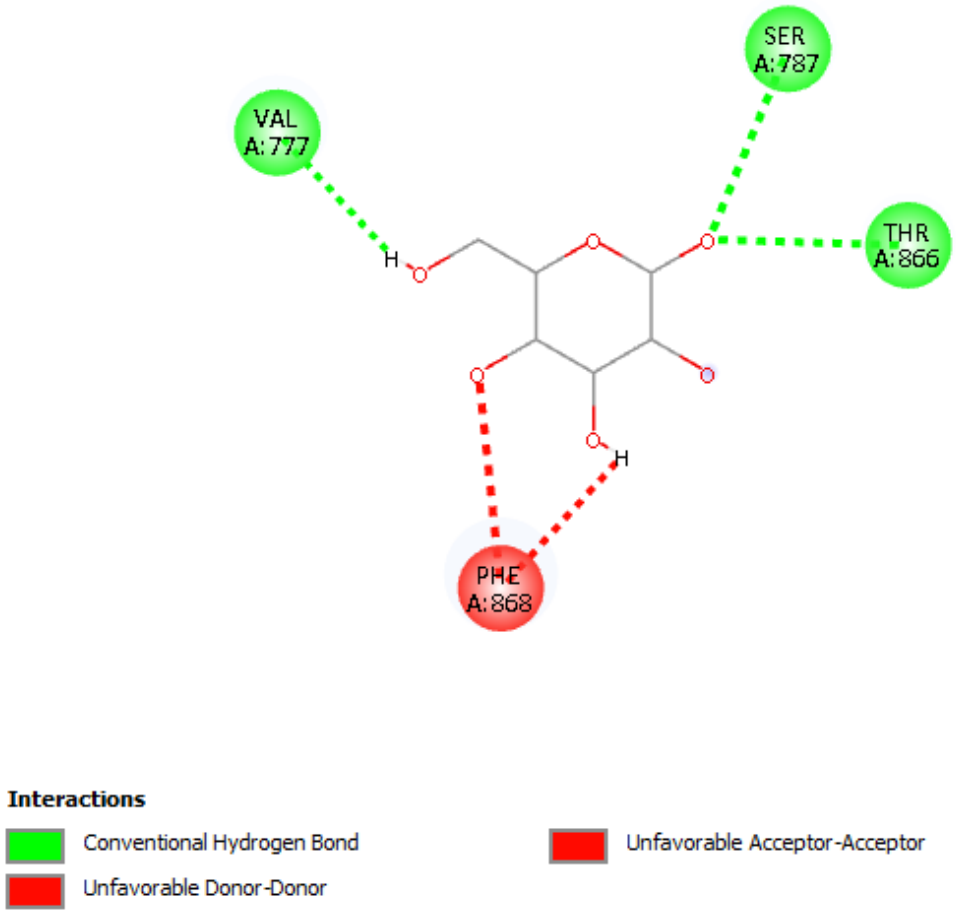

FIGURE 4.26: Molecular interaction analysis of Hexose with the HER2.

4.5.1.18 Betaine–HER2 Interaction Analysis

The molecular interaction analysis of Betaine with the HER2 is shown in Figure 4.27. The ligand formed three conventional hydrogen bonds with Ser787 (3.08 Å), Asp867 (3.15 Å), and Phe868 (2.96 Å), establishing favorable interactions within the receptor binding pocket.

In addition, attractive charge and π–anion interactions were observed with Asp867, while carbon hydrogen bonds were established with Phe868, further strengthening

the protein–ligand interactions. The quaternary ammonium and carboxyl functional groups of Betaine facilitated these electrostatic and hydrogen-bond interactions, thereby enhancing the stability of the protein–ligand complex.

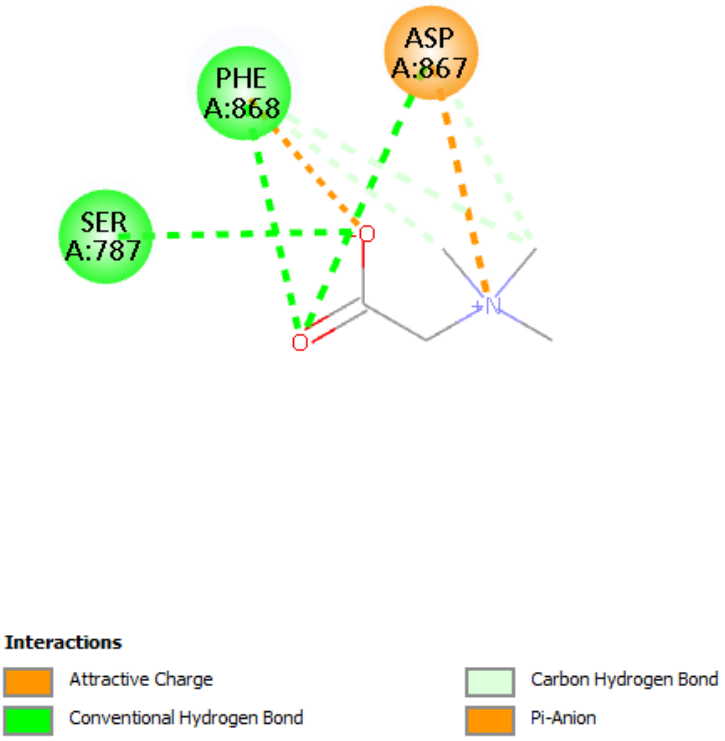

FIGURE 4.27: Molecular interaction analysis of Betaine with the HER2.

4.5.1.19 β-D-Glucose–HER2 Interaction Analysis

The molecular interaction analysis of β-D-Glucose with the HER2 is shown in Figure 4.28. The ligand formed four conventional hydrogen bonds involving Thr866 (2.74 Å), two interactions with Ser787 (2.44 Å), and Asp867 (2.59 Å), establishing favorable interactions within the receptor binding pocket. In addition, one carbon hydrogen bond was established with Arg788 (2.66 Å), further contributing to the stability of the ligand–protein complex. The multiple hydroxyl groups present on the non-aromatic pyranose ring promoted hydrogen-bond formation, thereby

facilitating stable binding within the receptor binding pocket. Nevertheless, one unfavorable donor–donor interaction involving Asp867 was also observed.

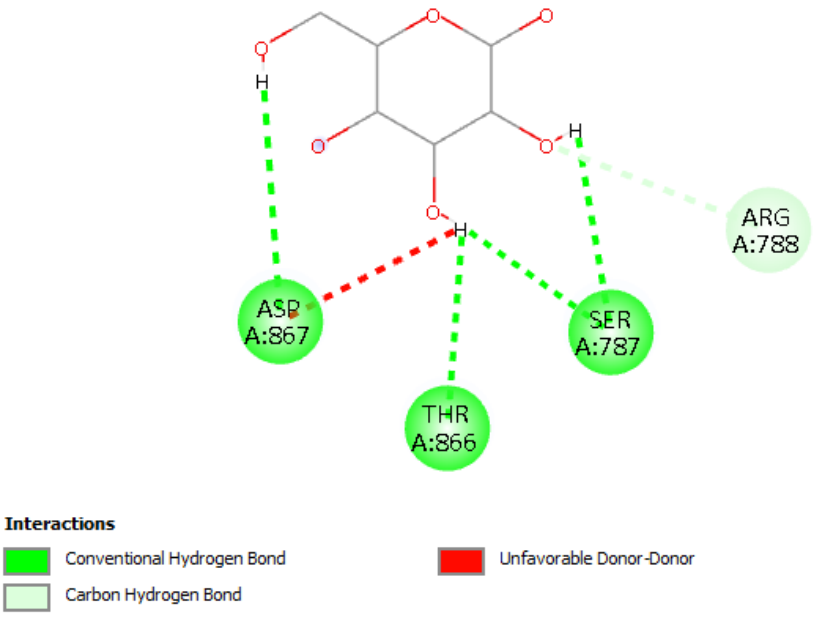

FIGURE 4.28: Molecular interaction analysis of β-D-Glucose with the HER2.

4.5.1.20 L-Tryptophan–HER2 Interaction Analysis

The molecular interaction analysis of L-tryptophan with the HER2 is shown in Figure 4.29. The ligand established five conventional hydrogen bonds with Ser787 (2.37 Å), Lys753 (2.54 Å and 2.58 Å), and Ala751 (3.17 Å), establishing favorable interactions within the receptor binding pocket. In addition, one carbon hydrogen bond was formed with Thr866. The indole ring of L-tryptophan participated in one pi–sigma interaction with Leu789 and three pi–alkyl interactions involving Val777, Leu800, and Leu870, further contributing to the stabilization of the protein–ligand complex. Overall, the predominance of hydrogen-bonding and hydrophobic interactions indicates stable binding of L-tryptophan within the HER2 receptor binding pocket.

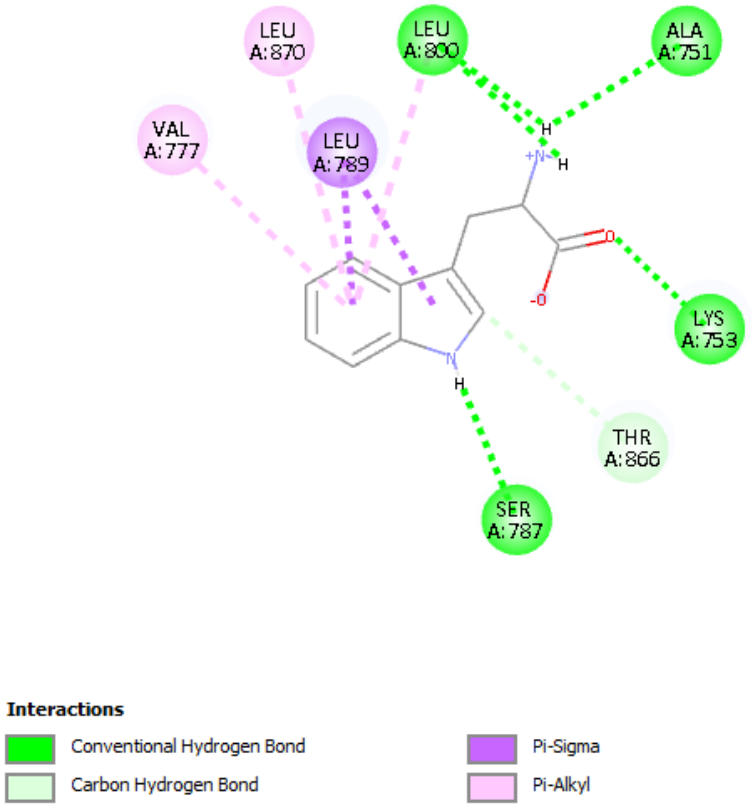

FIGURE 4.29: Molecular interaction analysis of L-tryptophan with the HER2.

4.5.1.21 L-Isoleucine–HER2 Interaction Analysis

The molecular interaction analysis of L-isoleucine with the HER2 is shown in Figure 4.30. The ligand formed six conventional hydrogen bonds with Ser787 (3.13 Å), Thr866 (2.90 Å), Asp867 (2.98 Å), and three interactions with Phe868 (2.17 Å), establishing favorable interactions within the receptor binding pocket. In addition, alkyl interactions were observed with Lys753, Leu800, and Leu870, further contributing to the stabilization of the ligand–protein complex. The amino and carboxyl functional groups of L-isoleucine facilitated hydrogen-bond formation, while its branched aliphatic side chain contributed to hydrophobic interactions, thereby promoting stable binding within the receptor binding pocket. Nevertheless, an unfavorable negative–negative interaction was also observed; however, the

overall interaction profile remained favorable because of the predominance of stabilizing interactions.

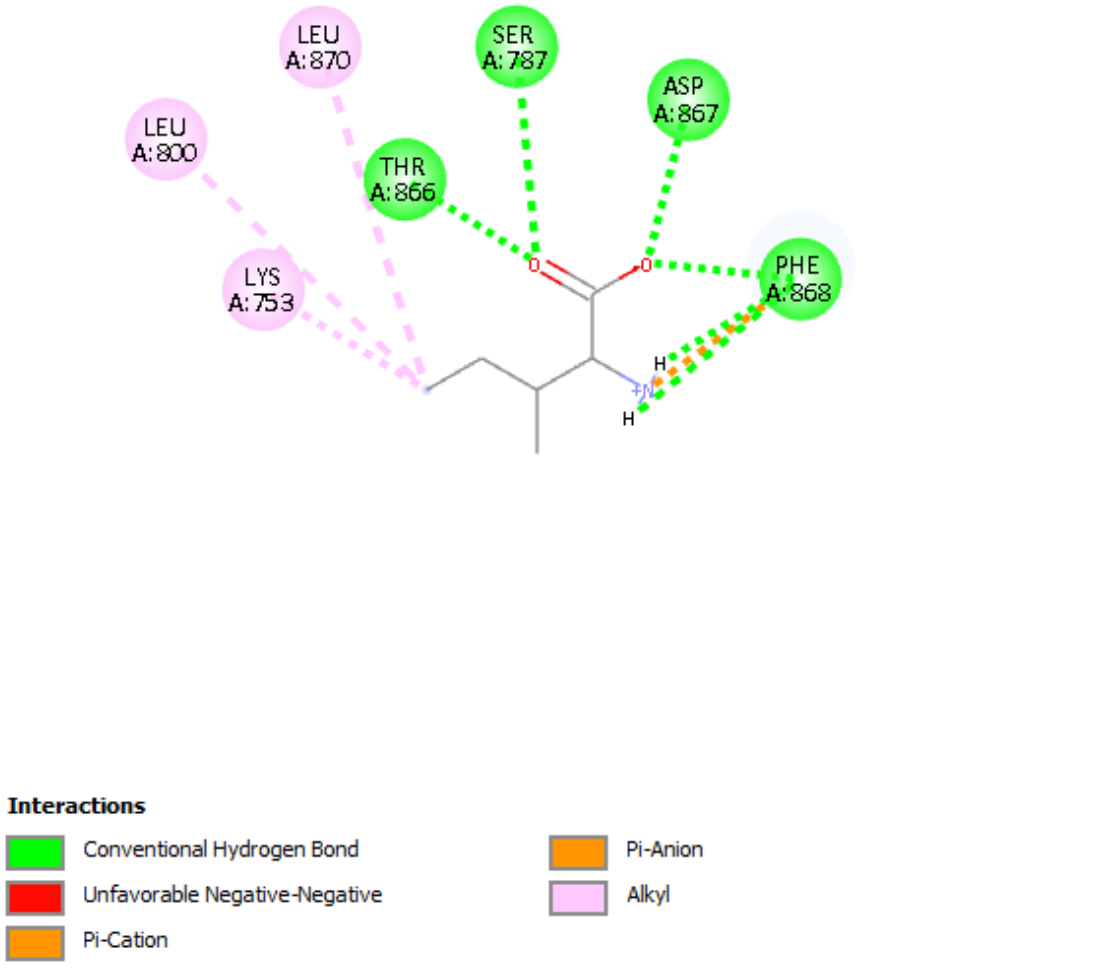

FIGURE 4.30: Molecular interaction analysis of L-isoleucine with the HER2.

4.5.1.22 L-Glutamic Acid–HER2 Interaction Analysis

The molecular interaction analysis of L-glutamic acid with the HER2 is shown in Figure 4.31. The ligand formed five conventional hydrogen bonds with Lys753 (3.16 Å and 2.14 Å), Leu800, Thr866, Ser787, and Phe868, establishing favorable interactions within the receptor binding pocket. The amino and carboxyl functional groups of L-glutamic acid facilitated hydrogen-bond formation, thereby enhancing the stability of the protein–ligand complex.

Nevertheless, one unfavorable negative–negative interaction involving Asp867 was also observed; however, the overall interaction profile remained favorable because of the predominance of stabilizing interactions.

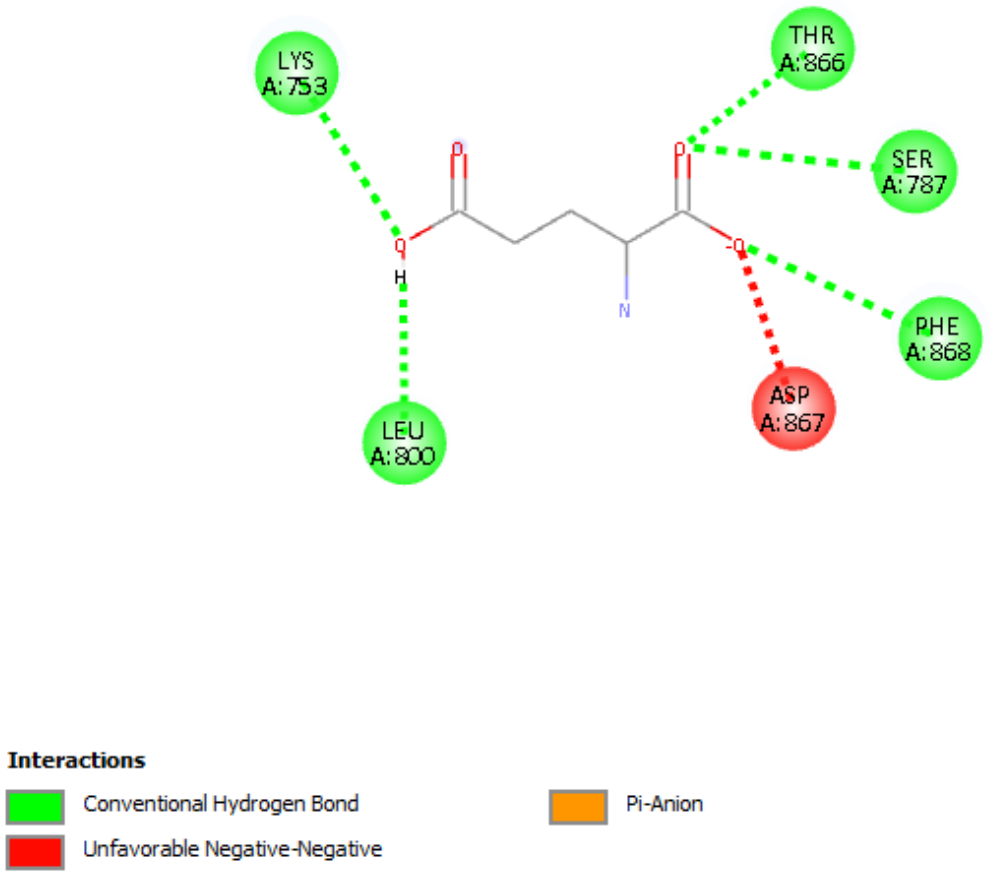

FIGURE 4.31: Molecular interaction analysis of L-glutamic acid with the HER2.

4.5.1.23 L-Lysine–HER2 Interaction Analysis

The molecular interaction analysis of L-lysine with the HER2 is shown in Figure 4.32. The ligand formed four conventional hydrogen bonds, including two interactions with Thr866 (2.27 Å and 2.88 Å), one interaction with Ser787 (2.94 Å), and one interaction with Phe868 (2.89 Å), establishing favorable interactions within the receptor binding pocket.

In addition, one attractive charge interaction was observed with Asp867. The amino and carboxyl functional groups of L-lysine facilitated hydrogen-bonding and electrostatic interactions, thereby enhancing the stability of the protein–ligand complex.

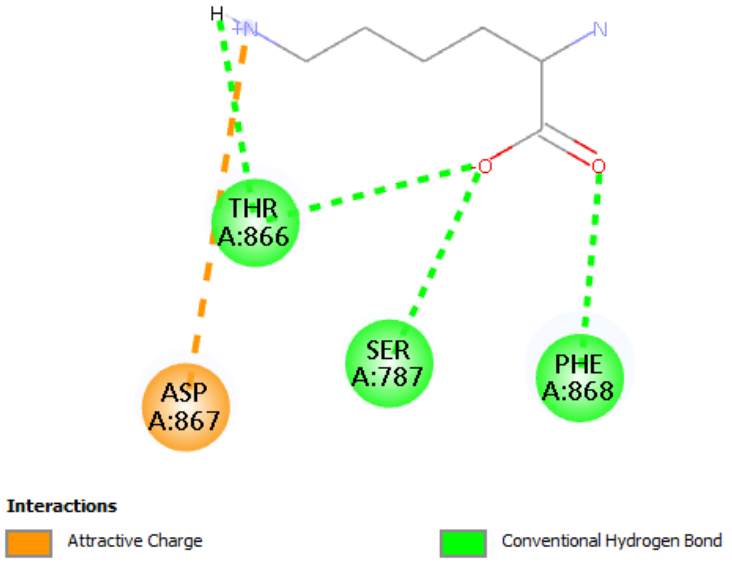

FIGURE 4.32: Molecular interaction analysis of L-lysine with the HER2.

4.5.1.24 L-Aspartic Acid–HER2 Interaction Analysis

The molecular interaction analysis of L-aspartic acid with the HER2 is shown in Figure 4.33. The ligand formed five conventional hydrogen bonds with Ser787 (2.97 Å), Thr866 (2.20 Å, 2.76 Å, and 2.78 Å), and Phe868 (2.95 Å), establishing favorable interactions within the receptor binding pocket. In addition, attractive charge and π–anion interactions were observed with Lys753, while a further π–anion interaction was established with Phe868.

The amino and carboxyl functional groups of L-aspartic acid facilitated hydrogen-bonding and electrostatic interactions, thereby enhancing the stability of the protein–ligand complex.

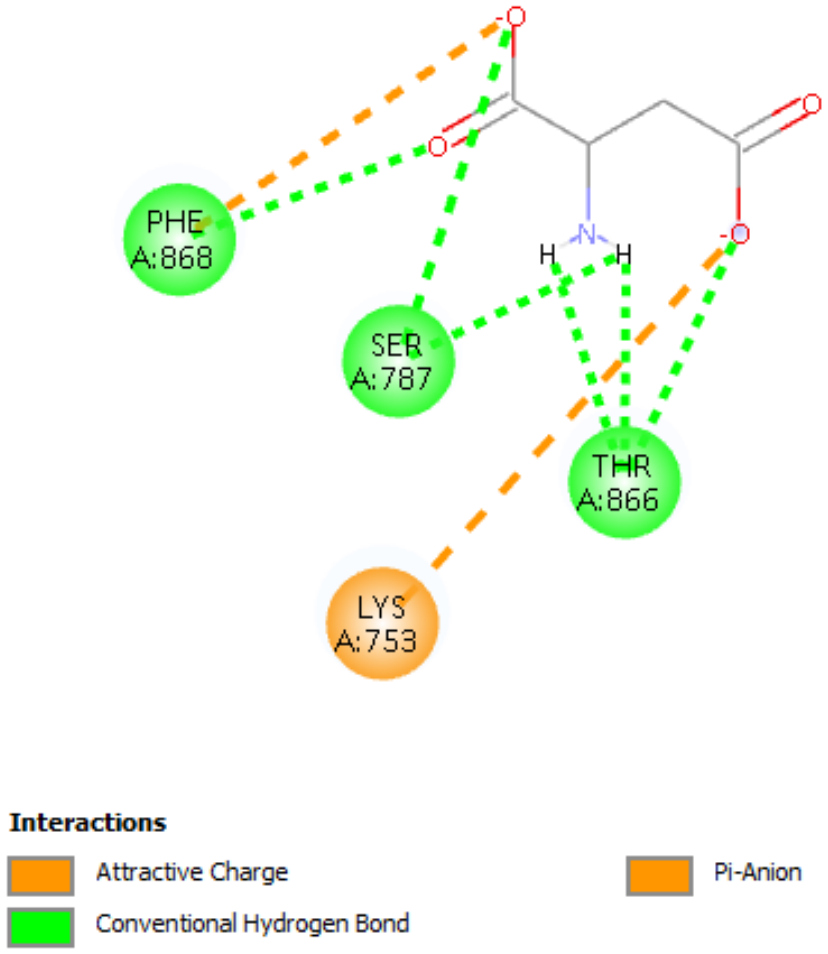

FIGURE 4.33: Molecular interaction analysis of L-aspartic acid with the HER2.

Collectively, the interaction analysis demonstrated that the selected phytochemicals established multiple favorable interactions within the binding pockets of the target proteins, including conventional hydrogen-bonds, salt-bridges, attractive-charge interactions, and π-mediated interactions.

These molecular contacts contributed to the stability of the ligand–protein complexes and were consistent with the molecular docking results. Among the investigated compounds, L-tryptophan exhibited a diverse interaction profile with key active-site residues across the selected target proteins.

It indicates stable binding within the receptor binding pockets and supporting its potential as a promising lead compound for further investigation.

4.6 Lead Compound Selection

Among the ten selected phytochemicals, eight compounds complied with Lipinski's RO5, exhibiting acceptable molecular weight (≤500 Da), suitable lipophilicity (logP), and permissible numbers of hydrogen bond donors and acceptors. In contrast, Inulin and PNPP disodium hexahydrate exhibited multiple violations of the drug-likeness criteria and were therefore excluded from subsequent molecular docking studies.

Following the comprehensive evaluation of physicochemical properties, ADMET profiles, molecular docking, and protein–ligand interaction analyses, L-tryptophan [(2S)-2-ammonio-3-(1H-indol-3-yl)propanoate] emerged as the most promising lead compound. It demonstrated a balanced pharmacokinetic and safety profile, complete compliance with Lipinski's RO5, favorable predicted toxicity, and stable interactions with all selected breast cancer-associated target proteins. Although Tamoxifen exhibited stronger docking scores against the selected targets, L-tryptophan displayed favorable drug-likeness, stable binding interactions, and a superior predicted safety profile, supporting its potential as a promising natural lead compound for further investigation.

4.6.1 ADMET Analysis

4.6.1.1 Absorption

L-tryptophan exhibited relatively high predicted human intestinal absorption (75.06%) together with good Caco-2 permeability, indicating efficient gastrointestinal uptake compared with the other selected phytochemicals.

4.6.1.2 Distribution

The compound showed moderate plasma protein binding and limited penetration across the blood–brain barrier and central nervous system. This characteristic is

advantageous for minimizing potential CNS-related adverse effects in non-CNS-targeted cancer therapy.

4.6.1.3 Metabolism

L-tryptophan did not exhibit inhibitory effects toward the major CYP enzymes, suggesting a low potential for drug–drug interactions and predictable metabolic behavior.

4.6.1.4 Excretion

The compound demonstrated moderate predicted total clearance and was not predicted to be a substrate of the renal OCT2 transporter, indicating that renal OCT2-mediated elimination is unlikely to play a major role in its excretion.

4.6.1.5 Toxicity

L-tryptophan was predicted to be non-mutagenic, non-hepatotoxic, and non cardiotoxic, with no evidence of skin sensitization, indicating a favorable safety profile. Based on the comprehensive evaluation of physicochemical properties, ADMET characteristics, molecular docking, and protein–ligand interaction analyses, L-tryptophan was identified as the most promising lead compound among the selected phytochemicals. It exhibited the most favorable overall docking performance against the selected target proteins, with docking scores of -7.6 kcal/mol against AR, -7.0 kcal/mol against ERα, and -7.4 kcal/mol against HER2. Furthermore, interaction analysis revealed multiple conventional hydrogen bonds, attractive charge interactions, and π-mediated interactions with key active-site residues, supporting the formation of stable protein–ligand complexes.

Together with its favorable ADMET profile, including efficient intestinal absorption, predictable metabolic behavior, moderate clearance, and low predicted toxicity, these findings support the selection of L-tryptophan as the lead compound for subsequent comparison with the reference drug, Tamoxifen.

4.7 Drug Selection

The KEGG database identified several therapeutic agents associated with breast cancer treatment, including Tamoxifen, Fulvestrant, Raloxifene, Toremifene, Letrozole, Anastrozole, Exemestane, Lapatinib, Alpelisib, and Capecitabine. Monoclonal antibody therapies were not included in this study due to their high molecular weight and their limited compatibility with conventional molecular docking and ADMET prediction methods. In addition, cytotoxic chemotherapeutic agents were not selected as reference compounds because their mechanisms of action are not directly associated with the receptor-mediated signaling pathways investigated in the present study.

Among the remaining small-molecule therapeutic agents, Tamoxifen was selected as the reference drug because of its widespread clinical use, well-established efficacy in breast cancer treatment, and extensively characterized pharmacokinetic profile. Moreover, Tamoxifen has been widely employed as a reference compound in computational studies involving breast cancer-associated targets. Therefore, it was used as the benchmark drug for comparative molecular docking, protein–ligand interaction, and pharmacokinetic analyses against the androgen receptor (AR), ERα, and HER2. The selected phytochemicals derived from *Helianthus tuberosus* were subsequently compared with Tamoxifen to evaluate their therapeutic potential.

4.7.1 Tamoxifen

Tamoxifen is a selective estrogen receptor modulator (SERM) that is widely used for the treatment and prevention of hormone receptor-positive breast cancer [122]. Its therapeutic activity is primarily attributed to its ability to competitively bind to estrogen receptors in breast tissue, thereby blocking estrogen-dependent signaling pathways involved in tumor initiation and progression [122]. Owing to its proven clinical efficacy and long-established therapeutic use, Tamoxifen has become one of the most widely prescribed endocrine therapies for breast cancer

management [123]. Consequently, it was selected as the reference drug for comparative molecular docking, protein–ligand interaction, and pharmacokinetic analyses in the present study.

Figure 4.34 illustrates the molecular mechanism through which Tamoxifen exerts its therapeutic effects in ER-positive breast cancer. By competitively binding to estrogen receptors (ER), Tamoxifen prevents the interaction of estrogen (E2) with its receptor, thereby inhibiting receptor activation. This suppresses the activation of estrogen response elements (EREs) and limits the recruitment of transcriptional coactivators, resulting in reduced expression of estrogen-responsive genes.

Furthermore, Tamoxifen suppresses the PI3K/AKT/mTOR signaling pathway, leading to decreased transcription of genes associated with cell proliferation, survival, and tumor progression. Collectively, these mechanisms inhibit breast cancer cell proliferation and slow disease progression [124].

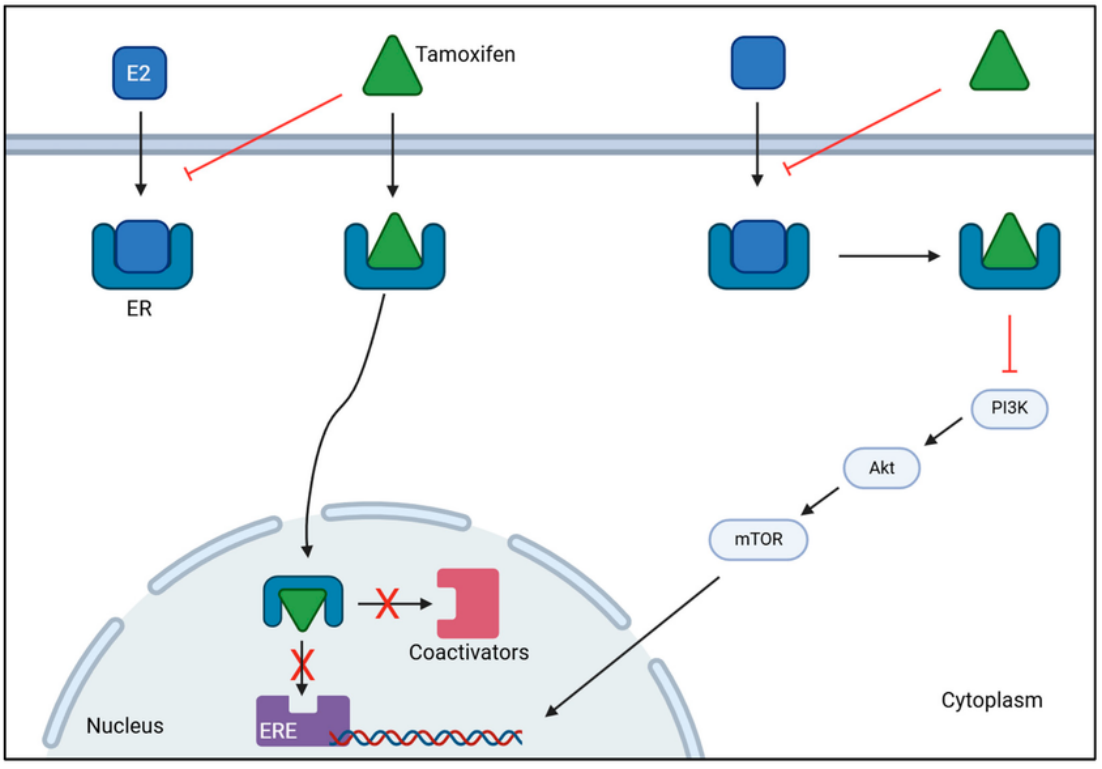

FIGURE 4.34: Mechanism of action of Tamoxifen in estrogen receptor-positive (ER-positive) breast cancer cells [124].

4.7.2 Physicochemical Properties

The physicochemical properties of Tamoxifen obtained from the PubChem database are summarized in Table 4.21. Tamoxifen has a molec. formula of $C_{26}H_{29}NO$ and a molec. weight of 371.52 g/mol. These physicochemical characteristics support its suitability as an orally active therapeutic agent and contribute to its pharmacokinetic behavior. Three dimensional structure of tamoxifen is shown in Figure 4.35.

TABLE 4.21: Physicochemical characteristics of Tamoxifen (PubChem).

Property	**Value**
Compound Name	Tamoxifen
PubChem CID	2733526
Molecular Formula	$C_{26}H_{29}NO$
Molecular Weight	371.52 g/mol

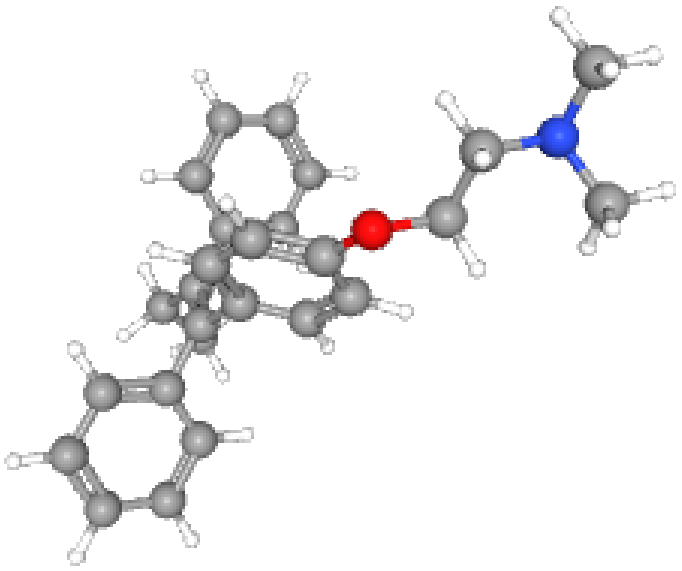

FIGURE 4.35: Three-dimensional (3D) structure of Tamoxifen retrieved from PubChem.

4.7.3 Lipinski's Rule of Five

The Lipinski's RO5 assessment for Tamoxifen, obtained using the SwissADME web server, is summarized in Table 4.22. Tamoxifen exhibited a molecular weight of 371.51 g/mol, two hydrogen bond acceptors, no hydrogen bond donors, and eight rotatable bonds. Although the compound showed one Lipinski violation due to its consensus LogP value of 6.06, which exceeds the recommended threshold of 5, it satisfied the overall drug-likeness criteria. Therefore, Tamoxifen was considered a suitable candidate for oral administration.

TABLE 4.22: Lipinski's Rule of Five properties of Tamoxifen (SwissADME).

Property	**Value**
Compound	Tamoxifen
Molecular Weight (MW)	371.51 g/mol
Consensus LogP	6.06
Hydrogen Bond Acceptors (HBA)	2
Hydrogen Bond Donors (HBD)	0
Rotatable Bonds (RB)	8
Lipinski's Rule	Yes (1 violation: LogP $>$ 5)

4.7.4 ADMET Analysis of Tamoxifen

The pharmacokinetic and toxicity characteristics of Tamoxifen were evaluated through ADMET analysis to assess its suitability as a therapeutic agent. Predictions related to absorption, distribution, metabolism, excretion, and toxicity were generated using the pkCSM web server, providing valuable insights into the compound's pharmacokinetic behavior and safety profile.

4.7.4.1 Absorption Profile

The absorption characteristics of Tamoxifen predicted by the pkCSM web server are summarized in Table 4.23. Tamoxifen exhibited low water solubility (−5.929 log mol/L) and favorable Caco-2 permeability (1.065), indicating good membrane permeability. A high predicted human intestinal absorption value of 96.885% suggests efficient uptake following oral administration.

In addition, Tamoxifen showed low skin permeability, indicating limited potential for transdermal absorption. The compound was also predicted to act as both a substrate and an inhibitor of P-glycoprotein, suggesting that efflux transporters may influence its absorption and overall pharmacokinetic behavior.

TABLE 4.23: Absorption properties of Tamoxifen predicted using pkCSM.

Property	**Value**
Water solubility (log mol/L)	−5.929
Caco-2 permeability (log Papp in 10^{-6} cm/s)	1.065
Human intestinal absorption (%)	96.885
Skin permeability (log Kp)	−2.737
P-glycoprotein substrate	Yes
P-glycoprotein I inhibitor	Yes
P-glycoprotein II inhibitor	Yes

4.7.4.2 Distribution Profile

The pkCSM web server was used to predict the distribution properties of Tamoxifen, and the corresponding results are presented in Table 4.24.

The predicted volume of distribution at steady state (VD_{ss}) of 0.83 log L/kg suggests that Tamoxifen is distributed beyond the bloodstream into body tissues.

The low fraction unbound (Fu) value of 0.093 indicates extensive plasma protein binding.

Furthermore, a blood–brain barrier (BBB) permeability value of 1.329 suggests that Tamoxifen readily crosses the BBB. The predicted central nervous system (CNS) permeability value of −1.473 indicates moderate penetration into the central nervous system.

TABLE 4.24: Distribution properties of Tamoxifen predicted using pkCSM.

Property	**Value**
VD_{ss} (human) (log L/kg)	0.83
Fraction unbound (Fu)	0.093
BBB permeability (log BB)	1.329
CNS permeability (log PS)	−1.473

4.7.4.3 Metabolism Profile

The metabolism-related properties of Tamoxifen are given in Table 4.25. The results indicate that Tamoxifen is predicted to be a substrate of CYP3A4 but not CYP2D6, suggesting that CYP3A4 plays a major role in its metabolism.

In addition, Tamoxifen was predicted to inhibit CYP1A2 and CYP2D6, indicating the potential for drug–drug interactions involving compounds metabolized by these enzymes.

No inhibitory activity was predicted against CYP2C19, CYP2C9, or CYP3A4, suggesting a lower likelihood of interactions involving these metabolic pathways.

TABLE 4.25: Metabolism properties of Tamoxifen predicted using pkCSM.

Property	**Predicted Value**
CYP2D6 substrate	No
CYP3A4 substrate	Yes
CYP1A2 inhibitor	Yes
CYP2C19 inhibitor	No
CYP2C9 inhibitor	No
CYP2D6 inhibitor	Yes
CYP3A4 inhibitor	No

4.7.4.4 Excretion Profile

The excretion profile of Tamoxifen is presented in Table 4.26. The predicted total clearance value of 0.556 indicates moderate elimination of the compound from the body. In addition, Tamoxifen was not predicted to be a substrate of the renal organic cation transporter 2 (OCT2), suggesting that OCT2-mediated renal excretion is unlikely to contribute significantly to its overall clearance.

TABLE 4.26: Excretion properties of Tamoxifen predicted using pkCSM.

Property	**Value**
Total clearance	0.556
Renal OCT2 substrate	No

4.7.4.5 Toxicity Profile

The toxicity analysis of Tamoxifen is provided in Table 4.27. The results predicted positive AMES toxicity and inhibitory activity against both hERG I and hERG II channels. The predicted maximum tolerated dose in humans was 0.313

TABLE 4.27: Toxicity properties of Tamoxifen predicted using pkCSM.

Property	**Value**
AMES toxicity	Yes
Maximum tolerated dose (human) (log mg/kg/day)	0.313
hERG I inhibitor	Yes
hERG II inhibitor	Yes
LD_{50} (oral rat acute) (mol/kg)	2.285
LOAEL (oral rat chronic) (log mg/kg/-day)	0.41
Hepatotoxicity	No
Skin sensitization	No
Tetrahymena pyriformis toxicity	0.316
Minnow toxicity	0.6

log mg/kg/day, whereas the oral rat acute toxicity (LD_{50}) and chronic toxicity (LOAEL) values were estimated to be 2.285 mol/kg and 0.41 log mg/kg/day, respectively. In contrast, no hepatotoxicity or skin sensitization potential was predicted. Furthermore, the predicted *Tetrahymena pyriformis* toxicity and minnow toxicity values were 0.316 and 0.6, respectively, providing additional insight into the environmental and biological toxicity profile of Tamoxifen.

4.7.5 Molecular Docking of Tamoxifen with Target Proteins

The molecular docking results of Tamoxifen against the selected breast cancer-associated target proteins are summarized in Table 4.28. Among the evaluated

targets, Tamoxifen exhibited the strongest binding affinity toward the androgen receptor (AR), with a docking score of −9.2 kcal/mol, followed by the HER2 (−8.6 kcal/mol) ERα (−7.8 kcal/mol).

These docking scores indicate favorable interactions between Tamoxifen and the selected target proteins, supporting the formation of stable protein–ligand complexes and confirming its suitability as a reference compound for subsequent comparative analyses.

TABLE 4.28: Molecular docking results of Tamoxifen against breast cancer-associated target proteins.

Protein	**Cavity Volume (Å^3)**	**Docking Score (kcal/-mol)**	**Structure**
AR	2398	−9.2	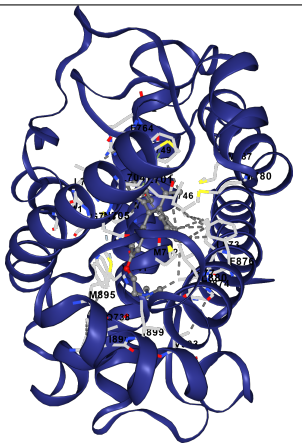
ERα	1983	−7.8	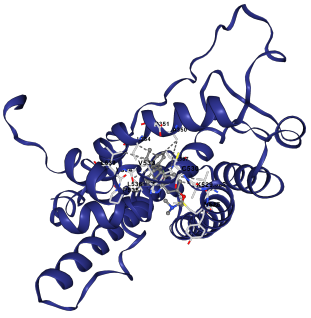
HER2	1099	−8.6	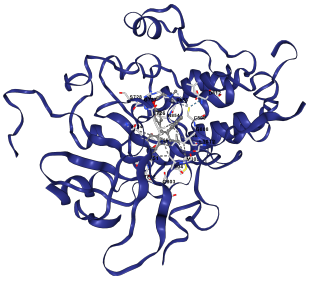

4.7.5.1 Tamoxifen–AR Interaction Analysis

The molecular interaction analysis of Tamoxifen with the androgen receptor (AR) is shown in Figure 4.36. The reference drug established one π–donor hydrogen bond with Gln711 (3.97 Å) and two pi–pi T-shaped interactions with Trp741 (5.06 Å) and Phe764 (5.48 Å). In addition, two π–σ interactions involving Met742 and Met780 (4.42 Å) were identified.

The aromatic phenyl rings of Tamoxifen also participated in multiple hydrophobic alkyl and π–alkyl interactions with Met745, Met749, Leu704, Leu873, Ala877, and Met895, thereby contributing to the stabilization of the protein–ligand complex within the receptor binding pocket.

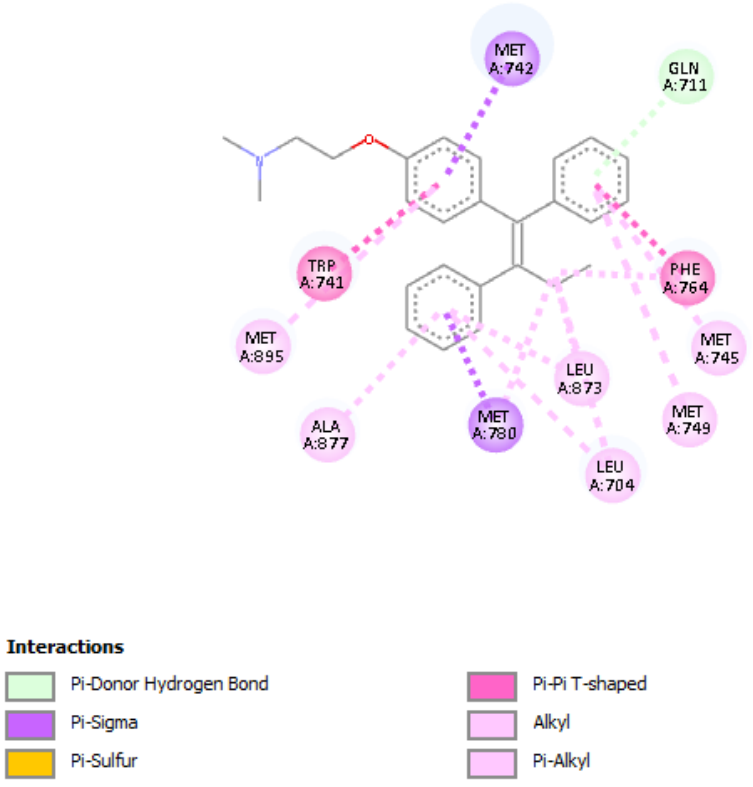

FIGURE 4.36: Interaction profile of Tamoxifen with the androgen receptor (AR).

4.7.5.2 Tamoxifen–ERα Interaction Analysis

The molecular interaction analysis of Tamoxifen with ERα is shown in Figure 4.37. The reference drug exhibited one π–σ interaction with Ile424 (4.10 Å) and established several hydrophobic alkyl and π–alkyl interactions with Met421, Met388, Leu525, Ala350, Leu346, and Leu387.

The three aromatic phenyl rings of Tamoxifen facilitated these hydrophobic interactions, thereby contributing to the stabilization of the protein–ligand complex and promoting favorable binding within the receptor binding pocket.

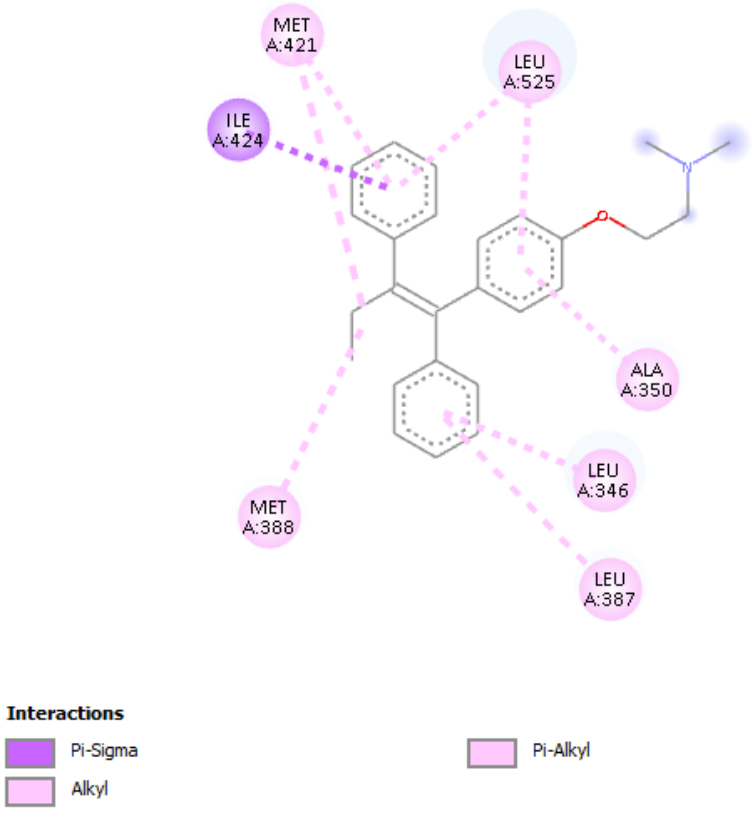

FIGURE 4.37: Interaction profile of Tamoxifen with (ERα).

4.7.5.3 Tamoxifen–HER2 Interaction Analysis

The molecular interaction analysis of Tamoxifen with the HER2 is shown in Figure 4.38. The ligand established one π–donor hydrogen bond with Thr866 (4.15 Å), establishing favorable interactions within the receptor binding pocket. In addition, one π–sulfur interaction was observed with Cys809 (5.10 Å). The aromatic phenyl

rings of Tamoxifen further participated in one alkyl interaction with Ala751 and four π–alkyl interactions involving Leu726, Leu856, Leu1012, and Val734, thereby contributing to the stabilization of the protein–ligand complex through hydrophobic contacts.

Overall, the predominance of hydrophobic interactions together with the π–donor hydrogen bond suggests stable binding of Tamoxifen within the HER2 receptor binding pocket.

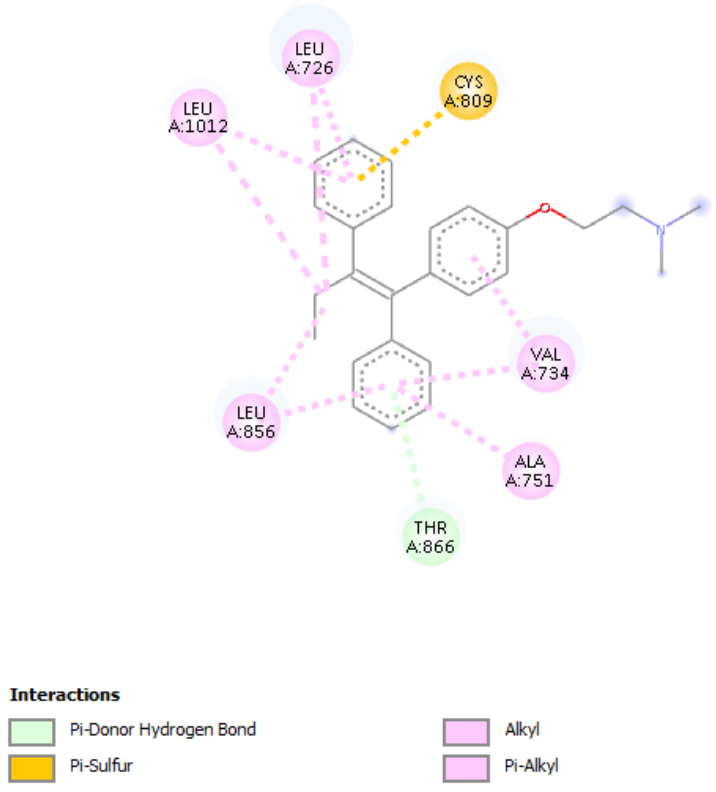

FIGURE 4.38: Interaction profile of Tamoxifen with HER2.

4.8 Comparison of Lead Compound and Drug

L-tryptophan and Tamoxifen were comparatively evaluated based on their physicochemical properties, ADMET profiles, molecular docking results, and protein–ligand interaction patterns. This comprehensive comparison was performed to

assess the therapeutic potential of L-tryptophan relative to the reference drug against the selected breast cancer-associated target proteins.

4.8.1 Comparison of Physicochemical Properties

The physicochemical properties of L-tryptophan and Tamoxifen are compared in Table 4.29. L-tryptophan possesses a lower molec. weight (204.22 g/mol) than Tamoxifen (371.52 g/mol), which is generally considered favorable for drug-likeness and oral bioavailability. In addition, the lower lipophilicity of L-tryptophan compared with Tamoxifen further supports its favorable physicochemical profile. Overall, these characteristics suggest that L-tryptophan possesses desirable physicochemical properties.

TABLE 4.29: Comparative physicochemical characteristics of the lead compound and the reference drug.

Property	**Lead Compound**	**Reference Drug**
Compound Name	L-Tryptophan	Tamoxifen
PubChem CID	6923516	2733526
Molecular Formula	$C_{11}H_{12}N_2O_2$	$C_{26}H_{29}NO$
Molecular Weight	204.22 g/mol	371.52 g/mol

4.8.2 Comparative Evaluation of Lipinski's RO5 (Lead Compound vs. Tamoxifen)

The comparison of the Lipinski's RO5 parameters for L-tryptophan and Tamoxifen is presented in Table 4.30. L-tryptophan exhibited a lower molecular weight, lower lipophilicity (LogP = 0.92), and fewer rotatable bonds than Tamoxifen, indicating favorable physicochemical characteristics for oral drug development. Although Tamoxifen satisfied most of Lipinski's criteria, it exhibited one violation because its LogP value (6.06) exceeded the recommended threshold of 5. In contrast,

L-tryptophan complied with all Lipinski's RO5 criteria, demonstrating favorable drug-like characteristics.

Furthermore, both compounds possessed acceptable numbers of H-bond donors and acceptors, supporting their potential to interact effectively with biological targets. Overall, these findings suggest that L-tryptophan exhibits a more favorable drug-likeness profile than Tamoxifen.

TABLE 4.30: Comparative evaluation of Lipinski's RO5 parameters for L-tryptophan and Tamoxifen.

Property	**L-Tryptophan**	**Tamoxifen**
Molecular Weight (MW)	204.22 g/mol	371.51 g/mol
LogP (Consensus)	0.92	6.06
Hydrogen Bond Acceptors (HBA)	2	2
Hydrogen Bond Donors (HBD)	2	0
Rotatable Bonds (RB)	3	8
Lipinski's Rule Compliance	Yes	Yes (1 violation: LogP > 5)

4.8.3 ADMET Properties Comparison

A comparative ADMET analysis of L-tryptophan and Tamoxifen was performed to evaluate their pharmacokinetic characteristics and predicted toxicity profiles. Key parameters related to absorption, distribution, metabolism, excretion, and toxicity were compared to assess their suitability as potential therapeutic agents for breast cancer treatment.

4.8.3.1 Comparative Assessment of Absorption

The comparative absorption properties of L-tryptophan and Tamoxifen are presented in Table 4.31.

L-tryptophan showed higher aqueous solubility (−2.891 log mol/L) than Tamoxifen (−5.929 log mol/L), indicating improved dissolution potential in biological fluids. Conversely, Tamoxifen exhibited greater Caco-2 permeability (1.065) and predicted human intestinal absorption (96.885%) than L-tryptophan (0.800 and 75.06%, respectively), suggesting more efficient intestinal uptake.

Both compounds displayed comparable skin permeability and were identified as P-glycoprotein substrates. However, only Tamoxifen was predicted to inhibit both P-glycoprotein I and II, whereas L-tryptophan showed no inhibitory activity toward either transporter.

Overall, despite the superior intestinal absorption predicted for Tamoxifen, L-tryptophan demonstrated a favorable absorption profile owing to its higher aqueous solubility and lack of predicted P-glycoprotein inhibitory activity.

TABLE 4.31: Comparative analysis of the predicted absorption properties of L-tryptophan and Tamoxifen.

Property	**L-Tryptophan**	**Tamoxifen**
Water solubility (log mol/L)	−2.891	−5.929
Caco-2 permeability (log Papp in 10^{-6} cm/s)	0.800	1.065
Human intestinal absorption (%)	75.06	96.885
Skin permeability (log Kp)	−2.735	−2.737
P-glycoprotein substrate	Yes	Yes
P-glycoprotein I inhibitor	No	Yes
P-glycoprotein II inhibitor	No	Yes

4.8.3.2 Comparative Assessment of Distribution

The comparative distribution profiles of L-tryptophan and Tamoxifen are presented in Table 4.32. The results demonstrated clear differences in the predicted distribution behavior of the two compounds.

Tamoxifen showed a higher volume of distribution ($VD_{ss} = 0.83$ log L/kg), together with increased blood–brain barrier permeability (log BB = 1.329) and central nervous system permeability (log PS = −1.473), indicating more extensive tissue distribution and enhanced penetration into the brain and central nervous system.

Conversely, L-tryptophan exhibited a higher fraction unbound (Fu = 0.555), suggesting that a larger proportion of the compound remains freely available in the systemic circulation for pharmacological activity.

Overall, these findings indicate that Tamoxifen is more widely distributed throughout body tissues, whereas L-tryptophan may provide greater systemic availability because of its higher unbound fraction while exhibiting limited penetration into the central nervous system.

TABLE 4.32: Comparative analysis of the predicted distribution properties of L-tryptophan and Tamoxifen.

Property	**L-Tryptophan**	**Tamoxifen**
VD_{ss} (Human) (log L/kg)	−0.14	0.83
Fraction unbound (Fu)	0.555	0.093
BBB permeability (log BB)	0.016	1.329
CNS permeability (log PS)	−2.909	−1.473

4.8.3.3 Comparative Assessment of Metabolism

The comparative metabolism properties of L-tryptophan and Tamoxifen are presented in Table 4.33.

L-tryptophan demonstrated a favorable predicted metabolic profile, as it was not identified as either a substrate or an inhibitor of the evaluated cytochrome P450 (CYP450) enzymes.

In contrast, Tamoxifen was predicted to be a substrate of CYP3A4 and an inhibitor of CYP1A2 and CYP2D6.

The absence of predicted CYP450 substrate and inhibitory activity for L-tryptophan suggests a lower likelihood of CYP450-mediated drug–drug interactions and more predictable metabolic behavior.

Overall, these findings indicate that L-tryptophan possesses favorable metabolic characteristics that may contribute to improved safety and reduced variability in drug metabolism.

TABLE 4.33: Comparative analysis of the predicted metabolism-related properties of L-tryptophan and Tamoxifen.

Property	**L-Tryptophan**	**Tamoxifen**
CYP2D6 substrate	No	No
CYP3A4 substrate	No	Yes
CYP1A2 inhibitor	No	Yes
CYP2C19 inhibitor	No	No
CYP2C9 inhibitor	No	No
CYP2D6 inhibitor	No	Yes
CYP3A4 inhibitor	No	No

4.8.3.4 Comparative Assessment of Excretion

The comparative excretion parameters of L-tryptophan and Tamoxifen are presented in Table 4.34.

L-tryptophan showed a higher predicted total clearance value (0.84) than Tamoxifen (0.556), indicating a greater rate of elimination from the body.

Furthermore, both compounds were predicted to be non-substrates of the renal organic cation transporter 2 (OCT2), suggesting that this transporter is unlikely to play a significant role in their renal excretion.

Overall, these findings indicate that L-tryptophan possesses favorable predicted excretion characteristics that may reduce systemic accumulation and support its potential as a therapeutic candidate.

TABLE 4.34: Comparative analysis of the predicted excretion properties of L-tryptophan and Tamoxifen.

Property	**L-Tryptophan**	**Tamoxifen**
Total clearance	0.84	0.556
Renal OCT2 substrate	No	No

4.8.3.5 Comparative Assessment of Toxicity Profiles

The comparative assessment of the toxicity profiles of L-tryptophan and Tamoxifen is presented in Table 4.35. The results indicate that L-tryptophan exhibited a more favorable predicted safety profile than Tamoxifen.

L-tryptophan was predicted to be non-mutagenic (AMES negative) and showed no inhibitory activity toward hERG I or hERG II channels, whereas Tamoxifen demonstrated positive AMES toxicity and potential inhibition of both hERG channels.

In addition, L-tryptophan exhibited a higher predicted maximum tolerated dose and lower predicted chronic toxicity than Tamoxifen, further supporting its favorable toxicological profile. Both compounds were predicted to be non-hepatotoxic and non-sensitizing to the skin.

Overall, these findings suggest that L-tryptophan possesses a more favorable predicted toxicity profile while maintaining desirable pharmacological characteristics.

These in silico toxicity predictions indicate that L-tryptophan may have a lower risk of adverse effects during therapeutic use.

TABLE 4.35: Comparative analysis of the predicted toxicity profiles of L-tryptophan and Tamoxifen.

Property	**L-Tryptophan**	**Tamoxifen**
AMES toxicity	No	Yes
Maximum tolerated dose (human) (log mg/kg/day)	0.764	0.313
hERG I inhibitor	No	Yes
hERG II inhibitor	No	Yes
Oral rat acute toxicity (LD_{50}) (mol/kg)	2.338	2.285
Oral rat chronic toxicity (LOAEL) (log mg/kg/day)	0.791	0.41
Hepatotoxicity	No	No
Skin sensitization	No	No
Tetrahymena pyriformis toxicity	0.283	0.316
Minnow toxicity	2.297	0.6

4.8.4 Docking Results Comparison

Molecular docking analysis was performed to compare the binding affinities of L-tryptophan and Tamoxifen toward the selected breast cancer-associated target proteins. The docking scores provided insight into the predicted strength of protein–ligand interactions and the relative binding potential of each compound.

4.8.4.1 Comparative Molecular Docking Evaluation of AR

The comparative assessment of the molecular docking results of L-tryptophan and Tamoxifen against the androgen receptor (AR) is presented in Table 4.36. Tamoxifen exhibited a stronger predicted binding affinity, with a docking score of −9.2 kcal/mol, compared with L-tryptophan (−7.6 kcal/mol). These results

indicate that Tamoxifen has a greater predicted binding affinity toward the AR binding pocket than L-tryptophan.

TABLE 4.36: Comparative molecular docking evaluation of the androgen receptor (AR).

Compound	**Best Docking Score (kcal/mol)**	**Binding Strength**
Tamoxifen	−9.2	Strong
L-Tryptophan	−7.6	Moderate

4.8.4.2 Comparative Molecular Docking Evaluation of ERα

The comparison of the molecular docking results of L-tryptophan and Tamoxifen against the estrogen receptor alpha (ERα) is presented in Table 4.37. Tamoxifen exhibited a slightly stronger predicted binding affinity, with a docking score of −7.8 kcal/mol, compared with L-tryptophan (−7.0 kcal/mol). Although Tamoxifen demonstrated greater predicted binding affinity toward ERα, L-tryptophan also exhibited favorable binding to the receptor, supporting its selection as the lead compound for subsequent comparative analyses.

TABLE 4.37: Comparative molecular docking evaluation of (ERα).

Compound	**Best Docking Score (kcal/mol)**	**Binding Strength**
Tamoxifen	−7.8	Strong
L-Tryptophan	−7.0	Moderate

4.8.4.3 Comparative Molecular Docking Evaluation of HER2

The comparative assessment of the molecular docking results of L-tryptophan and Tamoxifen against HER2 is presented in Table 4.38. Tamoxifen exhibited a stronger predicted binding affinity, with a docking score of −8.6 kcal/mol, whereas

L-tryptophan showed a docking score of −7.4 kcal/mol. The lower docking score of Tamoxifen indicates greater predicted binding affinity toward the HER2 receptor. Although L-tryptophan demonstrated comparatively lower predicted binding affinity, its favorable drug-likeness, pharmacokinetic characteristics, and predicted safety profile suggest that it remains a promising natural lead compound for further investigation against HER2.

TABLE 4.38: Comparative molecular docking evaluation of (HER2).

Compound	**Best Docking Score (kcal/mol)**	**Binding Strength**
Tamoxifen	−8.6	Strong
L-Tryptophan	−7.4	Moderate

4.8.5 Interaction Analysis Comparison

The interaction analysis demonstrated that both L-tryptophan and Tamoxifen established favorable interactions with the selected target proteins through hydrogen-bonding, hydrophobic interactions, electrostatic interactions, and van der Waals contacts. However, differences were observed in the interacting amino acid residues and binding patterns, reflecting variations in their predicted binding modes and affinities toward the receptor proteins.

4.8.5.1 Interaction Analysis Comparison of L-Tryptophan and Tamoxifen with AR

The interaction analysis comparison of L-tryptophan and Tamoxifen with the androgen receptor (AR) is presented in Figure 4.39. L-tryptophan established multiple conventional hydrogen bonds with key amino acid residues, including Pro682, Gly683, Val685, and Gln711. In addition, attractive charge interactions, a salt bridge, and several π-mediated interactions contributed to its favorable binding within the receptor binding pocket.

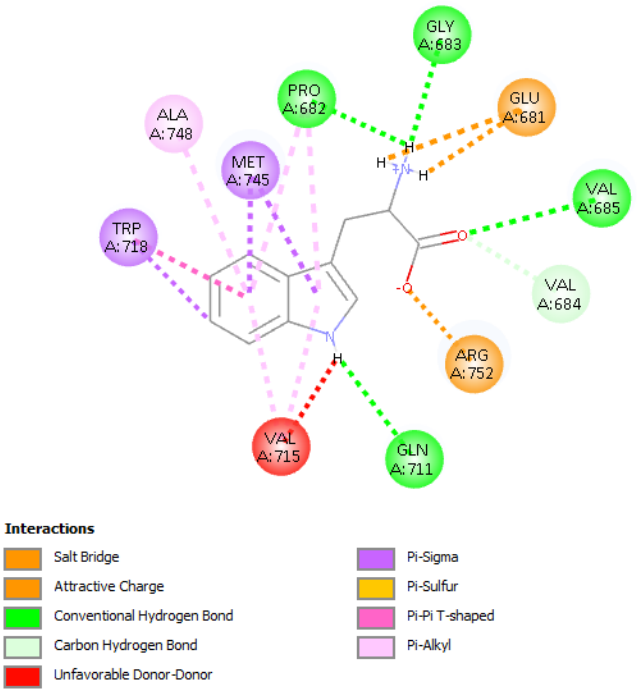

(a) L-Tryptophan

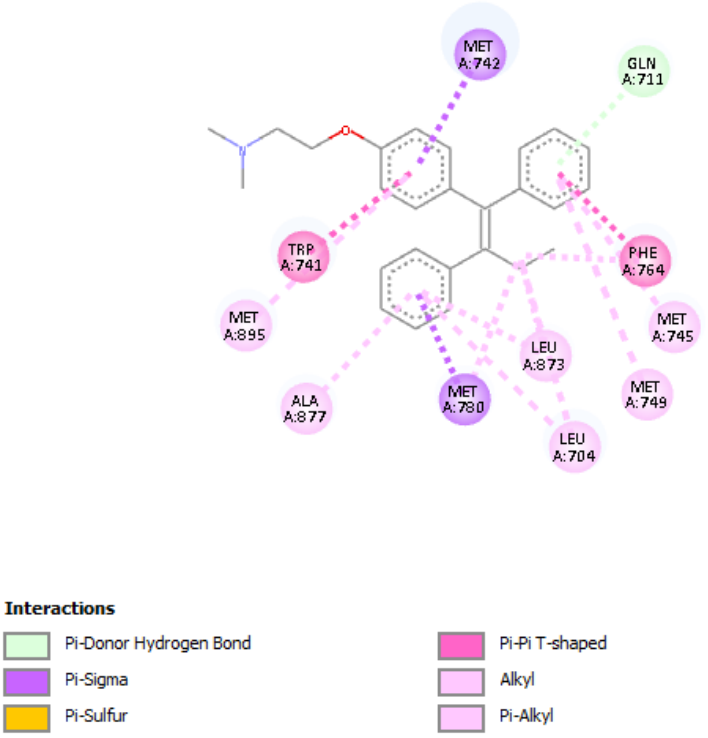

(b) Tamoxifen

FIGURE 4.39: Interaction analysis comparison of L-Tryptophan and Tamoxifen with the androgen receptor (AR).

The indole ring of L-tryptophan further participated in π–sigma, pi–pi T-shaped, and pi–alkyl interactions with active-site residues. In contrast, Tamoxifen interacted predominantly through hydrophobic alkyl and π–alkyl interactions, together with pi–pi T-shaped, pi–sigma, and pi–donor hydrogen bond interactions. The three aromatic phenyl rings of Tamoxifen played a major role in mediating these hydrophobic interactions.

Although Tamoxifen exhibited a stronger predicted binding affinity (-9.2 kcal/-mol) than L-tryptophan (-7.6 kcal/mol), L-tryptophan formed a greater number of conventional hydrogen bonds and electrostatic interactions, indicating a favorable and complementary binding mode within the AR binding pocket.

4.8.5.2 Interaction Analysis Comparison of L-Tryptophan and Tamoxifen with ERα

The comparative interaction analysis of L-tryptophan and Tamoxifen with the estrogen receptor alpha (ERα) is presented in Figure 4.40. L-tryptophan established several conventional hydrogen bonds with Glu323, Arg394, and Pro325, together with attractive charge, carbon hydrogen bond, and hydrophobic interactions, contributing to favorable binding within the receptor binding pocket. The indole ring of L-tryptophan further participated in π–sulfur and π–alkyl interactions with key active-site residues.

In contrast, Tamoxifen interacted predominantly through π–σ, alkyl, and π–alkyl interactions involving Ile424, Met421, Met388, Leu525, Ala350, Leu346, and Leu387. The three aromatic phenyl rings of Tamoxifen played a major role in mediating these hydrophobic interactions. Although Tamoxifen exhibited a stronger predicted binding affinity (-7.8 kcal/mol) than L-tryptophan (-7.0 kcal/mol), L-tryptophan established a broader range of conventional hydrogen-bonding and electrostatic interactions, indicating a favorable binding mode within the ERα binding pocket.

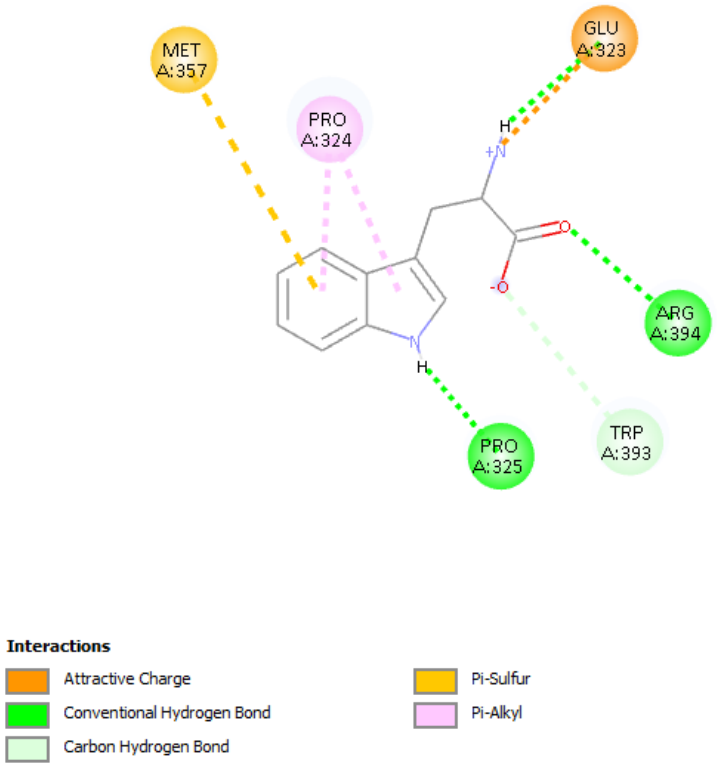

(a) L-Tryptophan

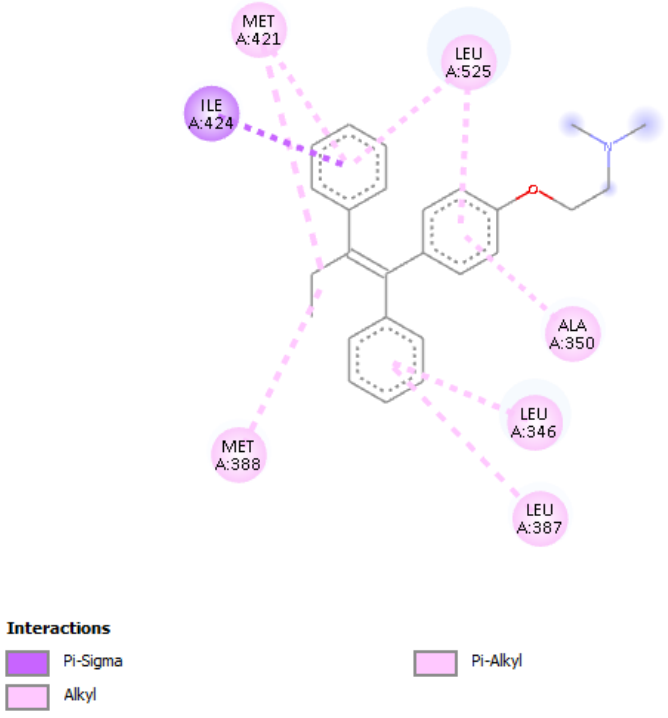

(b) Tamoxifen

FIGURE 4.40: Comparative interaction analysis of L-Tryptophan and Tamoxifen with ERα.

4.8.5.3 Interaction Analysis Comparison of L-Tryptophan and Tamoxifen with HER2

The comparative interaction analysis of L-tryptophan and Tamoxifen with HER2 is presented in Figure 4.41. L-tryptophan established multiple conventional hydrogen bonds with key amino acid residues, including Ser787, Lys753, Ala751, and Leu800, together with carbon hydrogen, π–σ, and π–alkyl interactions, contributing to favorable binding within the receptor binding pocket.

In contrast, Tamoxifen interacted predominantly through hydrophobic interactions, including alkyl, π–alkyl, and π–sulfur interactions, together with one π–donor hydrogen bond involving Thr866. The extensive hydrophobic interactions of Tamoxifen were consistent with its stronger predicted binding affinity (-8.6 kcal/mol) compared with L-Tryptophan (-7.4 kcal/mol).

Although Tamoxifen exhibited greater predicted binding affinity toward HER2, L-Tryptophan formed multiple conventional hydrogen bonds together with hydrophobic interactions and demonstrated superior drug-likeness, pharmacokinetic characteristics, and predicted safety profile, supporting its potential as a promising natural lead compound for further investigation.

Overall, the comparative analysis demonstrated that L-tryptophan possesses favorable physicochemical, pharmacokinetic, and predicted safety characteristics relative to Tamoxifen. Although Tamoxifen exhibited stronger predicted binding affinities toward the androgen receptor (AR), ERα, and HER2, L-tryptophan established favorable protein–ligand interactions with all selected target proteins and exhibited a favorable overall drug-like profile.

Furthermore, L-tryptophan fully satisfied with Lipinski's RO5 and demonstrated favorable predicted pharmacokinetic and toxicity characteristics compared with the reference drug. Collectively, these findings suggest that L-tryptophan is a promising bioactive compound and may represent as a potential lead compound for the development of novel breast cancer therapeutics. Its favorable ADMET profile, combined with its ability to interact with multiple breast cancer-related targets,

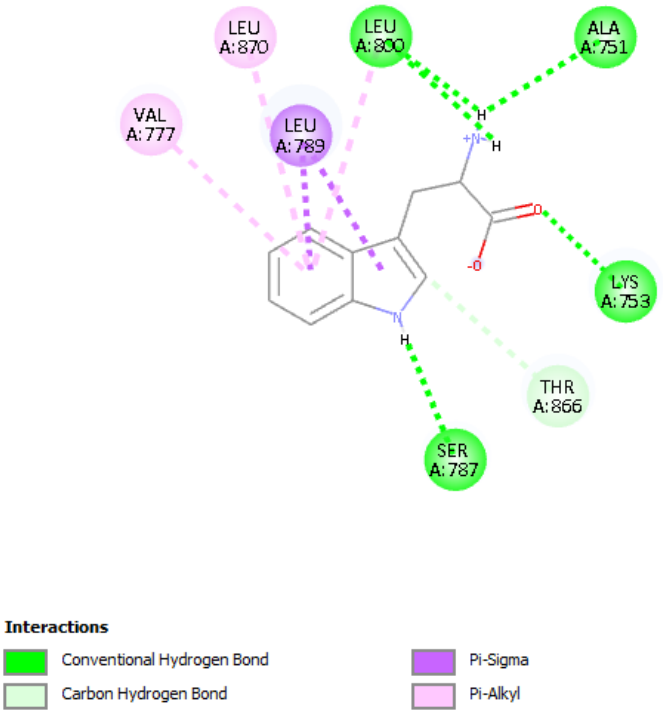

(a) L-Tryptophan

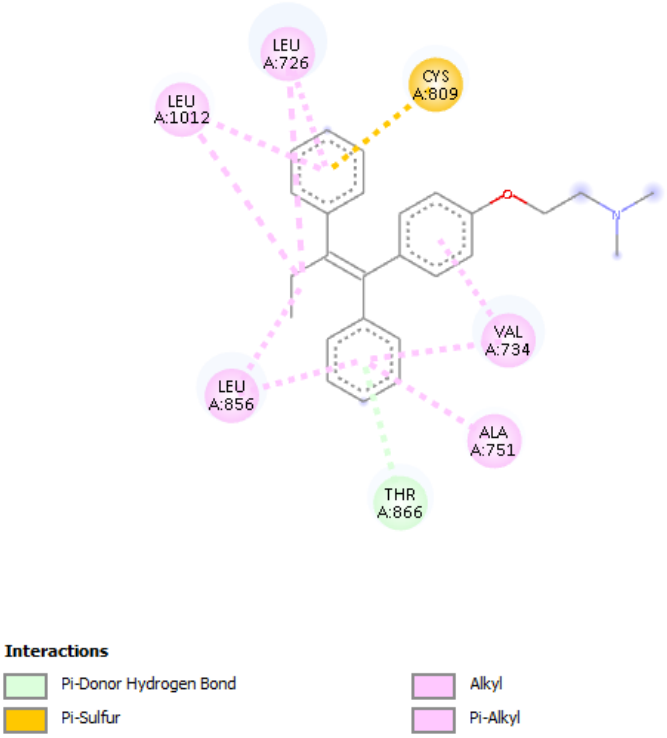

(b) Tamoxifen

FIGURE 4.41: Comparative interaction analysis of L-Tryptophan and Tamoxifen with HER2.

highlights its potential for further investigation. Nevertheless, these computational findings should be assessed through *in vitro* and *in vivo* investigations to establish its efficacy, safety and therapeutic potential before clinical application.

Chapter 5

Discussions

The present investigation evaluated the anticancer potential of L-tryptophan derived from *Helianthus tuberosus* was investigated against selected breast cancer target proteins using an in silico workflow. The computational analyses included physicochemical characterization, prediction of ADMET properties, molecular docking, and protein–ligand interaction assessment. The results demonstrated that L-tryptophan exhibits physicochemical properties consistent with a promising drug candidate. Its relatively low molecular weight, low lipophilicity, and fulfillment of Lipinski's RO5 criteria indicate favorable drug-like characteristics for oral administration [125]. Additionally, L-tryptophan showed greater aqueous solubility than Tamoxifen, suggesting improved dissolution in physiological fluids, which may contribute to better oral bioavailability.

The ADMET properties analysis further supported the appropriateness of L-tryptophan as a potential lead compound. The compound exhibited a balanced predicted pharmacokinetic profile, good aqueous solubility, absence of predicted cytochrome P450 inhibitory activity, and a more favorable predicted toxicity profile than Tamoxifen. In addition, the absence of predicted AMES toxicity and hERG channel inhibition suggests a lower potential risk of mutagenicity and cardiotoxicity. Computational evaluation of pharmacokinetic behavior and drug-likeness has become an important component of pharmaceutical research,

facilitating the early identification of promising therapeutic candidates and enhancing the efficiency of the medicine development process [126].

The desirable ADMET profile of L-tryptophan indicates that the compound possesses characteristics important for early-stage drug development. The successful progression of potential therapeutic agents into preclinical studies largely depends on achieving an appropriate balance of ADMET properties. Therefore, the encouraging pharmacokinetic predictions observed in the present study support the continued investigation of L-tryptophan as a potential therapeutic candidate for breast cancer.

Although numerous metabolites have been identified in Helianthus tuberosus, only selected compounds were considered during the preliminary screening process. Their selection was based on published phytochemical evidence, the availability of reliable three-dimensional structures in the PubChem database, and their reported biological significance. Among the screened metabolites, L-tryptophan demonstrated the most favorable overall profile by combining acceptable physicochemical characteristics, promising ADMET properties, and comparatively better interactions with the selected breast cancer target proteins. Consequently, L-tryptophan was chosen for detailed analysis and discussion in the present study.

Comparison of the docking outcomes revealed that Tamoxifen bound more strongly than L-tryptophan to AR, ERα, and HER2, as reflected by its more favorable predicted binding affinity values. Although L-tryptophan showed lower binding affinity than Tamoxifen, it formed stable interactions with all selected target proteins through hydrogen bonds, electrostatic contacts, and π-mediated interactions. It also adopted favorable binding conformations within the receptor active sites. The stronger binding of Tamoxifen was expected because it is an approved breast cancer drug, whereas L-tryptophan was evaluated as a potential lead phytochemical.

The proteins selected for molecular docking represent key therapeutic targets involved in different molecular subtypes of breast cancer. Estrogen receptor alpha

(ERα) plays a central role in the development and treatment of hormone receptor-positive breast cancer, whereas HER2 is frequently overexpressed in HER2-positive tumors and is associated with increased tumor aggressiveness and poor prognosis. In addition, the androgen receptor (AR) is expressed in various breast cancer subtypes, including a subset of triple-negative breast cancers. Therefore, assessing the interaction of L-tryptophan with ERα, HER2, and AR enabled a comprehensive evaluation of its potential therapeutic relevance across multiple forms of breast cancer rather than restricting the analysis to a single subtype [127].

While molecular docking offers valuable insights into protein–ligand binding, it provides only a static representation of molecular interactions. Important factors such as protein flexibility, solvent effects, and the cellular environment are not fully captured by this approach.Therefore, molecular dynamics simulations and experimental validation are required to assess the binding behavior and biological relevance of the protein–ligand systems obtained through molecular docking.

In addition to the molecular docking, quantitative structure activity relationship (QSAR) analysis is a valuable computational technique used to estimate the biological activity of compounds based on their structural characteristics. However, QSAR modelling was not performed in the present study because the primary objective was to evaluate the selected metabolite using molecular docking and ADMET analysis, and the available dataset was not sufficient for developing a reliable predictive model. Future investigations integrating QSAR analysis, molecular dynamics simulations, and experimental validation would provide a more detailed understanding of the structure–activity relationships, binding stability, and therapeutic potential of L-tryptophan against breast cancer-associated targets [128, 129].

Previous studies have demonstrated that indole-containing compounds possess significant anticancer potential through modulation of estrogen receptor signaling, downregulation of the PI3K/AKT/mTOR signaling pathway, stimulation of apoptotic cell death, and inhibition of cancer cell proliferation [127, 130]. As L-tryptophan contains an indole ring, the interaction patterns observed in the present study are consistent with the reported biological activities of indole-containing

compounds. However, the present computational findings alone do not confirm these mechanisms, and experimental validation is required to establish the underlying molecular pathways.

While *Helianthus tuberosus* has been extensively studied for its nutritional value and various pharmacological properties, including antioxidant and antidiabetic activities, its potential against breast cancer has received comparatively limited attention. Furthermore, the computational assessment of L-tryptophan derived from *H. tuberosus* against androgen receptor (AR), estrogen receptor alpha (ERα), and HER2 has not been comprehensively investigated in the available literature.

By integrating molecular docking with ADMET prediction, the present study provides preliminary evidence supporting the potential of this naturally occurring metabolite as a lead candidate for breast cancer research. These findings contribute additional knowledge to the existing literature and provide a basis for future experimental validation.

The identification of L-tryptophan as a bioactive constituent of *Helianthus tuberosus* further highlights the therapeutic potential of naturally occurring phytochemicals in cancer research. Natural compounds remain an important source of potential therapeutic agents due to their remarkable structural diversity, biological compatibility, and capacity to interact with multiple molecular targets. These properties highlight the potential of L-tryptophan as a promising scaffold for structural modification and the development of new anticancer therapeutics. The outcomes of this study establish a scientific foundation for future experimental research to validate the anticancer efficacy of L-tryptophan against breast cancer.

Overall, the findings indicate that L-tryptophan possesses desirable physicochemical, pharmacokinetic, and predicted safety characteristics together with stable interactions against breast cancer-associated target proteins. Although Tamoxifen demonstrated stronger predicted binding affinities toward AR, ERα, and HER2, L-tryptophan exhibited superior drug-likeness, an acceptable predicted pharmacokinetic profile, lower predicted toxicity, and favorable protein–ligand interactions, highlighting its potential as a natural lead phytochemical for future research.

Since the present findings are based entirely on computational analyses, additional *in vitro* and *in vivo* studies are required to validate the biological activity, safety, pharmacokinetic behavior, and therapeutic efficacy of L-tryptophan before its potential clinical application can be established.

Chapter 6

Conclusion and Future Recommendations

6.1 Conclusion

The present study conducted a comprehensive *in silico* evaluation of bioactive phytochemicals obtained from *Helianthus tuberosus* (Jerusalem artichoke) to assess their anticancer potential against three key molecular targets associated with breast cancer: the androgen receptor (AR), estrogen receptor alpha (ERα), and human epidermal growth factor receptor 2 (HER2).Based on physicochemical characterization, Lipinski's RO5 evaluation, ADMET prediction, molecular docking, and protein–ligand interaction analysis, L-tryptophan emerged as the most promising phytochemical among the selected bioactive compounds. L-tryptophan was characterized by favorable physicochemical and drug-like properties, meeting all Lipinski's RO5 requirements while exhibiting a promising predicted pharmacokinetic profile and lower predicted toxicity relative to Tamoxifen.

Although Tamoxifen achieved more favorable predicted binding affinity scores against AR, ERα, and HER2, L-tryptophan formed stable interactions with each of the selected target proteins through hydrogen bonds, electrostatic contacts, hydrophobic interactions, and π-mediated interactions, indicating its promise as a

natural lead phytochemical. Collectively, these findings suggest that L-tryptophan represents a promising candidate for continued investigation as a natural lead phytochemical in breast cancer drug development while also demonstrating the potential of *Helianthus tuberosus* as a rich source of bioactive compounds. However, further experimental validation through in vitro and in vivo studies is required to verify the biological activity, pharmacokinetic properties, safety, and therapeutic efficacy of L-tryptophan before its clinical potential can be fully established.

6.2 Future Recommendations

The findings of this computational investigation provide a basis for several directions of future research. Experimental studies, including *in vitro* and *in vivo* investigations, should be conducted to confirm the anticancer activity of L-tryptophan and to further evaluate its pharmacokinetic properties, toxicity profile, and therapeutic efficacy against breast cancer. In addition, molecular dynamics simulations are recommended to examine the stability and dynamic behavior of the ligand–protein complexes under physiological conditions, thereby complementing the molecular docking results. Structural modification of L-tryptophan may also be considered to enhance its binding affinity, target selectivity, and pharmacokinetic performance while preserving its favorable predicted safety profile. Moreover, future investigations should assess the therapeutic potential of combining L-tryptophan with established anticancer drugs, such as Tamoxifen, to determine possible synergistic effects. Further research should also examine the activity of L-tryptophan against additional breast cancer-related molecular targets and signaling pathways, including the PI3K/AKT/mTOR pathway. Finally, other bioactive phytochemicals from *Helianthus tuberosus* should be systematically evaluated to identify additional natural compounds with potential applications in breast cancer therapy.

Bibliography

[1] S. Wang, A. Wang, R. Chen, D. Xu, H. Wang, F. Jiang, H. Liu, W. Qian, and W. Fan, "Haplotype-resolved chromosome-level genome of hexaploid jerusalem artichoke provides insights into its origin, evolution, and inulin metabolism," *Plant Communications*, vol. 5, no. 3, 2024.

[2] V. Liava, A. Karkanis, N. Danalatos, and N. Tsiropoulos, "Cultivation practices, adaptability and phytochemical composition of jerusalem artichoke (helianthus tuberosus l.): A weed with economic value," *Agronomy*, vol. 11, no. 5, p. 914, 2021.

[3] Y. Wang, G. Wang, Z. Zhou, Y. Zong, L. Wang, S. Yang, Y. Zhang, and X. Sun, "Transcriptome analysis for genes involved in fructan biosynthesis in the jerusalem artichoke (helianthus tuberosus l.)," *Biotechnology & Biotechnological Equipment*, vol. 36, no. 1, pp. 472–480, 2022.

[4] T. N. Smekalova, N. V. Lebedeva, and L. Y. Novikova, "Morphological analysis of jerusalem artichoke (helianthus tuberosus l.) accessions of different origin from vir collection," in *Proc. Latv. Acad. Sci. Sect. B*, vol. 73, 2019, pp. 502–512.

[5] N. Abdalla, N. Arafa, H. Taha, M. I. Ragab, S. El-Miniawy, I. Tóth, S. Kovács, and H. R. El-Ramady, "An overview on anatomy of jerusalem artichoke (helianthus tuberosus l.)," *Environment, Biodiversity and Soil Security*, vol. 5, no. 2021, pp. 121–130, 2021.

[6] A. A. Manokhina, A. S. Dorokhov, T. P. Kobozeva, T. N. Fomina, and O. A. Starovoitova, "Varietal characteristics of jerusalem artichoke as a high

nutritional value crop for herbivorous animal husbandry," *Applied Sciences*, vol. 12, no. 9, p. 4507, 2022.

[7] Y. Wang, Y. Zhao, F. Xue, X. Nan, H. Wang, D. Hua, J. Liu, L. Yang, L. Jiang, and B. Xiong, "Nutritional value, bioactivity, and application potential of jerusalem artichoke (helianthus tuberosus l.) as a neotype feed resource," *Animal Nutrition*, vol. 6, no. 4, pp. 429–437, 2020.

[8] P. Boonmahome, J. Namwongsa, N. Vorasoot, S. Jogloy, N. Riddech, S. Boonlue, and W. Mongkolthanaruk, "Single and co-inoculum of endophytic bacteria promote growth and yield of jerusalem artichoke through upregulation of plant genes under drought stress," *PLoS One*, vol. 18, no. 6, p. e0286625, 2023.

[9] M. Bembenek, V. Melnyk, B. Karwat, M. Hnyp, Ł. Kowalski, and Y. Mosora, "Jerusalem artichoke as a raw material for manufacturing alternative fuels for gasoline internal combustion engines," *Energies*, vol. 17, no. 10, p. 2378, 2024.

[10] D.-H. Kim, W. Lee, Y. Pyo, and D.-K. Choi, "Phytochemical composition and mechanistic pharmacology of jerusalem artichoke (helianthus tuberosus l.): Implications for functional and therapeutic applications," *Current Issues in Molecular Biology*, vol. 48, no. 2, p. 180, 2026.

[11] R. F. Tapera, X. Siwe-Noundou, L. J. Shai, and S. Mokhele, "Exploring the therapeutic potential, ethnomedicinal values, and phytochemistry of helianthus tuberosus l.: A review," *Pharmaceuticals*, vol. 17, no. 12, p. 1672, 2024.

[12] M. M. Showkat, A. B. Falck-Ytter, and K. O. Strætkvern, "Phenolic acids in jerusalem artichoke (helianthus tuberosus l.): Plant organ dependent antioxidant activity and optimized extraction from leaves," *Molecules*, vol. 24, no. 18, p. 3296, 2019.

[13] J. W. Wang, L. Fang, J. Yu, L. Zhao, J. Yao, H. Li, and X. Chen, "The protective effect of jerusalem artichoke polysaccharides against oxidative damage to biomolecules," *Journal of Food Bioactives*, vol. 17, 2022.

[14] E. I. Obeagu and G. U. Obeagu, "Breast cancer: A review of risk factors and diagnosis," *Medicine*, vol. 103, no. 3, p. e36905, 2024.

[15] X. Yang, D. Yang, X. Qi, X. Luo, and G. Zhang, "Endocrine treatment mechanisms in triple-positive breast cancer: from targeted therapies to advances in precision medicine," *Frontiers in Oncology*, vol. 14, p. 1467033, 2025.

[16] L. Liao, "Inequality in breast cancer: Global statistics from 2022 to 2050," *The Breast*, vol. 79, p. 103851, 2025.

[17] A. N. Giaquinto, H. Sung, K. D. Miller, J. L. Kramer, L. A. Newman, A. Minihan, A. Jemal, and R. L. Siegel, "Breast cancer statistics, 2022," *CA: a cancer journal for clinicians*, vol. 72, no. 6, pp. 524–541, 2022.

[18] C. Valenza, B. Taurelli Salimbeni, C. Santoro, D. Trapani, G. Antonarelli, and G. Curigliano, "Tumor infiltrating lymphocytes across breast cancer subtypes: current issues for biomarker assessment," *Cancers*, vol. 15, no. 3, p. 767, 2023.

[19] L. Clusan, F. Ferrière, G. Flouriot, and F. Pakdel, "A basic review on estrogen receptor signaling pathways in breast cancer," *International journal of molecular sciences*, vol. 24, no. 7, p. 6834, 2023.

[20] A. Anestis, I. Zoi, A. G. Papavassiliou, and M. V. Karamouzis, "Androgen receptor in breast cancer—clinical and preclinical research insights," *Molecules*, vol. 25, no. 2, p. 358, 2020.

[21] D. Molehin, S. Filleur, and K. Pruitt, "Regulation of aromatase expression: Potential therapeutic insight into breast cancer treatment," *Molecular and cellular endocrinology*, vol. 531, p. 111321, 2021.

[22] B. Sawicka, D. Skiba, P. PszczóÅ, I. Aslan, J. Sharifi, B. Krochmal-Marczak *et al.*, "Jerusalem artichoke (helianthus tuberosus l.) as a medicinal plant and its natural products," *Cellular and Molecular Biology*, vol. 66, no. 4, pp. 160–177, 2020.

[23] National Center for Biotechnology Information, "Pubchem taxonomy summary for taxonomy 4233, helianthus tuberosus (jerusalem artichoke)," https://pubchem.ncbi.nlm.nih.gov/taxonomy/Helianthus-tuberosus, 2026, accessed: 2026-06-30.

[24] D. Zhan, C. Si, Z. Bie, L. Wang, X. Sun, S. Yang, and Q. Zhong, "Genome size variation provided novel insights into agronomic trait correlated effects and revealed intraspecific diversity in jerusalem artichoke (helianthus tuberosus l.)," *South African Journal of Botany*, vol. 161, pp. 12–20, 2023.

[25] Q. Zhong, S. Yang, X. Sun, L. Wang, and Y. Li, "The complete chloroplast genome of the jerusalem artichoke (helianthus tuberosus l.) and an adaptive evolutionary analysis of the ycf2 gene," *PeerJ*, vol. 7, p. e7596, 2019.

[26] R. S. Sharoffidin, J. Y. Salomiddin, S. B. Sharifzoda, K. Abdukarimzoda, A. Zare, N. M. Mussin, K. R. Zhilisbayeva, N. Tanideh, and A. Tamadon, "Unveiling the medicinal potential of helianthus tuberosus: A comprehensive bibliometric study," *European Journal of Integrative Medicine*, p. 102608, 2026.

[27] S. Diez, M. C. Tarifa, D. M. Salvatori, and L. Franceschinis, "Functional ingredients based on jerusalem artichoke: technological properties, antioxidant activity, and prebiotic capacity," in *Biology and Life Sciences Forum*, vol. 40, no. 1. MDPI, 2025, p. 24.

[28] M.-Y. Wang, Z.-L. Ma, C.-L. He, and X.-Y. Yuan, "The antioxidant activities of flavonoids in jerusalem artichoke (helianthus tuberosus l.) leaves and their quantitative analysis," *Natural product research*, vol. 36, no. 4, pp. 1009–1013, 2022.

[29] Y. Mu, W. Gao, S. Lv, F. Li, Y. Lu, and C. Zhao, "The antioxidant capacity and antioxidant system of jerusalem artichoke (helianthus tuberosus l.) tubers in relation to inulin during storage at different low temperatures," *Industrial Crops and Products*, vol. 161, p. 113229, 2021.

[30] Y. Mu, B. Zhang, S. Lv, F. Li, and C. Zhao, "The role of inulin in maintaining antioxidant capacity and enzymatic activities of jerusalem artichoke (helianthus tuberosus l.) cultivars during cold storage," *Antioxidants*, vol. 14, no. 9, p. 1109, 2025.

[31] M. Y. Mostafa, "Utilization of jerusalem artichoke (helianthus tuberosus l.) tubers powder in preparing healthy crackers with antioxidant, anti-inflammatory, and anti-diabetic properties," *Biological and Biomedical Journal*, vol. 3, no. 1, pp. 137–153, 2025.

[32] B. Krochmal-Marczak, B. Sawicka, and P. Barbaś, "Utility meaning of jerusalem artichoke," in *Jerusalem Artichoke Food Science and Technology: Helianthus Tuberosus*. Springer, 2022, pp. 91–138.

[33] E. Generalov, L. Yakovenko, A. Sinitsyn, A. Alekseev, O. Sinitsyna, K. Abduvosidov, V. Minaichev, and L. Generalova, "Anti-inflammatory effects of helianthus tuberosus l. polysaccharide and its limited gene expression profile," *International Journal of Molecular Sciences*, vol. 26, no. 16, p. 7885, 2025.

[34] X. Wan, Z. Liu, Y. Wang, Y. Yin, X. Cai, L. Gao, Q. Wang, Y. Li, and C. Zhou, "Antiviral activity against respiratory syncytial virus of polysaccharide from jerusalem artichoke (helianthus tuberosus l.)," *BioMed Research International*, vol. 2022, no. 1, p. 1809879, 2022.

[35] A. G. Atiyah, M. S. Hasan, and M. S. Owain, "The role of ozonated jerusalem artichoke ointment on the healing of surgically created full-thickness cutaneous wounds in rabbits," *Veterinary Medicine International*, vol. 2024, no. 1, p. 9966943, 2024.

[36] S. H. Kim, B. K. Kim, B. Y. Park, J. M. Kim, Y. J. Lee, M. K. Lee, S.-T. Yee, and M. Y. Kang, "Effects of jerusalem artichoke extract and inulin on blood glucose levels and insulin secretion in streptozotocin induced diabetic mice," *The Journal of Korean Diabetes*, vol. 22, no. 1, pp. 60–70, 2021.

[37] J. Li, S. Jia, C. Yuan, B. Yu, Z. Zhang, M. Zhao, P. Liu, X. Li, and B. Cui, "Jerusalem artichoke inulin supplementation ameliorates hepatic lipid metabolism in type 2 diabetes mellitus mice by modulating the gut microbiota and fecal metabolome," *Food & Function*, vol. 13, no. 22, pp. 11 503–11 517, 2022.

[38] H. Takahashi, A. Nakajima, Y. Matsumoto, H. Mori, K. Inoue, H. Yamanouchi, K. Tanaka, Y. Tomiga, M. Miyahara, T. Yada *et al.*, "Administration of jerusalem artichoke reduces the postprandial plasma glucose and glucose-dependent insulinotropic polypeptide (gip) concentrations in humans," *Food & nutrition research*, vol. 66, pp. 10–29 219, 2022.

[39] F. Beyazyüz, E. Arslan, and G. Koygun, "Investigation of cytotoxic, antimetastatic and apoptotic activities of jerusalem artichoke (helianthus tuberosus l.) extracts: Comparison with mcf-7 and mcf-12a cells," *Kahramanmaraş Sütçü İmam Üniversitesi Tarım ve Doğa Dergisi*, vol. 27, no. 2, pp. 293–303, 2024.

[40] K. R. Ahmed and N. Shaban, "Anticancer effect of artichoke and fennel seeds extracts on oral squamous cell carcinoma cell line: In vitro study," *Egyptian Dental Journal*, vol. 70, no. 4, pp. 3295–3303, 2024.

[41] A. M. Mathew, Z. Deng, C. J. Nelson, T. G. Mayberry, Q. Bai, M. Lequio, E. Fajardo, H. Xiao, M. R. Wakefield, and Y. Fang, "Artichoke as a melanoma growth inhibitor," *Medical Oncology*, vol. 40, no. 9, p. 262, 2023.

[42] D. S. Chauhan, P. Vashisht, R. P. Bebartta, D. Thakur, and V. Chaudhary, "Jerusalem artichoke: A comprehensive review of nutritional composition, health benefits and emerging trends in food applications," *Comprehensive Reviews in Food Science and Food Safety*, vol. 24, no. 1, p. e70114, 2025.

[43] R. Ruttanaprasert, S. Jogloy, A. Janket, P. Siripipatthana, T. Senawong, and C. Aninbon, "Adaptive responses of jerusalem artichoke to mid-season drought: effects on phenolic compounds and p-coumaric acid content," *BMC Plant Biology*, vol. 25, no. 1, p. 893, 2025.

[44] N. Afoakwah, Y. Zhao, W. Tchabo, Y. Dong, J. Owusu, and G. Mahunu, "Studies on the extraction of jerusalem artichoke tuber phenolics using microwave-assisted extraction optimized conditions," *Food Chemistry Advances*, vol. 3, p. 100507, 2023.

[45] N. A. Afoakwah, W. Tchabo, and P. Owusu-Ansah, "Ultrasound-assisted extraction (uae) of jerusalem artichoke tuber bio-active ingredient using optimized conditions of box-behnken response surface methodology," *Heliyon*, vol. 10, no. 4, 2024.

[46] A. M. Mounir, A. El-Hefny, S. Mahmoud, and A. El-Tanahy, "Effect of low gamma irradiation doses on growth, productivity and chemical constituents of jerusalem artichoke (helianthus tuberosus) tubers," *Bulletin of the National Research Centre*, vol. 46, no. 1, p. 146, 2022.

[47] L. Kaszás, T. Alshaal, H. El-Ramady, Z. Kovács, J. Koroknai, N. Elhawat, É. Nagy, Z. Cziáky, M. Fári, and É. Domokos-Szabolcsy, "Identification of bioactive phytochemicals in leaf protein concentrate of jerusalem artichoke (helianthus tuberosus l.)," *Plants*, vol. 9, no. 7, p. 889, 2020.

[48] A. Galkina, N. Krause, M. Lenz, C. G. Daniliuc, M. Kaiser, and T. J. Schmidt, "Antitrypanosomal activity of sesquiterpene lactones from helianthus tuberosus l. including a new furanoheliangolide with an unusual structure," *Molecules*, vol. 24, no. 6, p. 1068, 2019.

[49] J. Bokić, J. Kojić, J. Krulj, L. Pezo, V. Banjac, V. Tumbas Šaponjac, V. Travičić, D. A. Moreno, and M. Bodroža-Solarov, "Bioactive, mineral and antioxidative properties of gluten-free chicory supplemented snack: Impact of processing conditions," *Foods*, vol. 11, no. 22, p. 3692, 2022.

[50] X. Yuan and Q. Yang, "Simultaneous quantitative determination of 11 sesquiterpene lactones in jerusalem artichoke (Helianthus tuberosus l.) leaves by ultra high performance liquid chromatography with quadrupole time-of-flight mass spectrometry," *Journal of Separation Science*, vol. 40, no. 7, pp. 1457–1464, Apr. 2017.

[51] M. A. Shariati, M. U. Khan, L. Hleba, C. K. de Souza, Z. Tokhtarov, S. Terentev, S. Konovalov, F. Arduvanova, N. Batishcheva, I. Shigapov, E. S., and M. Kantimerova, "Topinambur (the jerusalem artichoke): Nutritional value and its application in food products: An updated treatise," *Journal of Microbiology, Biotechnology and Food Sciences*, vol. 10, no. 6, p. e4737, Jun. 2021.

[52] B. Bogucka and K. Jankowski, "Jerusalem artichoke: Quality response to potassium fertilization and irrigation in poland," *Agronomy*, vol. 10, no. 10, p. 1518, 2020.

[53] A. Díaz, M. A. García, and C. Dini, "Jerusalem artichoke flour as food ingredient and as source of fructooligosaccharides and inulin," *Food Research International*, vol. 165, p. 112463, 2023.

[54] I. A. Rubel, M. A. Iraporda, C. Gervasi, S. G. Genovese, and N. E. Manrique, "Inulin from jerusalem artichoke: From biosynthesis to application," *Bioactive Carbohydrates and Dietary Fibre*, vol. 26, p. 100281, 2021.

[55] D. C. Mudannayake, D. D. Jayasena, K. M. S. Wimalasiri, C. S. Ranadheera, and S. Ajlouni, "Inulin fructans–food applications: A review," *International Journal of Food Science and Technology*, vol. 57, no. 9, pp. 5764–5780, 2022.

[56] S. Khamwan, S. Boonlue, and W. Mongkolthanaruk, "Production of fructan synthesis/hydrolysis of endophytic bacteria involved in inulin production in jerusalem artichoke," *3 Biotech*, vol. 12, no. 11, p. 296, 2022.

[57] R. Hong and B. Xu, "Breast cancer: An up-to-date review," *Cancer Communications*, vol. 42, no. 10, pp. 913–936, Oct. 2022.

[58] X. Xiong, Y. Wang, X. Bai, Y. Wang, and Y. Song, "Breast cancer: Pathogenesis and treatments," *Signal Transduction and Targeted Therapy*, vol. 10, p. 49, 2025.

[59] L. J. Grimm, E. F. Conant, S. C. Partridge, and W. A. Berg, "Ductal carcinoma in situ: State-of-the-art review," *Radiology*, vol. 302, no. 2, pp. 246–255, Feb. 2022.

[60] J. A. Mouabbi, A. M. Gilcrease, A. M. Thompson, F. Meric-Bernstam, V. Valero, and B. Lim, "Invasive lobular carcinoma: An understudied subtype of breast cancer," *Breast Cancer Research and Treatment*, vol. 193, no. 2, pp. 253–264, Jun. 2022.

[61] E. Orrantia-Borunda, P. Anchondo-Nuñez, L. E. Acuña-Aguilar, F. O. Gómez-Valles, and C. A. Ramírez-Valdespino, "Subtypes of breast cancer," in *Breast Cancer*, H. N. Mayrovitz, Ed. Brisbane, Australia: Exon Publications, 2022, ch. 3.

[62] M. Tufail, J. Cui, and C. Wu, "Breast cancer: Molecular mechanisms of underlying resistance and therapeutic approaches," *American Journal of Cancer Research*, vol. 12, no. 7, pp. 2920–2949, 2022.

[63] M. Hashemi, H. Z. Arani, S. Orouei, S. M. Rezaei, F. Nikkhah, M. K. Jolly, N. Esmaeili, and H. Heidari, "Emt mechanism in breast cancer metastasis and drug resistance: Revisiting molecular interactions and biological functions," *Biomedicine & Pharmacotherapy*, vol. 155, p. 113774, Nov. 2022.

[64] S. D. Nathanson, M. Detmar, T. P. Padera, and L. R. Yates, "Mechanisms of breast cancer metastasis," *Clinical & Experimental Metastasis*, vol. 39, no. 1, pp. 117–137, Feb. 2022.

[65] A. Glaviano, F. Buono, M. D. Laurentiis, M. D. Maio, and N. Normanno, "Resistance to cdk4/cdk6 inhibitors in breast cancer: Mechanisms and therapeutic strategies," *Drug Resistance Updates*, vol. 74, p. 101062, May 2024.

[66] K. Čermáková, P. Souček, and M. Ehrlich, "Targeting the pi3k/akt/mtor pathway in breast cancer," *Biomedicines*, vol. 11, no. 1, p. 109, Jan. 2023.

[67] A. F. Wali, A. Rashid, N. A. Alharbi, M. A. Alshammari, S. A. Bhat, M. A. Almatroudi, and G. M. Ashraf, "Pi3k/akt/mtor pathway in breast cancer pathogenesis and therapy: Insights into phytochemical-based therapeutics," *Clinical and Experimental Medicine*, vol. 25, no. 1, p. 245, 2025.

[68] K. P. S. Raghav and M. M. Moasser, "Molecular pathways and mechanisms of her2 in cancer therapy," *Clinical Cancer Research*, vol. 29, no. 13, pp. 2351–2361, Jul. 2023.

[69] M. Tufail, J. Cui, and C. Wu, "Dna repair pathways in breast cancer: From mechanisms to clinical applications," *Breast Cancer Research and Treatment*, vol. 200, no. 3, pp. 305–321, Aug. 2023.

[70] Y. Qu, S. Qin, Z. Yang, Z. Li, Q. Liang, T. Long, W. Wang, D. Zeng, Q. Zhao, Z. Dai, Q. Ni, F. Zhao, W. Kim, and J. Hou, "Targeting the dna repair pathway for breast cancer therapy," *Biomedicine & Pharmacotherapy*, vol. 165, p. 115250, Sep. 2023.

[71] J. Bai, Y. Gao, and G. Zhang, "The treatment of breast cancer in the era of precision medicine," *Cancer Biology & Medicine*, vol. 22, no. 4, pp. 322–347, 2025.

[72] Y. Wang and A. Minden, "Molecular combination therapies for breast cancer," *International Journal of Molecular Sciences*, vol. 23, no. 19, p. 11046, Sep. 2022.

[73] V. P. Chavda, L. V. Nalla, P. Balar, R. Bezbaruah, V. Apostolopoulos, R. K. Singla, A. Khadela, L. Vora, and V. N. Uversky, "Advanced phytochemical-based nanocarrier systems for the treatment of breast cancer," *Cancers*, vol. 15, no. 4, p. 1023, Feb. 2023.

[74] A. Mazurakova, L. Koklesova, M. Samec, K. Kudela, K. Kajo, V. Škuciová, D. Büsselberg, P. Kubatka, and O. Golubnitschaja, "Anti-breast cancer effects of phytochemicals: Primary, secondary, and tertiary care," *EPMA Journal*, vol. 13, no. 2, pp. 315–334, Apr. 2022.

[75] A. F. Wali, J. R. Pillai, S. Talath, P. Shivappa, S. B. Sridhar, M. El-Tanani, I. R. Rangraze, O. I. Mohamed, and N. N. A. Ani, "Phytochemicals in breast cancer prevention and treatment: A comprehensive review," *Current Issues in Molecular Biology*, vol. 47, no. 1, p. 30, Jan. 2025.

[76] H. Wu, W. J. van der Pol, L. G. Dubois, C. D. Morrow, and T. O. Tollefsbol, "Dietary supplementation of inulin contributes to the prevention of estrogen receptor-negative mammary cancer by alteration of gut microbial communities and epigenetic regulations," *International Journal of Molecular Sciences*, vol. 24, no. 10, p. 9015, May 2023.

[77] H. Wu, M. M. Rahman, and T. O. Tollefsbol, "Combined phytochemical sulforaphane and dietary fiber inulin contribute to the prevention of er-negative breast cancer via pi3k/akt/mtor pathway," *Nutrients*, vol. 17, no. 12, p. 2023, Jun. 2025.

[78] Y. Hussain, H. Khan, W. Alam, M. Aschner, K. F. Alsharif, and L. Saso, "Flavonoids targeting the mtor signaling cascades in cancer: A potential crosstalk in anti-breast cancer therapy," *Oxidative Medicine and Cellular Longevity*, vol. 2022, p. 4831833, Jun. 2022.

[79] F. Beyazyüz, B. Yılmaz, E. Demirpolat, S. Erdem, C. Dayan, and M. A. Onur, "Investigation of cytotoxic, antimetastatic and apoptotic activities of jerusalem artichoke (helianthus tuberosus l.) extracts: Comparison with mcf-7 and mcf-12a cells," *KSU Journal of Agriculture and Nature*, vol. 27, no. 2, pp. 293–303, 2024.

[80] K. S. Alharbi, A. Hussain, A. H. A. Bratty, M. A. Alhazmi, M. M. Nasif, S. Javed, F. Anwar, J. Iqbal *et al.*, "Medicinal plant-derived nutraceuticals: An innovative approach to breast cancer prevention and treatment," *Journal of Food Biochemistry*, vol. 46, no. 5, p. e14030, May 2022.

[81] D. A. Paramita, I. W. Sudarsa, I. M. Muliarta, and I. K. Sudiana, "Regulation of p53 by curcuma longa extract in triple-negative breast cancer cells," *Medical Archives (Medicina Glasnik)*, vol. 19, no. 2, pp. 165–171, Aug. 2022.

[82] D. Hermansyah, D. Agustina, R. H. Prasetyo, and R. D. Setijanto, "Combination of curcuma longa and phyllanthus niruri extracts inhibits triple-negative breast cancer cell growth through apoptosis induction," *Indonesian Journal of Cancer Chemoprevention*, vol. 14, no. 1, pp. 22–30, 2023.

[83] D. Hermansyah, D. A. Paramita, I. W. Sudarsa, I. M. Muliarta, and I. K. Sudiana, "Curcuma longa extract inhibits migration by reducing mmp-9 and rac-1 expression in highly metastatic breast cancer cells," *Research in Pharmaceutical Sciences*, vol. 19, no. 2, pp. 157–166, Apr. 2024.

[84] B. T. Tung, N. T. T. Ha, N. T. H. Trang, N. T. T. Hien, and D. T. T. Huong, "Evaluation of cytotoxic effects of camellia sinensis extracts on human breast cancer cells," *VNU Journal of Science: Medical and Pharmaceutical Sciences*, vol. 40, no. 4, pp. 69–77, 2024.

[85] R. Tamang, R. Chaudhary, P. R. Adhikari, B. K. Shah, and S. S. A. An, "Sustainable synthesis of camellia sinensis-mediated silver nanoparticles for biomedical applications: Mechanistic insights into their anticancer activity," *Biomaterials Advances*, vol. 166, p. 214072, Jan. 2025.

[86] P. Theivendren, M. Ravichandran, M. M. Akhtar, and S. K. Sahu, "Camellia sinensis polyphenols as natural stat inhibitors for breast cancer therapy," *Pharmacological Research – Modern Chinese Medicine*, vol. 14, p. 100521, Mar. 2025.

[87] M. D. Vélez, M. A. Llano-Ramírez, C. Ramón, J. Rojas, C. Bedoya, S. Arango-Varela, G. A. Santa-Gonzalez, and M. Gil, "Antioxidant capacity and cytotoxic effect of an optimized extract of isabella grape (vitis labrusca) on breast cancer cells," *Heliyon*, vol. 9, no. 11, p. e21827, Nov. 2023.

[88] A. Mokashi, N. V. Borkar, P. Sharma, H. P. Patil, and S. B. Jadhav, "Virtual screening and network pharmacology-based study to elucidate the pharmacological mechanism of vitis vinifera against breast cancer," *Clinical Breast Cancer: Health and Perspectives*, vol. 4, no. 1, p. e143521, Feb. 2024.

[89] S. A. Ahmed, P. S. Tabassum, S. A. Falak, A. V. D. Ahmad, and M. S. Shaikh, "Molecular docking and network pharmacology: Investigating vitis vinifera phytoconstituents as multi-target therapeutic agents against breast cancer," *Journal of Pharmaceutical Sciences and Computational Chemistry*, vol. 1, no. 2, pp. 116–134, 2025.

[90] J. Farheen, M. H. A. Bratty, S. H. Omar, M. A. Alhazmi, A. H. Alhadrami, and K. S. Alharbi, "Vitis vinifera-derived silver nanoparticles: A promising green nanotherapeutic strategy for breast cancer treatment," *Journal of Drug Delivery Science and Technology*, vol. 92, p. 105332, Feb. 2024.

[91] I. Zafar, H. M. Ali, M. Arif, M. Adnan, M. Ahsan, A. Ali, S. R. Hassan, J. Sharifi-Rad, and R. Ullah, "In silico and in vitro study of bioactive compounds of nigella sativa against breast cancer," *Frontiers in Molecular Biosciences*, vol. 10, p. 1205362, Jun. 2023.

[92] R. Arif, M. Ahsan, H. M. Ali, I. Zafar, M. Adnan, A. Ali, and R. Ullah, "Network pharmacology and experimental validation to explore the mechanisms underlying the anticancer potential of nigella sativa phytochemicals against breast cancer," *Pharmaceuticals*, vol. 17, no. 1, p. 84, Jan. 2024.

[93] W. A. Baig, K. Alwosaibai, K. M. Al-Jubran, T. M. Chaudhry, N. Al-Dowish, F. Alsaffar, and M. A. Alam, "Synergistic anti-cancer effects of nigella sativa seed oil and conventional cytotoxic agent against human breast cancer," *Drug Metabolism and Personalized Therapy*, vol. 37, no. 3, pp. 315–321, Sep. 2022.

[94] A. N. Usman, S. M. Tahir, R. Natzir, B. Bahar, and V. Hadju, "Ginger potency on the prevention and treatment of breast cancer," *Breast Disease*, vol. 42, no. 3, pp. 281–290, May 2023.

[95] J. Mathiyazhagan, M. C. Jayakumar, V. Duraipandiyan, N. A. Al-Dhabi, K. Velmurugan, and S. Karthikeyan, "Preventive effect of combined zingiber officinale and tinospora cordifolia extract on dmba-induced mammary carcinogenesis via suppression of mtor signaling pathway," *Nutrition and Cancer*, vol. 74, no. 5, pp. 1857–1871, May 2022.

[96] R. Alhaddad, M. H. A. Bratty, S. H. Omar, A. H. Alhazmi, K. S. Alharbi, and J. Farheen, "Green synthesis of zingiber officinale-mediated zinc oxide nanoparticles and their anticancer efficacy against breast cancer," *Future Science OA*, vol. 10, no. 1, p. FSO948, Jan. 2024.

[97] K. Raval and T. Ganatra, "Basics and applications of molecular docking," *IP International Journal of Comprehensive and Advanced Pharmacology*, vol. 7, no. 1, pp. 4–11, Apr. 2022.

[98] S. Singh, S. Kaur, and N. Sharma, "Molecular docking and dynamics simulation," in *Bioinformatics*. Amsterdam, Netherlands: Elsevier, 2022, pp. 291–304.

[99] M. T. Muhammed, A. H. Al-Salami, A. M. Hassan, A. A. Al-Khuzai, and M. A. Al-Mulla, "Molecular docking in drug discovery: Recent advances and challenges," *Letters in Drug Design & Discovery*, vol. 21, no. 4, pp. 638–651, May 2024.

[100] J. M. Paggi, D. N. Santiago, and D. L. Mobley, "The art and science of molecular docking," *Annual Review of Biochemistry*, vol. 93, pp. 245–271, Jul. 2024.

[101] A. K. Subramani, P. Kumar, V. Rajakumar, M. Govindaraju, and K. V. G. Sankar, "Qsar, molecular docking, and admet studies of coumarin conjugates as potential anticancer agents," *Molecules*, vol. 27, no. 19, p. 6423, Sep. 2022.

[102] S. S. Panda, N. M. S. Siraj, A. A. Al-Majed, H. M. Refat, and M. M. Ghorab, "Design, synthesis, biological evaluation, and molecular docking studies of curcumin hybrid conjugates as potential anticancer agents," *Pharmaceuticals*, vol. 15, no. 10, p. 1251, Oct. 2022.

[103] M. S. Taghizadeh, S. Jahandideh, R. Mahboobi, and S. Samarghandian, "Natural products targeting overexpressed receptors in breast cancer: A review of molecular mechanisms and therapeutic potential," *PLoS ONE*, vol. 17, no. 5, p. e0267961, May 2022.

[104] A. Zochedh, N. Boussekine, A. Bouraiou, M. Bensouici, and A. Baghiani, "Molecular docking, molecular dynamics simulation, and admet studies of naringin as a potential therapeutic agent against breast cancer," *Journal of Molecular Structure*, vol. 1272, p. 134149, Jan. 2023.

[105] N. He, Y. Wang, J. Liu, Y. Li, X. Zhang, R. Zhang, and Y. Wang, "Plasticizers inducing breast cancer through network toxicology, molecular docking, and experimental validation," *Ecotoxicology and Environmental Safety*, vol. 284, p. 116866, Oct. 2024.

[106] H. Sung, J. Ferlay, R. L. Siegel, M. Laversanne, I. Soerjomataram, A. Jemal, and F. Bray, "Global cancer statistics 2020: Globocan estimates of incidence and mortality worldwide for 36 cancers in 185 countries," *CA: A Cancer Journal for Clinicians*, vol. 71, no. 3, pp. 209–249, May 2021.

[107] A. G. Waks and E. P. Winer, "Breast cancer treatment: A review," *JAMA*, vol. 321, no. 3, pp. 288–300, Jan. 2019.

[108] A. Peters and P. Tadi, "Aromatase inhibitors," in *StatPearls*. Treasure Island, FL: StatPearls Publishing, 2026, available from: https://www.ncbi.nlm.nih.gov/books/NBK557856/.

[109] Q. Qi, "Breast cancer targeting her2: Mechanisms, resistance and emerging therapies," *Theoretical Natural Science*, vol. 77, pp. 70–79, 2025.

[110] R. Chauhan, J. Bhattacharya, R. Solanki, F. J. Ahmad, B. Alankar, and H. Kaur, "Gud-ve: Visualization tool for physicochemical properties of proteins," *MethodsX*, vol. 10, p. 102226, 2023.

[111] G. Henrique, A. Caminero, and R. L. Calil, "Absorption matters: A closer look at popular oral bioavailability rules for drug approvals," *Molecular Informatics*, vol. 42, no. 11, p. 2300072, 2023.

[112] D. E. V. Pires, T. L. Blundell, and D. B. Ascher, "pkcsm: Predicting small-molecule pharmacokinetic and toxicity properties using graph-based signatures," *Journal of Medicinal Chemistry*, vol. 58, no. 9, pp. 4066–4072, 2015.

[113] M. Mihăşan, "What in silico molecular docking can do for the bench-working biologists," *Journal of Biosciences*, vol. 37, no. 6, pp. 1089–1095, 2012.

[114] S. Agnihotry, R. K. Pathak, D. B. Singh, A. Tiwari, and I. Hussain, "Protein structure prediction," in *Bioinformatics: Methods and Applications*. Amsterdam, Netherlands: Elsevier, 2022, pp. 177–188.

[115] A. M. Davis and P. D. Leeson, "Physicochemical properties," in *The Royal Society of Chemistry eBooks*. Royal Society of Chemistry, 2023, ch. 1, pp. 1–28.

[116] A. A. Tokmakov, A. Kurotani, and K.-I. Sato, "Protein pi and intracellular localization," *Frontiers in Molecular Biosciences*, vol. 8, p. 775736, 2021.

[117] E. Gasteiger, C. Hoogland, A. Gattiker, S. Duvaud, M. R. Wilkins, R. D. Appel, and A. Bairoch, "Protein identification and analysis tools on the expasy server," in *The Proteomics Protocols Handbook*, J. M. Walker, Ed. Totowa, NJ: Humana Press, 2005, pp. 571–607.

[118] X. Zhou, Y. Zhang, C. Zhang, J. Ma, Y. Li, D. Kihara, J. Yang, and Y. Zhang, "I-tasser-mtd: A deep-learning-based platform for multidomain protein structure and function prediction," *Nature Protocols*, vol. 17, no. 10, pp. 2326–2353, Oct. 2022.

[119] Z. S. A. Shehri, A. A. Alshammari, A. M. Alqahtani, A. A. Alghamdi, and M. A. Aljohani, "Machine learning-based virtual screening and molecular docking of phytochemicals: Applying lipinski's rule of five to improve drug-likeness," *Crystals*, vol. 15, no. 5, p. 445, 2025.

[120] U. A. Çevik, A. Isik, and A. Karakaya, "Admet and physicochemical assessments in drug design," in *Computational Methods for Rational Drug Design*. Hoboken, NJ: John Wiley & Sons, 2024, pp. 123–151.

[121] X.-Y. Meng, H.-X. Zhang, M. Mezei, and M. Cui, "Molecular docking: A powerful approach for structure-based drug discovery," *Current Computer-Aided Drug Design*, vol. 7, no. 2, pp. 146–157, Jun. 2011.

[122] M. Ghanavati, Y. Khorshidi, M. Shadnoush, M. E. Akbari, S. H. Ardehali, Y. Chavarri-Guerra, A. Akbari, M. Rezaei, and H. R. Mirzaei, "Tamoxifen use and risk of endometrial cancer in breast cancer patients: A systematic review and dose–response meta-analysis," *Cancer Reports*, vol. 6, no. 4, p. e1806, 2023.

[123] A. Howell and S. J. Howell, "Tamoxifen evolution," *British Journal of Cancer*, vol. 128, no. 3, pp. 421–425, Feb. 2023.

[124] E. Carvalho, S. Canberk, F. Schmitt, and N. Vale, "Molecular subtypes and mechanisms of breast cancer: Precision medicine approaches for targeted therapies," *Cancers*, vol. 17, no. 7, p. 1102, Apr. 2025.

[125] C. A. Lipinski, F. Lombardo, B. W. Dominy, and P. J. Feeney, "Experimental and computational approaches to estimate solubility and permeability in drug discovery and development settings," *Advanced Drug Delivery Reviews*, vol. 46, no. 1–3, pp. 3–26, Mar. 2001.

[126] A. Daina, O. Michielin, and V. Zoete, "Swissadme: A free web tool to evaluate pharmacokinetics, drug-likeness and medicinal chemistry friendliness of small molecules," *Scientific Reports*, vol. 7, p. 42717, Mar. 2017.

[127] J. S. Sidhu, R. K. Singla, Mayank, and V. Jaitak, "Indole derivatives as anticancer agents for breast cancer therapy: A review," *Anti-Cancer Agents in Medicinal Chemistry*, vol. 21, no. 2, pp. 160–173, 2021.

[128] A. Tropsha, O. Isayev, A. Varnek, G. Schneider, and A. Cherkasov, "Integrating qsar modelling and deep learning in drug discovery: the emergence of deep qsar," *Nature Reviews Drug Discovery*, vol. 23, no. 2, pp. 141–155, 2024.

[129] M. Shah, M. Patel, M. Shah, M. Patel, and M. Prajapati, "Computational transformation in drug discovery: A comprehensive study on molecular docking and quantitative structure activity relationship (qsar)," *Intelligent Pharmacy*, vol. 2, no. 5, pp. 589–595, 2024.

[130] K. Kaur and V. Jaitak, "Recent development in indole derivatives as anticancer agents for breast cancer," *Current Topics in Medicinal Chemistry*, vol. 19, no. 13, pp. 1160–1186, 2019.